ABSTRACT

Title of Document: THE *P–T–t* HISTORY OF A BARROVIAN SEQUENCE IN DUTCHESS COUNTY, NEW YORK, AND THE ADJACENT PART OF CONNECTICUT

Yan Chen, Master of Science, 2009

Directed By: Professor Michael Brown and Associate Research Scientist Philip M. Piccoli Department of Geology

The *P–T–t* history of a Barrovian sequence in Dutchess County, New York and the adjacent part of Connecticut was studied. Using the average *P–T* mode in THERMOCALC, the following *P–T* results were calculated for the garnet, staurolite, kyanite and sillimanite-K-feldspar zones (1σ uncertainties): 5.2±0.8 kbar, 570±12°C; 5.9±1.1 kbar, 557±12°C; 6.4±1.1 kbar, 600±29°C; and 7.4±1.4 kbar, 752±68°C, respectively. Phase equilibria modeling in the MnNCKFMASHTO system yields peak *P–T* results consistent with the average *P–T* results.

Monazite ages were obtained for the garnet, staurolite, kyanite and sillimanite-K-feldspar zones (2σ uncertainties): 455±6 and 453±10 Ma; 451±9 and 438±8 Ma; 478±6, 431±4 and 425±8 Ma; 533±7 Ma, 507±6, 506±4 Ma and 472±5 Ma, respectively. These ages help to constrain the timing of the Taconic and Salinic orogenic events.

THE *P–T–t* HISTORY OF A BARROVIAN SEQUENCE IN DUTCHESS COUNTY, NEW YORK, AND THE ADJACENT PART OF CONNECTICUT

by

Yan Chen

Thesis submitted to the Faculty of the Graduate School of the
University of Maryland, College Park, in partial fulfillment
of the requirements for the degree of
Master of Science
2009

Advisory Committee:
Professor Michael Brown, Chair
Associate Research Scientist Philip M. Piccoli, Co-Chair
Assistant Professor Aaron Martin, Committee Member

Acknowledgements

I would like to thank my committee members Drs. Michael Brown, Phil Piccoli and Aaron Martin for their help and effort in reaching this point. I would like to thank Drs. Bill McDonough and Sarah Penniston-Dorland for their help in shaping my research purpose.

I would like to thank, again, Drs. Michael Brown and Phil Piccoli for all their help, in training my scientific research attitude, in teaching me English and for supporting me in the past four years. I thank Dr. Phil Piccoli for helping me with all of the EPMA work and staying late in the probe room after work hours.

I would like to thank Barry Reno and Fawna Korhonen for their help and support during my research. I thank Satoshi Saito for helping me collect samples.

I would like to thank Drs. Wei Chunjing and Richard White for their help in phase equilibrium modeling. I thank Dr. Stan Mertzman for his patience in XRF whole rock analysis.

And I thank all other teachers and graduate students who have given support to my study.

Table of Contents

List of Tables

List of Figures

Chapter 1: Introduction

The Appalachian orogen is a Paleozoic orogen with long-lived accretionary history, including the opening and closing of the Iapetus Ocean, followed by collisional orogenesis in response to closing of the Rheic Ocean (e.g., van Staal, 2005; Zagorevski et al., 2006). The Iapetus Ocean started to open in the latest Neoproterozoic (ca. 570 Ma) producing a rift–drift transition along the Laurentian passive margin, achieved a width of about 5000 km by the late Cambrian (500–490 Ma), and was closed in successive events related to the accretion of arcs and microcontinents during the Ordovician and early Silurian (van Staal, 1998; McLennan et al., 2001; van Staal, 2005). The Rheic Ocean opened when the microcontinent Avalonia rifted from Gondwana during the Lower to Middle Ordovician, and was closed in the collision between Gondwana and Laurentia in the Permian (van Staal, 2005). The various orogenic events are generally grouped into five, as follows: the Lower to Middle Ordovician Taconic, early to late Silurian Salinic, latest Silurian to Lower Devonian Acadian, Middle Devonian to early Carboniferous Neoacadian, and Carboniferous to Permian Alleghanian (van Staal, 2005).

The Taconic Orogeny (470–455 Ma) in western New England has been interpreted as the result of the accretion of magmatic arcs to the Laurentian margin (Stanley & Ratcliffe, 1985; Karabinos et al., 2003). However, reconstruction of a tectonic model for the Taconic Orogeny is not straightforward. Intense metamorphism associated with the Taconic Orogeny and overprinting by the subsequent orogenic events, especially the Acadian Orogeny, partly or completely

erased the previous pressure, temperature and geochronology (*P–T–t*) records, making it difficult to reconstruct the *P–T–t* history of the Taconic klippen. The purpose of this study is to unravel the *P–T–t* history of the Taconic Barrovian sequence in Dutchess County, New York, and the adjacent part of Connecticut using an integrated approach including petrography, mineral chemistry and phase equilibria modeling in combination with electron probe microanalyzer (EPMA) dating of monazite. Methods of phase equilibria modeling and monazite geochronology are introduced below.

1.1 Phase Equilibria Modeling Using THERMOCALC

The program THERMOCALC was developed by Powell & Holland (1988) in order to address thermobarometry problems. It is based on a large internally-consistent thermodynamic dataset (Holland & Powell, 1998) which has been continuously updated over the past twenty years (e.g., Powell & Holland, 2008). Various types of phase diagram and average *P–T* can be calculated using THERMOCALC to quantify the *P–T* history of a rock. A *P–T* pseudosection is an equilibrium phase diagram for a fixed bulk composition, which provides information on possible mineral assemblages and the proportions and compositions of minerals in a *P–T* range. The average *P–T* method, which is based on an internally-consistent thermodynamic dataset, obtains an optimal *P–T* from an independent set of reactions representing all the equilibria rather than a subset of the equilibria (Powell & Holland, 1994).

In this thesis, I present a detailed study of phase equilibria modeling by constructing *P–T* pseudosections in the chemical system including MnO, Na_2O, CaO,

K_2O, FeO, MgO, Al_2O_3, SiO_2, Fe_2O_3, TiO_2 and H_2O (MnNCKFMASHTO) and calculating average *P–T* conditions of samples from the garnet, staurolite, kyanite, and sillimanite–K-feldspar zones of the Barrovian sequence in Dutchess County, New York and the adjacent part of Connecticut.

1.2 Monazite Geochronology

1.2.1 An Introduction to Monazite

Monazite is a light rare earth element (LREE)-enriched orthophosphate with an idealized formula of [(LREE)PO_4]. Compositional variation in monazite is caused by two types of substitutions: (1) isomorphous substitution at either of the two independent cation sites (LREE or P), and (2) coupled substitution at both sites (Williams et al., 2007). The isomorphous substitution includes: (1) the substitution of one rare earth element (REE) by another REE or Y, i.e., $LREE^{3+} \leftrightarrow Y^{3+}$ (REE^{3+}); (2) the substitution of rare earth elements (REEs) by non-REE species (other than Y), for example, the brabantite [(Ca, Th)PO_4] substitution ($2REE^{3+} \leftrightarrow Ca^{2+} + Th^{4+}$), and (3) the substitution of P by Si, for example, $PO_4^{3+} \leftrightarrow SiO_3^{2-} + F^-$. The second type of substitution involves a coupled substitution at both cation sites, for example, the huttonite substitution ($P^{5+} + REE^{3+} \leftrightarrow Si^{4+} + Th^{4+}$). Through the brabantite and huttonite substitutions, monazite can contain significant concentrations of thorium (Th) and uranium (U; U is incorporated into monazite in a similar way as Th), which makes monazite a potential mineral for absolute dating.

1.2.2 Monazite EPMA Geochronology

Different from traditional isotopic geochronology methods, electron probe microanalyzer (EPMA) dating of monazite is based on the total UO_2, ThO_2 and PbO concentrations in monazite. The application of this chemical dating method to monazite was proposed by Suzuki et al. (1991). Similar methods have been used on uraninite, huttonite and thorite (e.g., Cameron-Schimann, 1978; Parslow, 1985; Bowles, 1990). The advantages of this method include *in situ* dating, high-spatial resolution (3-5 μm beam) and non-destructive analysis. One disadvantage is the relatively large uncertainty related to a single date, however, this can be minimized by increasing the number of analyses.

Uranium has three natural radioactive isotopes, ^{238}U (99.2743%), ^{235}U (0.7200%) and ^{234}U (0.0057%; this is an intermediate daughter whose abundance can vary in some materials). The ratio of ^{238}U and ^{235}U today is 137.88. Thorium has only one relatively stable radioactive isotope which is ^{232}Th. The decay mechanism, half lives and decay constants of ^{238}U, ^{235}U and ^{232}Th are:

$^{238}U \rightarrow {}^{206}Pb + 8\alpha$ with $t_{1/2} = 4.47 \times 10^{9}$yr and $\lambda 1 = 1.551 \times 10^{-10}$yr^{-1},

$^{235}U \rightarrow {}^{207}Pb + 7\alpha$ with $t_{1/2} = 704 \times 10^{6}$yr and $\lambda 2 = 9.848 \times 10^{-10}$yr^{-1}, and

$^{232}Th \rightarrow {}^{208}Pb + 6\alpha$ with $t_{1/2} = 14 \times 10^{9}$yr and $\lambda 3 = 4.9475 \times 10^{-10}$yr^{-1}.

The number of Pb atoms produced as a function of time and corresponding parent isotopes are $^{208}Pb = {}^{232}Th \cdot (e^{\lambda_{232} t} - 1)$, $^{207}Pb = {}^{235}U \cdot (e^{\lambda_{235} t} - 1)$ and $^{206}Pb = {}^{238}U \cdot (e^{\lambda_{238} t} - 1)$. The total Pb measured today can be expressed by the following equation:

$$Total\ Pb = Pb_{initial} + \ Th \cdot (e^{\lambda_{232}t} - 1) + U \cdot \frac{1}{138.88} \cdot (e^{\lambda_{235}t} - 1) + U \cdot \frac{137.88}{138.88} \cdot (e^{\lambda_{238}t} - 1),$$

where Pb, $Pb_{initial}$, Th and U represent the number of atoms of the corresponding elements. $Pb_{initial}$ in monazite is assumed to be zero. The final equation using the oxide concentrations in wt.% is:

$$\frac{PbO}{W_{PbO}} = \frac{ThO_2}{W_{ThO_2}} \cdot (e^{\lambda_{232}t} - 1) + \frac{UO_2}{W_{UO_2}} \cdot \frac{1}{138.88} \cdot (e^{\lambda_{235}t} - 1) + \frac{UO_2}{W_{UO_2}} \cdot \frac{137.88}{138.88} \cdot (e^{\lambda_{238}t} - 1),$$

where W_i refers to the molecular weight of i (i = PbO, UO_2, ThO_2). An approximation is made in calculating W_{PbO} by assuming an atomic weight of 207.2 for PbO other than the true atomic weight in each sample. The uncertainty on the age introduced by this approximation is less than 1 Ma.

Many studies have focused on improving the analytical technique and protocol of EPMA dating of monazite (e.g., Pyle et al., 2005b; Williams et al., 2007) as well as the format of reporting data (e.g., Williams, 2006). One challenge of using this technique is how to report and analyze the age data in an appropriate statistical fashion. Monazite age data are currently reported in the literature in one or several of the following formats: probability density or histogram plot (e.g., Pyle et al., 2005a; Martin et al., 2007), the range of age data (e.g., Kelts et al., 2008), a weighted average with or without the MSWD value (e.g., Kelly et al., 2005) and an average calculated using the tanh estimator (e.g., Kelsey et al., 2003). Probability density plots or histogram plots are used to show the distribution of data and compare data from different populations. However, this comparison is semi-qualitative rather than quantitative. Comparing ages quantitatively from different populations is commonly required in geochronological studies, but few studies use inferential statistics to

quantify the difference between populations. In this study, a new statistical method is proposed to report and compare monazite age data.

1.3 Structure of the Thesis

Following this chapter, chapter two introduces the regional geology of the study area and the research history; chapter three examines the petrography and mineral chemistry of representative samples; chapter four includes phase equilibria modeling using THERMOCALC and estimation of pressure and temperature conditions using *P–T* pseudosections and the average *P–T* method; chapter five examines the timing of metamorphism through the application of monazite geochronology; chapter six discusses the significance of the thesis and summarizes the conclusion.

Chapter 2: Regional Geology

The study area is located in southeastern New York and western Connecticut (Figure 2-1). In the field area, the metamorphic grade increases gradually from west to east with a Barrovian sequence of metamorphic zones as follows: chlorite, biotite, garnet, staurolite, kyanite, sillimanite and sillimanite-K-feldspar zones (Figure 2-1). The protolith of the Barrovian sequence was deposited on the continental slope and rise of the Iapetus Ocean prior to or during the early stage of the Taconic Orogeny (Zen, 1972; Stanley & Ratcliffe, 1985), subsequently carried westward (present coordinates) and metamorphosed during the accretion of magmatic arcs to the Laurentian continental margin (Stanley & Ratcliffe, 1985). A detailed petrologic, structural and mineralogical study of the Barrovian sequence in Dutchess County was conducted in the 1930s (Barth, 1936; Balk, 1936) and a series of NNE-trending isograds have been mapped (Barth, 1936; Vidale, 1974). More recently, Whitney et al. (1996a, b) restudied the petrography and mineralogy and reported fluid infiltration into part of the study area.

The metamorphic geochronology in this area was studied by Long (1962) and Bence & McLelland (1976). K-Ar and Rb-Sr isotope ages (360–350 Ma) from biotite and muscovite separates were interpreted as the result of the latest regional thermal event at approximately 360–350 Ma ago (Long, 1962). A 430 ± 20 Ma Rb-Sr muscovite age combined with Rb-Sr whole-rock analysis was interpreted as the minimum age of an earlier metamorphic event (Long, 1962). However, similar ages (435 ± 3 to 370 ± 5 Ma) from ^{40}Ar-^{39}Ar biotite and muscovite separates were interpreted to be the result of continuous loss of argon during exhumation following

the Taconic Orogeny rather than representing two metamorphic events (Bence & McLelland, 1976). Both studies yielded cooling ages rather than the peak metamorphic ages. McLennan et al. (2001) studied detrital zircons from the Austin Glen Formation, a unit which has been interpreted to represent part of the Taconic foreland basin. Detrital zircons record predominantly Grenville ages of ca. 1.34–0.93 Ga. The absence of zircons with Taconic ages was interpreted to be the result of the lack of exposure of any coeval plutons (McLennan et al., 2001).

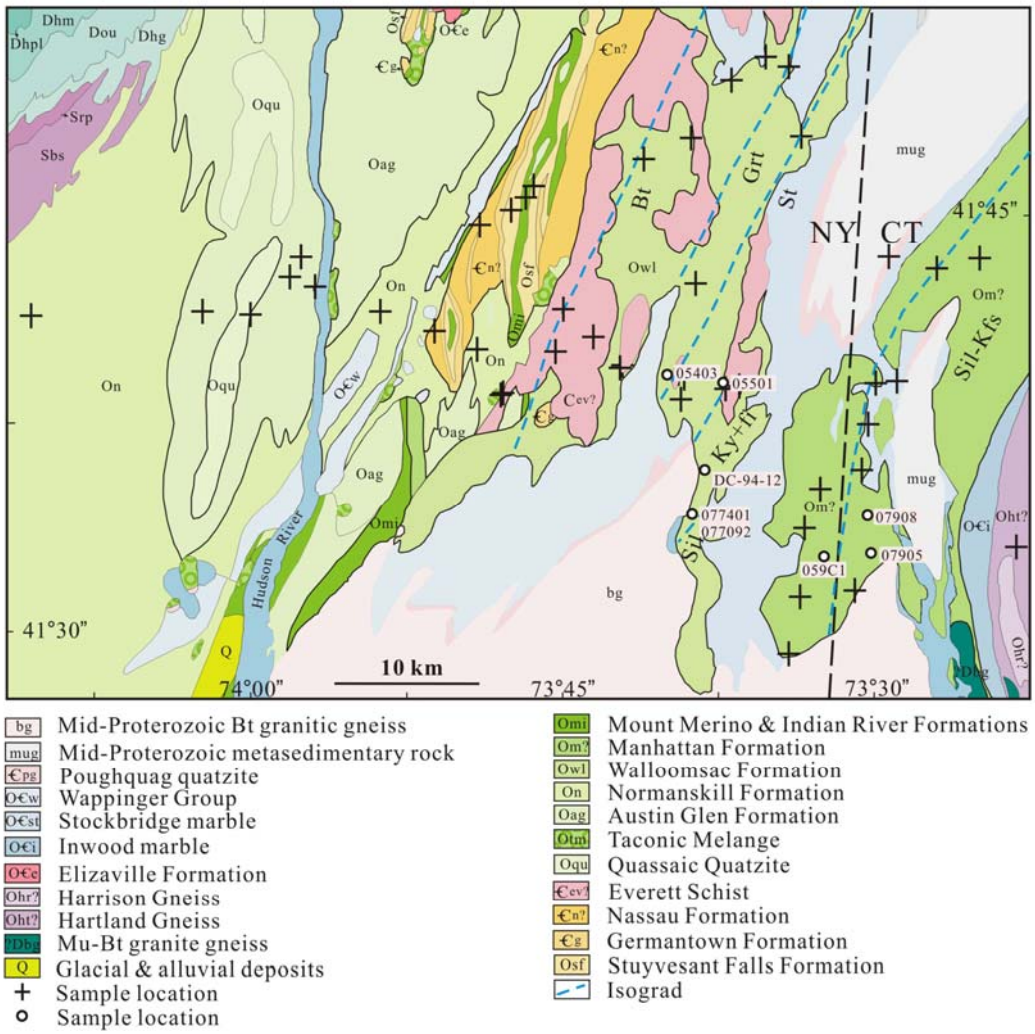

Figure 2-1. Geological map of the study area in Dutchess County, New York and adjacent part of Connecticut. Modified after Fisher et al. (1970) and Whitney et al. (1996a). Crosses and circles show sample locations.

P–T conditions were estimated by Whitney et al. (1996a) using conventional mineral thermobarometers and petrogenetic grids. The thermobarometric results are listed in Table 2-1.

Table 2-1. Thermobarometry results from Whitney et al. (1996a).

Zone	Assemblage	T(°C)*	P_{GPAQ}† (kbar)	P_{GPBM}†
Garnet	Rim	435–470		2.1–3.0
	Outer core	475–480		3.2–4.0
Lower St	Rim	450–480		3.7–4.0
	Outer core	505–520		5.5–5.6
Upper St	Rim	485–500		3.0–4.0
	Outer core	512–515		4.3–5.3
Kyanite	Rim	455–525	3.5–4.9‡	3.8–4.7
	Outer core	450–500	4.5–6.0	3.5–5.2
Sillimanite	Rim	580–590	3.8–4.7	4.6–5.7
	Outer core	585	4.0–5.1	4.4–5.6
Sil–Kfs	Rim	*c*.720	*c*.5–6	*c*.5–6
	Outer core	*c*.730	*c*.5–6	*c*.5–6

*Garnet–biotite geothermometry calibrations of Ferry & Spear (1978) with Berman (1990) garnet solution model and Hodges & Spear (1982) yielded similar results. The range reported represents values obtained from 2–3 garnet–biotite assemblages within the same thin section. †GPAQ=garnet–plagioclase-Al_2SiO_5-quartz geobarometry (Hodges & Spear, 1982; Koziol & Newton, 1989); GPMB=garnet–plagioclase–muscovite–biotite geobarometry of Ghent & Stout (1981), Hodges & Crowley (1985) and Hoisch (1990). Note: the calibration of Koziol & Newton (1989) consistently yields the highest pressure. ‡Fibrolitic sillimanite at garnet rim.

Chapter 3: Petrography and Mineral Chemistry

The petrography and mineral chemistry of the study area has been examined by Balk (1936), Barth (1936), and Whitney et al. (1996a). In this thesis, instead of describing the general petrography and mineral chemistry of each metamorphic zone, I have examined the petrography, mineral chemistry, bulk composition, and monazite geochronology of samples from the garnet, staurolite and kyanite zones, and the sillimanite plus sillimanite–K-feldspar zones combined (Figure 2-1, numbered sample locations). Samples from the chlorite and biotite zones are not studied extensively because of the difficulty of obtaining quantitative *P–T–t* information from the low-grade samples.

3.1 Analytical Methods

Mineral compositions and garnet X-ray element composition maps were obtained using the JEOL JXA-8900 SuperProbe in the Nanoscale Imaging Spectroscopy and Properties Laboratory (NISP) at the University of Maryland. An accelerating voltage of 15 kV, a cup current of 10 nA, and a 5 μm beam were used for most phases, and the same accelerating voltage (15 kV), a cup current of 50 nA, and a 1 μm beam were used for garnet single spot analyses along radial traverses in order to avoid inclusions. Natural mineral standards were analyzed as unknowns for quality control and those mostly resembled the unknown phases were used as standards (Appendix C).

Garnet X-ray element composition maps were collected at an accelerating voltage of 15 kV and a cup current of 200 nA with a 3 μm beam. The dwell time was 150 ms. The step size varied from 2 μm to 4 μm depending on the size of garnet.

3.2 Mineral Distribution

Based on a study of fifty three thin sections, the distribution of major and accessory minerals from the sub-chlorite zone through the sillimanite–K-feldspar zone is given in Table 3-1.

Table 3-1. Mineral distribution of the Barrovian sequence in the study area.

Zone	Sub-Chl	Chl	Bt	Grt	St	Ky	Sil	Sil-Kfs
N	6	8	6	8	4	9	4	8
Chl		√	√	√	†			
Bt			√	†	√	√	√	√
Grt				√	†	√	√	†
St					√	†	†	
Ky						†		
Sil							√	√
Kfs								√
Pl	√	√	√	√	†	√	√	√
Ms	√	√	√	√	√	√	√	†
Qtz	√	√	√	√	√	√	√	√
Ilm		†	√	√	√	√	√	√
Cld				†	†			
Cal	†	†						
Gr					†			
Ep					†			
Ap	√	√	√	√	√	√	√	√
Mnz	†	√	√	†	√	√	√	√
Zrn	†	√	√	√	√	√	√	√
Py	†	√	√	√	√	√	√	√
Tur				√	√	†	†	†
Aln			√	†	†			
Xen			√	†		†	√	†

Most mineral abbreviations are after Kretz (1983). "Xen" refers to xenotime.
"√" means the phase is observed in all samples examined.
"†" means the phase is observed in some but not all of the examined samples.
N is the number of samples studied.

3.3 Petrography and Mineral Chemistry of Representative Samples

Representative samples from the garnet, staurolite, kyanite and sillimanite–K-feldspar zones were examined in detail. Representative mineral analyses are listed in Tables 3-2 to 3-6. All mineral analyses are included in Appendix D.

3.3.1 Garnet Zone

A representative schist (05403) from the garnet zone contains idiomorphic garnet (0.5–1mm), biotite (0.1–0.5 mm) and ilmenite (0.3–0.8 mm) porphyroblasts in a matrix composed of fine-grained (10–50 μm) muscovite, chlorite, quartz and plagioclase with accessory zircon, apatite, tourmaline and pyrite (Figure 3-1).

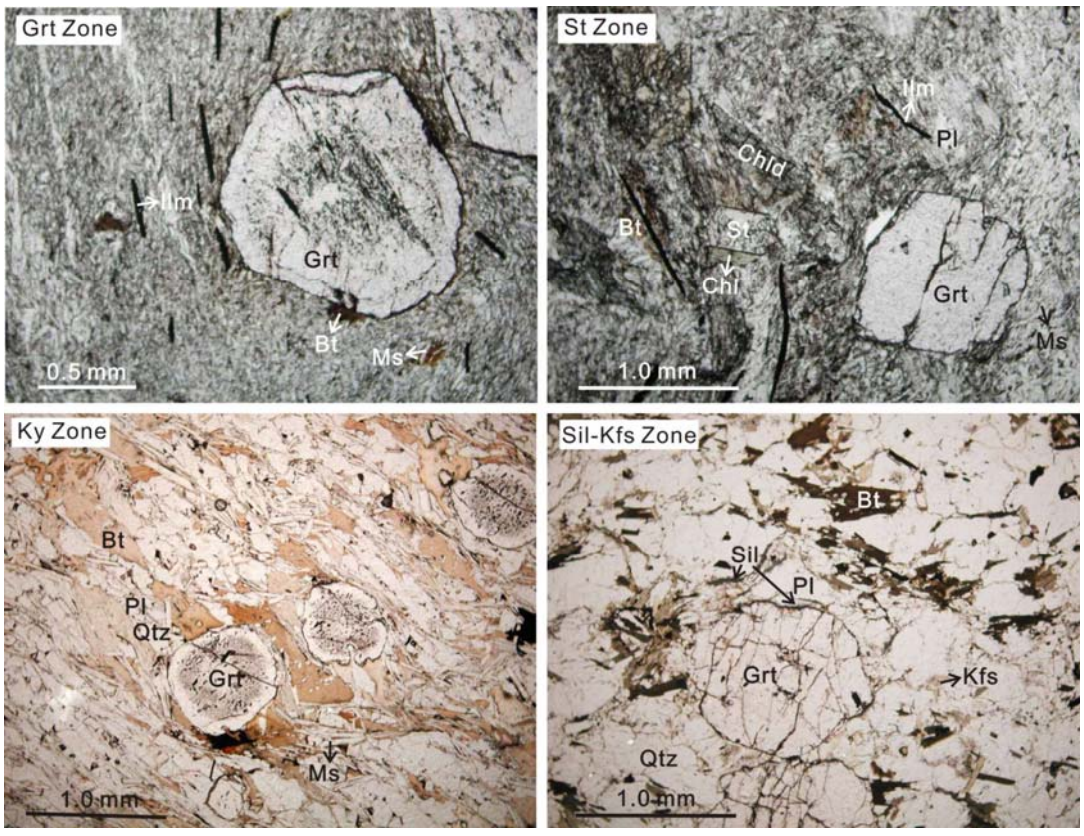

Figure 3-1. Photomicrographs of samples from the garnet, staurolite, kyanite and sillimanite–K-feldspar zones.

Millimeter-scale quartz veins containing quartz (0.3–1mm) and chlorite (~0.3 mm) occur parallel to the dominant foliation.

Garnet shows prograde growth zoning with decreasing spessartine (X_{Sps}, 0.25 to 0.04) and grossular (X_{Grs}, 0.15 to 0.05), and increasing almandine (X_{Alm}, 0.57 to 0.83) and pyrope (X_{Prp}, 0.03 to 0.07) components from the core to the rim (Figure 3-2). The *Mg#* increases from the core to the rim (0.06 to 0.08) but decreases through the outmost 10–20 μm of rim (0.08 to 0.07). An analysis close to the garnet rim with the highest *Mg#* was selected for use in the average *P–T* calculations.

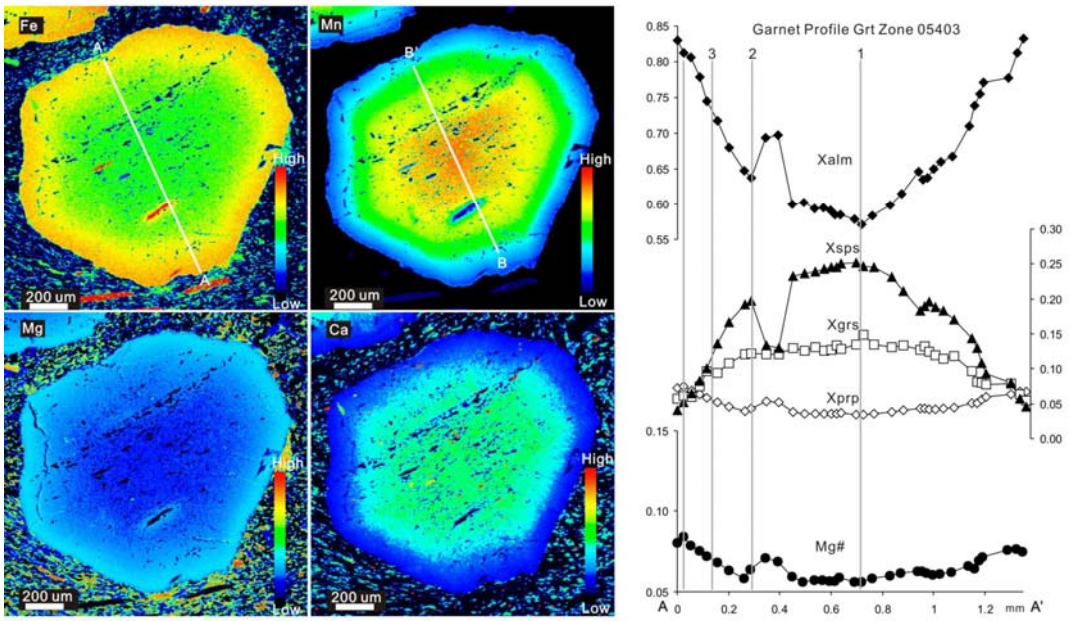

Figure 3-2. X-ray element composition maps and profiles of garnet from the garnet zone.

Muscovite close to garnet in the matrix (domain A) and muscovite close to the veins (domain B) were analyzed. Muscovite in domain A is homogeneous, whereas in domain B is heterogeneous with higher SiO_2 and lower Al_2O_3 in some analyses. The average of eight analyses from two muscovite grains in domain A was used for the

average *P–T* calculations. An analysis with the highest SiO_2 from muscovite in domain B was used for a second average *P–T* calculation for comparison.

Biotite is chemically homogeneous but grains in contact with garnet (e.g. Bt#2, see Appendix D for chemical composition) have a different composition compared to the biotite not in contact with garnet (Bt#3). The average composition of Bt#3 was used for the average *P–T* calculations.

Plagioclase in this sample is small in size (~10 μm), which makes it difficult to identify any potential compositional zoning. Analyses from different grains are indistinguishable within the analytical uncertainty. The average composition of three analyses from two plagioclase grains was used for the average *P–T* calculations.

Chlorite is small (~10 μm) in the matrix and coarse in the veins (100–300 μm). Chlorite in the veins is heterogeneous in composition and not selected for any average *P-T* calculation because it is suspected to be secondary. Chlorite in the matrix is usually too small to obtain multiple analyses. The average of three analyses from three chlorite grains is used for the average *P–T* calculations.

3.3.2 Staurolite Zone

Sample 05501 contains porphyroblasts of garnet (1–2mm), chloritoid (up to 3 mm in length), ilmenite (1–2 mm in length) and staurolite (~0.5 mm) in a matrix composed of biotite (~0.3 mm), muscovite (0.1–0.2 mm), plagioclase (0.1–0.5 mm) and graphite (<10 μm), with accessory monazite, zircon, apatite, tourmaline and pyrite (Figure 3-1). Crenulation cleavage is present and ilmenite is generally parallel to the foliation and some grains bend with the crenulation cleavage.

Idiomorphic garnet exhibits prograde growth zoning with decreasing X_{Sps} (0.17 to 0.05), and increasing X_{Alm} (0.72 to 0.83), X_{Prp} (0.05 to 0.09) and *Mg#* (0.07 to 0.09) from the core to the rim (Figure 3-3). The grossular component varies irregularly from 0.06 to 0.05 from the core to the rim with a drop to 0.04 in the outmost 50 μm rim. An analysis in the garnet rim with the highest *Mg#* was selected for use in the average *P–T* calculations.

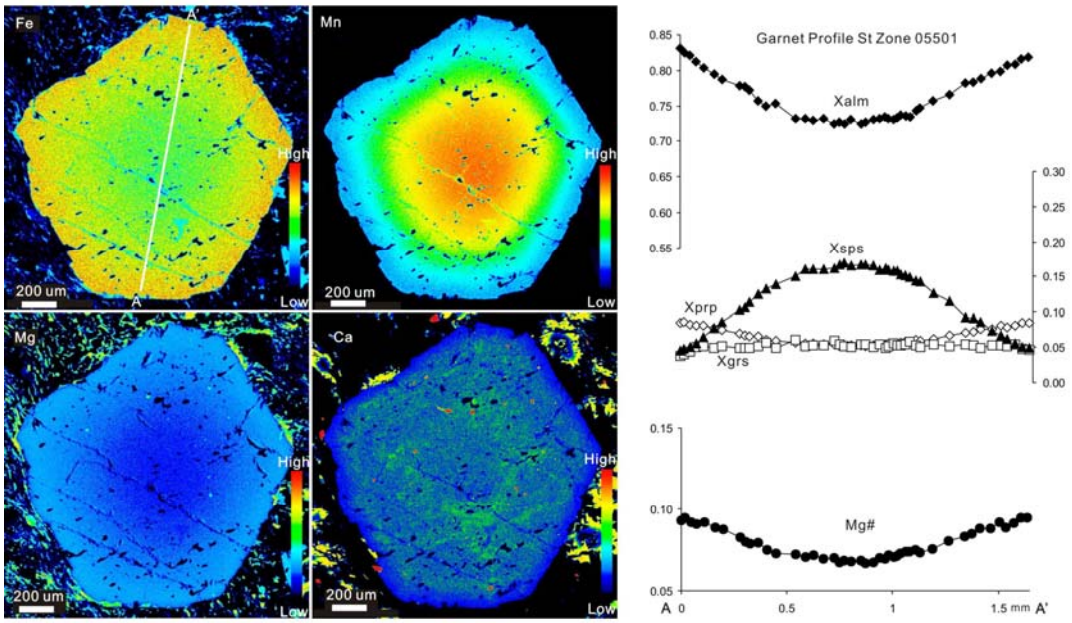

Figure 3-3. X-ray element composition maps and profiles of garnet from the staurolite zone.

Muscovite is homogeneous. The average composition of six analyses from muscovite close to garnet (but not in contact), and the average of eight analyses from muscovite close to chloritoid are used in the average *P-T* calculations.

Biotite is chemically heterogeneous in terms of FeO and MgO but is not systematically zoned. The average composition is used for the average *P-T* calculations.

Plagioclase (Pl#1, see Appendix D) close to garnet but not in contact (~1mm) is chemically zoned with increasing anorthite component from the core to the rim (X_{An}, 0.05–0.17). Pl#2 (about 5 mm from the garnet) is also chemically zoned (X_{An}, 0.19–0.24) but the limited number of analyses does not allow identification of systematic zoning. The rim composition of Pl#1 is used for the average *P–T* calculations.

Staurolite is irregularly zoned. The rim composition is used for the average *P–T* calculations.

Large tabular chloritoid porphyroblasts are oriented obliquely at low angle to the foliation (<20°), however, there are a few exceptions (>45°). Some chloritoid grains have been partially replaced by chlorite. Choritoid is chemically homogeneous. The average of 23 analyses from three grains is used for the average *P–T* calculations.

3.3.3 Kyanite Zone

Sample 077401 contains garnet (~0.5 mm), biotite (0.5–1 mm), muscovite (0.3–0.8 mm), plagioclase (0.01–0.1 mm), quartz (0.3–0.5 mm) and ilmenite (0.1–1 mm), with accessory monazite, apatite, pyrite, tourmaline and zircon (Figure 3-1). The foliation is defined by muscovite and biotite, and is crosscut by millimeter-scale quartz veins. Muscovite and biotite occur in the quartz veins.

Garnet has an inclusion-free core, an inclusion-rich mantle and an inclusion-free rim. Quartz and ilmenite inclusions (10–50 μm) in garnet form straight trails which are at high angle (>45°) with the matrix foliation. The X_{Alm} varies from 0.66 to 0.70 from the core to the mantle and increases to 0.74 within approximately the 50 μm-wide rim. X_{Sps} (0.10–0.13) and X_{Prp} (0.11–0.12) do not vary significantly from the

core to the rim. The X_{Grs} (0.10 to 0.04) decreases from the core to the rim. The *Mg#* is approximately constant from the core to the mantle (0.15–0.16) and decreases (0.13) at the rim (Figure 3-4). The average of analyses from the core and mantle and the analysis in the rim with the lowest Mg# were used for the average *P–T* calculations.

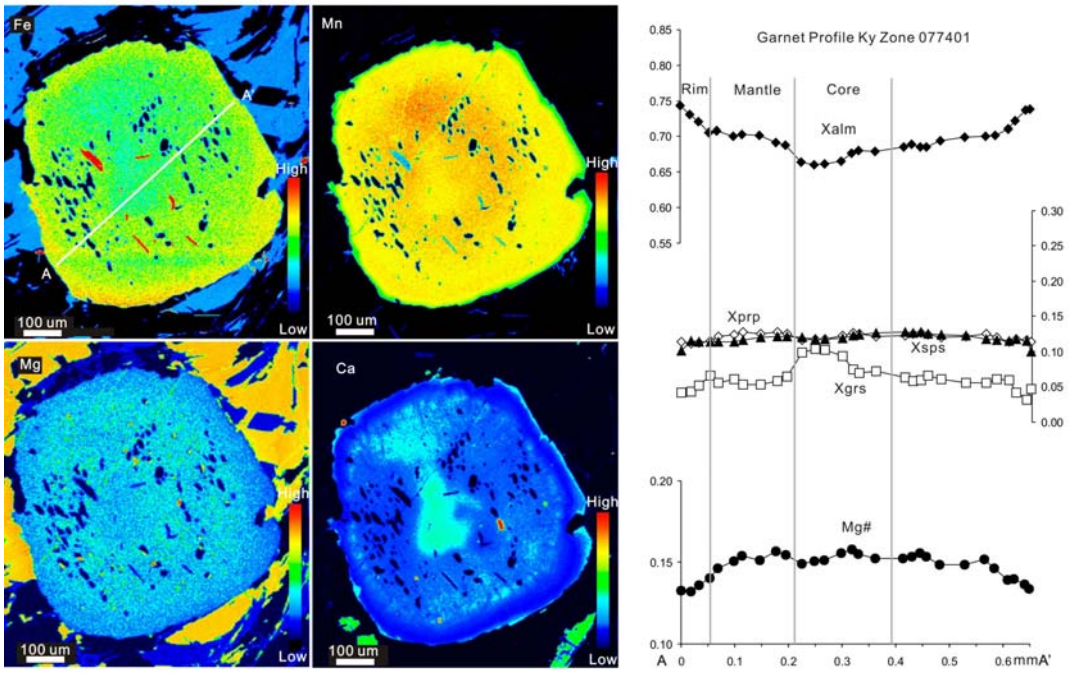

Figure 3-4. X-ray element composition maps and profiles of garnet from the kyanite zone.

Muscovite from different domains (A. close to garnet (less than 100 μm from garnet rim) but not in contact, B. about 2mm from the garnet rim, and C. close to the vein) has similar average compositions, although they are not all homogenous. The average composition of muscovite close to garnet is used for the average *P–T* calculations.

Biotite is chemically homogenous. The average composition of 14 analyses from two grains is used for the average *P–T* calculations.

Plagioclase shows irregular compositional zoning (X_{An}, 0.05–0.24). The rim composition is used for the average *P–T* calculations.

3.3.4 Sillimanite–K-feldspar Zone

Sample 07905 contains biotite (0.2–0.8 mm), garnet (0.5–1.5 mm), plagioclase (0.5–2 mm), K-feldspar (0.01–1 mm), sillimanite (~ 20 μm), quartz (~0.5 mm) and ilmenite (0.1–0.3 mm), with accessory zircon, monazite, apatite, tourmaline and pyrite (Figure 3-1). Sillimanite occurs along boundaries between feldspar, garnet and quartz. K-feldspar is locally sericitized.

Garnet is partially embayed by quartz, and replaced by biotite along cracks. Garnet X-ray element composition maps and compositional profiles show that X_{Sps} (0.16 to 0.11) decreases and X_{Alm} (0.67 to 0.73) increases from the core to the rim (Figure 3-5). X_{Prp} (0.10–0.11) is homogeneous from the core to the rim. X_{Grs} (0.06–0.07) is generally homogeneous from the core to the rim but with high-Ca rims occur locally (<10 μm thick). The *Mg#* varies little in the core (0.14–0.13) and decreases sharply to 0.12 at the rim. The average composition of analyses #2–#34 (see Appendix D) and the analysis in the rim with low *Mg#* are used for the average *P–T* calculations.

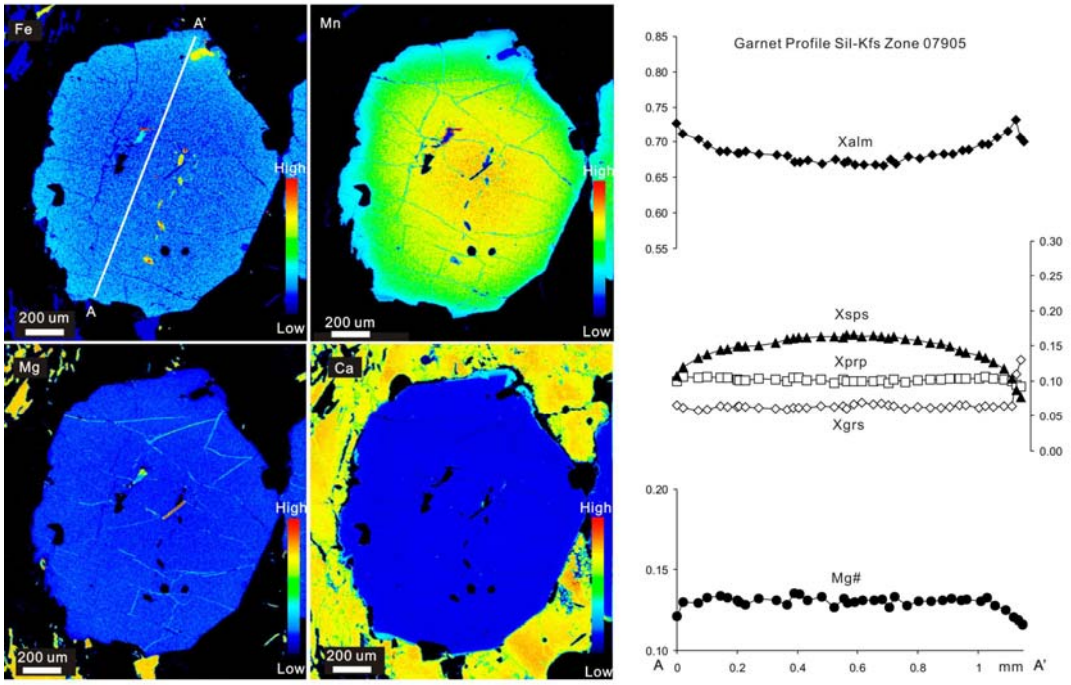

Figure 3-5. X-ray element composition maps and profiles of garnet from the sillimanite–K-feldspar zone.

Plagioclase in contact with garnet (Pl#1) has lower X_{An} (0.62) in the center, higher X_{An} (0.64) in the rim far from garnet, and the highest X_{An} (0.67) at the rim close to garnet. Plagioclase #2 (in contact with quartz and K-feldspar) shows irregular zoning (X_{An}, 0.59–0.64). The rim composition of Pl#1 (far from garnet) is used for the average *P-T* calculations.

Biotite is chemically homogenous. The average of 12 analyses from three grains is used for the average *P–T* calculations.

K-feldspar has an average composition of $Or_{0.98}$ with trace amount of Ca. The average of nine analyses from three grains is used for the average *P–T* calculations.

Table 3-2. Representative muscovite analyses.

	Garnet Zone		Staurolite Zone	Kyanite Zone
	matrix	vein	matrix	matrix
SiO_2	46.33	46.72	45.74	46.43
TiO_2	0.12	0.16	0.17	0.32
Al_2O_3	37.77	37.27	38.75	37.22
FeO	1.15	1.18	0.92	1.06
MnO	0.00	0.00	0.00	0.00
MgO	0.46	0.77	0.26	0.75
CaO	0.02	0.00	0.00	0.00
Na_2O	1.26	1.02	1.73	1.15
K_2O	9.35	9.69	8.52	9.67
F	0.00	0.06	0.00	0.02
Total	96.46	96.84	96.09	96.62
Si	6.05	6.09	5.97	6.06
Al^{IV}	1.95	1.91	2.03	1.94
Al^{VI}	3.86	3.81	3.93	3.79
Ti	0.01	0.02	0.02	0.03
Fe	0.13	0.13	0.10	0.12
Mn	0.00	0.00	0.00	0.00
Mg	0.09	0.15	0.05	0.15
Ca	0.00	0.00	0.00	0.00
Na	0.32	0.26	0.44	0.29
K	1.56	1.61	1.42	1.61
F	0.00	0.02	0.00	0.01
Ca+Na+K	1.88	1.87	1.86	1.90
OCT	4.09	4.10	4.10	4.09

Cations calculated on a 22-oxygen equivalents basis.
$OCT=Al^{VI}+Ti+Fe+Mn+Mg$

Table 3-3. Representative biotite analyses.

	Garnet Zone		Staurolite Zone	Kyanite Zone	Sil-Kfs Zone	
	contact Grt	matrix	matrix	matrix	matrix	in Grt rim
SiO_2	34.15	35.38	35.22	35.91	34.84	34.94
TiO_2	1.47	1.76	1.64	1.45	2.65	3.36
Al_2O_3	19.95	19.85	19.68	18.95	18.61	18.48
FeO	22.97	21.99	21.28	18.15	22.03	21.94
MnO	0.11	0.02	0.01	0.00	0.00	0.03
MgO	9.23	8.36	9.28	11.81	8.19	7.97
CaO	0.00	0.00	0.00	0.00	0.00	0.00
Na_2O	0.16	0.19	0.20	0.29	0.14	0.19
K_2O	8.22	9.17	8.83	9.00	10.10	9.90
Total	96.27	96.74	96.13	95.57	96.57	96.81
Si	5.21	5.35	5.34	5.40	5.33	5.32
Al^{IV}	2.79	2.65	2.66	2.60	2.67	2.68
Al^{VI}	0.79	0.89	0.85	0.76	0.69	0.64
Ti	0.17	0.20	0.19	0.16	0.31	0.39
Fe	2.93	2.78	2.70	2.28	2.82	2.80
Mn	0.01	0.00	0.00	0.00	0.00	0.00
Mg	2.10	1.89	2.10	2.65	1.87	1.81
Ca	0.00	0.00	0.00	0.00	0.00	0.00
Na	0.05	0.05	0.06	0.09	0.04	0.06
K	1.60	1.77	1.71	1.73	1.97	1.93
Ca+Na+K	1.65	1.82	1.77	1.81	2.01	1.98
OCT	6.01	5.76	5.83	5.85	5.68	5.64

Cations calculated on a 22-oxygen equivalents basis.
OCT=Al^{VI}+Ti+Fe+Mn+Mg

Table 3-4. Representative plagioclase and K-feldspar compositions.

	Garnet Zone	Staurolite Zone		Kyanite Zone		Sil-Kfs Zone		
	Pl	Pl		Pl		Pl		Kfs
		core	rim	core	rim	core	rim	
SiO_2	62.15	68.07	64.52	61.64	61.51	59.05	59.30	64.67
Al_2O_3	24.01	20.88	22.79	24.29	25.10	26.57	26.16	18.31
FeO	0.39	0.00	0.07	0.01	0.01	0.05	0.03	0.05
CaO	5.07	1.03	3.17	5.53	5.94	7.91	7.36	0.00
Na_2O	8.77	11.11	9.84	8.37	8.42	7.18	7.40	0.20
K_2O	0.02	0.04	0.05	0.05	0.07	0.09	0.08	16.50
Total	100.42	101.13	100.45	99.88	101.04	100.85	100.33	99.73
Si	2.75	2.94	2.83	2.74	2.70	2.62	2.64	3.00
Al	1.25	1.06	1.18	1.27	1.30	1.39	1.37	1.00
Fe	0.01	0.00	0.00	0.00	0.00	0.00	0.00	0.00
Ca	0.24	0.05	0.15	0.26	0.28	0.38	0.35	0.00
Na	0.75	0.93	0.84	0.72	0.72	0.62	0.64	0.02
K	0.00	0.00	0.00	0.00	0.00	0.01	0.00	0.98
Or	0.00	0.00	0.00	0.00	0.00	0.01	0.00	0.98
Ab	0.76	0.95	0.85	0.73	0.72	0.62	0.64	0.02
An	0.24	0.05	0.15	0.27	0.28	0.38	0.35	0.00

Cations calculated on an 8-oxygen basis.

Table 3-5. Representative chlorite, chloritoid and staurolite compositions.

	Garnet Zone		Staurolite Zone		
	Chl		Chld	St	
				core	rim
SiO_2	25.00		25.13	28.64	28.72
TiO_2	0.05		0.05	0.17	0.33
Al_2O_3	23.02		40.99	54.09	54.04
FeO	27.90		23.82	13.82	13.62
MnO	0.04		0.17	0.06	0.08
MgO	11.70		2.15	1.23	1.12
CaO	b.d.		b.d.	0.01	b.d.
Total	87.70		92.32	98.02	97.91
Si	5.32		2.06	2.06	2.07
Al^{IV}	2.68	Al	3.97	4.59	4.59
Al^{VI}	3.09				
Ti	0.01		0.00	0.01	0.02
Fe(ii)	4.96		1.64	0.83	0.82
Mn	0.01		0.01	0.00	0.00
Mg	3.71		0.26	0.13	0.12
Ca	0.00		0.00	0.00	0.00

Cations calculated on a 28-oxygen equivalents basis for chlorite, 12-oxygen equivalents basis for chloritoid and staurolite. b.d.= below detection limit.

Table 3-6. Representative garnet analyses.

	Garnet Zone		Staurolite Zone		Kyanite Zone		Sil-Kfs Zone	
	core	rim	core	rim	core	rim	core	rim
SiO_2	36.42	36.34	36.41	36.32	36.98	36.24	36.48	36.70
TiO_2	0.19	0.18	0.11	0.11	0.01	0.00	0.01	0.01
Al_2O_3	20.65	20.99	20.70	20.77	21.06	20.82	20.94	21.10
Fe_2O_3	1.34	0.09	0.51	1.12	0.89	0.85	0.00	0.00
FeO	24.98	36.17	31.63	35.66	28.56	28.56	29.77	32.21
MnO	10.64	1.76	7.21	2.11	6.31	5.28	7.16	4.99
MgO	0.83	1.77	1.30	2.08	2.84	2.77	2.50	2.54
CaO	5.07	1.95	1.86	1.58	3.34	1.60	2.14	2.15
Total	99.99	99.23	99.67	99.64	99.40	99.24	99.00	99.70
Si	2.97	2.97	2.98	2.97	3.01	2.98	3.00	2.99
Al^{IV}	0.03	0.03	0.02	0.03	0.00	0.02	0.00	0.01
Al^{VI}	1.95	2.00	1.98	1.97	2.02	2.00	2.03	2.02
Fe^{3+}	0.08	0.01	0.03	0.07	0.00	0.04	0.00	0.00
Ti	0.01	0.01	0.01	0.01	0.00	0.00	0.00	0.00
Fe^{2+}	1.70	2.48	2.17	2.44	1.96	2.20	2.05	2.20
Mn	0.73	0.12	0.50	0.15	0.35	0.30	0.41	0.28
Mg	0.10	0.22	0.16	0.25	0.34	0.34	0.31	0.31
Ca	0.44	0.17	0.16	0.14	0.29	0.14	0.19	0.19
X_{Alm}	0.57	0.83	0.72	0.82	0.66	0.74	0.69	0.74
X_{Prp}	0.03	0.07	0.05	0.09	0.12	0.11	0.10	0.10
X_{Grs}	0.15	0.06	0.05	0.05	0.10	0.05	0.06	0.06
X_{Sps}	0.25	0.04	0.17	0.05	0.12	0.10	0.14	0.09
Mg#	0.06	0.08	0.07	0.09	0.15	0.13	0.13	0.12

Cations calculated on a 12-oxygen basis. X_{Alm} = Fe(II)/(Fe(II)+Mn+Mg+Ca), X_{Grs} = Ca/(Fe(II)+Mn+Mg+Ca), X_{Sps} = Mn/(Fe(II)+Mn+Mg+Ca), X_{Prp} = Mg/(Fe(II)+Mn+Mg+Ca), Mg# = Mg/(Fe(II)+Mg)

Chapter 4: Phase Equilibria Modeling and Pressure–Temperature Estimation

The use of pressure and temperature (*P–T*) pseudosections (equilibrium phase diagrams for a fixed chemical composition) to evaluate the stability of mineral assemblages, the evolution from one assemblage to another, and the *P–T* conditions recorded by mineral core compositions is common (e.g., Johnson et al., 2003; Johnson & Brown, 2004). In this study, the average *P–T* method (Powell & Holland, 1988; Powell & Holland, 1994) was used to estimate the peak *P–T* conditions recorded by garnet rims and matrix minerals. *P–T* pseudosections and garnet composition isopleths were constructed in the MnNCKFMASHTO system to evaluate the stability and evolution of mineral assemblages as well as the *P–T* conditions recorded by garnet core compositions.

4.1 Average P–T Estimation

The *P–T* conditions recorded by minerals in equilibrium assemblages in samples from the garnet (05403), staurolite (05501), kyanite (077401) and sillimanite–K-feldspar zones (07905) were estimated using the average *P–T* mode in THERMOCALC 3.26 (Powell & Holland, 1988; Powell & Holland, 1994) and the internally consistent thermodynamic dataset of Holland & Powell (1998; updated 11/22/2003). Mineral assemblages in the samples were described in chapter 3. Mineral compositions used for the average *P–T* calculations are listed in Appendix A and the average *P–T* results are presented in Table 4-1.

Table 4-1. Calculated average *P–T* results compared with the *P–T* results from Whitney et al. (1996a)

Zone	Assemblage	avT	sdT	avP	sdP	Cor	sigfit	Whitney et al. (1996a)	
		°C		kbar				T °C	P_{GPBM}
Garnet	Ms 1†	570	12	5.2	0.8	0.55	0.83	435–470	2.1–3.0
	Ms 2†	576	18	5.6	1.1	0.52	1.48		
Staurolite	Ms 1‡	557	12	5.9	1.1	0.65	1.2	450–480	3.7–4.0
	Ms 2‡	557	12	5.9	1.1	0.65	1.2		
Kyanite	Grt core	603	28	7.1	1.1	0.77	0.51	450–500	3.5–5.2
	Grt rim	600	29	6.4	1.1	0.76	0.83	455–525	3.8–4.7
Sil-Kfs	Grt core	749	67	6.7	1.4	-0.14	0.31	c. 730	c. 5–6
	Grt rim	752	68	7.4	1.4	-0.11	0.64	c. 720	c. 5–6

† Ms 1: average of muscovite close to garnet, Ms 2: single analysis in vein, high SiO_2
‡ Ms 1: average of muscovite close to garnet, Ms 2: average of ms close to chloritoid
Abbreviations: av: average; sd: standard deviation; cor: correlation coefficient of average P and T; sigfit: sigma fit

The calculated average temperature of the mineral assemblages in the garnet, staurolite and kyanite zones are about 100 to 150 °C higher than those determined by Whitney et al. (1996a). The calculated temperature of the sillimanite–K-feldspar zone is similar to the result of Whitney et al. (1996a). The calculated average pressure of each zone is about 1 to 2 kbar higher than the results determined by Whitney et al. (1996a). The difference in *P–T* estimates could be due to the use of an internally-consistent thermodynamic dataset and a multi-equilibrium *P–T* method in this work (Powell & Holland, 1988; Holland & Powell, 1998) rather than the conventional thermobarometric methods used by Whitney et al. (1996a).

4.2 Phase Equilibria Modeling

The whole rock chemical compositions used in the construction of *P–T* pseudosections were obtained at the X-ray Laboratory of Franklin & Marshall College using XRF and iron titration methods described in Boyd & Mertzman (1987).

Aliquots of each sample were analyzed twice, independently, and the average composition was used for construction of pseudosections. This bulk composition was assumed to be the effective bulk composition during the initial stage of garnet nucleation. Bulk compositions of all samples are listed in Appendix E.

P–T pseudosections were constructed for samples from the garnet (05403), staurolite (05501), kyanite (077401, 077092) and sillimanite–K-feldspar zones (07905, 07908) in the model system including,MnO, Na_2O, CaO, K_2O, FeO, MgO, Al_2O_3, SiO_2, Fe_2O_3, TiO_2 and H_2O (MnNCKFMASHTO). Calculations were carried out using THERMOCALC v. 3.26 (Powell & Holland, 1988; Powell & Holland, 1994) and the internally consistent thermodynamic dataset of Holland & Powell (1998; ds55.txt, updated 11/22/2003). Quartz, plagioclase, muscovite, paragonite, chlorite, biotite, chloritoid, garnet, staurolite, kyanite, sillimanite, andalusite, potassium feldspar, ilmenite, magnetite, rutile, cordierite, clinozoisite, H_2O and melt (L) were considered in calculations. The activity–composition (*a–x*) model for garnet follows White et al. (2005), who combined the MnKFMASH *a-x* model of Mahar et al. (1997), the KFMASHTO *a–x* model of White et al. (2000) and the NCKFMASH *a–x* model of White et al. (2001) in a similar manner to Zeh & Holness (2003) but using a different Fe^{3+} endmember (khoharite versus andradite) and different W(alm-py) and W(py-spss) numbers (R.W. White, pers. comm., April, 2009). The *a–x* model for chlorite is a non order-disorder model involving a combination of the *a–x* model from Mahar et al. (1997) and the *a–x* model from Holland et al. (1998) as used in White et al. (2005; R.W. White, pers. comm., April, 2009). The *a–x* models for cordierite and staurolite involve a combination of the *a–x* models from Mahar et al. (1997) and the *a–x* models

from Holland et al. (1998) as used in White et al. (2005). The *a–x* model for chloritoid involves a combination of the *a–x* model from Maher et al. (1997) and the *a–x* model from White et al. (2000). The *a–x* models for the following phases are: biotite and ilmenite (from White et al., 2005), muscovite and paragonite (from Coggon & Holland, 2002), plagioclase and potassium feldspar (from Holland & Powell, 2003), magnetite (from White et al., 2002), and silicate melt (from White et al., 2007).

4.2.1 Garnet Zone

The *P–T* pseudosection constructed for sample 05403 is shown in Figure 4-1a. The equilibrium mineral assemblage, Chl + Ms + Bt + Grt + Pl + Qtz + Ilm, is stable over a *P–T* range of ~ 3–7 kbar and 500–590°C. The pseudosection is contoured with isopleths of almandine (X_{Alm}), spessartine (X_{Sps}) and grossular (X_{Grs}) components in garnet to investigate the *P–T* conditions at the initial stage of garnet growth recorded by garnet core compositions, and the possible *P–T* path recorded by garnet composition zoning. The average *P–T* result calculated from the garnet rim composition and matrix minerals is plotted as a 1σ uncertainty ellipse (see Powell & Holland, 1994 for definition).

The X_{Alm} isopleths in the Chl + Ms + Bt + Grt + Pl field are temperature-controlled and X_{Alm} increases with increasing temperature. The X_{Sps} isopleths generally follow the shape of the garnet-in line (pink solid line) and X_{Sps} decreases toward the higher *P–T* range. The X_{Grs} isopleths are linear within the field and X_{Grs} decreases toward high temperature and low pressure. Combined with the garnet

composition profiles (Figure 3-2), a prograde path of increasing temperature is predicted from the isopleths and garnet compositions.

The composition of the garnet core is X_{Alm} = 0.57, X_{Sps} = 0.25 and X_{Grs} = 0.15 (Table 3-6). However, the highest X_{Sps} in the garnet stability field is about 0.20, which is lower than the observed garnet core X_{Sps} value of 0.25. This inconsistency may be due to the bulk rock MnO concentration not being reflective of the MnO concentration of the chlorite and mica-bearing precursors, on which garnet most likely nucleated (e.g., Spear & Daniel, 2001; Hirsch et al., 2003). The pseudosection in Figure 4-1b was constructed by increasing the MnO concentration of the original composition (Figure 4-1a) from 0.17 wt.% to 0.24 wt.% and keeping all other elements the same. The topology of the two pseudosections is very similar except that the garnet-in line moves toward lower *P–T*. The *P–T* condition recorded by the garnet core, where the three isopleths intersect, is approximately 4.6 kbar and 520°C.

After initial growth of garnet cores, the garnet rims are assumed to be in equilibrium with the matrix minerals, whereas the interior is not in equilibrium. This process is recorded by the composition zoning in garnet (Figure 3-2). Due to this effect, the effective bulk composition during the growth of garnet was changing and different from the analyzed bulk composition. To obtain the effective bulk composition at peak *P–T* conditions, the components isolated within garnet have to be removed from the analyzed bulk composition. The method of removing the components that are sequestered in the interior of a monotonically-zoned garnet is described in Appendix B.

A representative garnet profile (Figure 3-2) was chosen to aid in the evaluation of the role of changing effective bulk composition. The interior of garnet (from the core to a position ~ 50 μm from the rim: B-B' in Figure 3-2) was removed from the bulk composition. The results of this modeling suggest that the effective MnO concentration in the rock was 0.08 wt.%. The bulk compositions used to construct the pseudosections in Figure 4-1 are listed in Table 4-2.

Table 4-2. Bulk rock compositions (mol. %) used for *P–T* pseudosection modeling.

	Original Composition Fig. 4-1a	High MnO Fig. 4-1b	Grt Fractioned Fig. 4-1c
SiO_2	70.22	70.22	70.75
Al_2O_3	13.39	13.39	13.37
Fe_2O_3	0.41	0.41	0.42
FeO	6.01	6.01	5.50
MnO	0.17	0.24	0.08
MgO	3.73	3.73	3.75
CaO	0.84	0.84	0.80
Na_2O	1.71	1.71	1.74
K_2O	2.67	2.67	2.73
TiO_2	0.85	0.85	0.86

The concentrations are on a LOI-free basis.

The stability field of the assemblage Chl + Ms + Bt + Grt + Pl in the pseudosection that models the garnet-fractioned system (Figure 4-1c) covers a smaller temperature range than the high-MnO pseudosection (Figure 4-1b). The garnet-in line and the entire equilibrium mineral assemblage field move toward higher pressure. The X_{Alm} isopleths increase first and then decrease as temperature increases (Figure 4-1c). The highest X_{Alm} isopleth (0.77) forms a closed shape in the fields Chl + Ms + Bt + Grt + Pl and Chl + Ms + Bt + Grt + Pl + St (Figure 4-1c), which is inside of the

average *P–T* ellipse. The X_{Sps} isopleths for the garnet rim composition (0.06–0.04) pass through the average *P–T* ellipse. Although the X_{Alm} and X_{Grs} isopleths for the garnet rim (X_{Alm} 0.81–0.83, X_{Grs} 0.07–0.06) do not intersect the equilibrium mineral assemblage field, the higher value for X_{Alm} (0.77) and the lower value for X_{Grs} (0.08) are close and additional adjustment of the effective bulk composition to obtain a better fit was deemed unnecessary.

The X_{Grs} of garnet (Figure 3-2) did not change significantly during most of the garnet growth from the core through the mantle (X_{Grs} 0.13–0.12). Therefore the *P–T* path should generally follow the 0.13–0.12 isopleths (represented by the grey band in Figure 4-1d) during this period of garnet growth until the shoulder of the mantle, where the garnet composition is X_{Sps} 0.18–0.19, X_{Alm} 0.64–0.65 and X_{Grs} 0.12–0.13 (stage 2 in Figure 3-2). At the rim, the X_{Grs} dropped to 0.10 in a distance of less than 100 μm, where the garnet composition is X_{Sps} 0.10, X_{Alm} 0.74 and X_{Grs} 0.10 (stage 3, Figure 3-2). Combining the isopleths, garnet composition and the average *P–T* result, a prograde *P–T* path is presented (Figure 4-1d). The garnet growth zoning records a temperature increase of about 50°C and a pressure increase of about 0.6 kbar from the

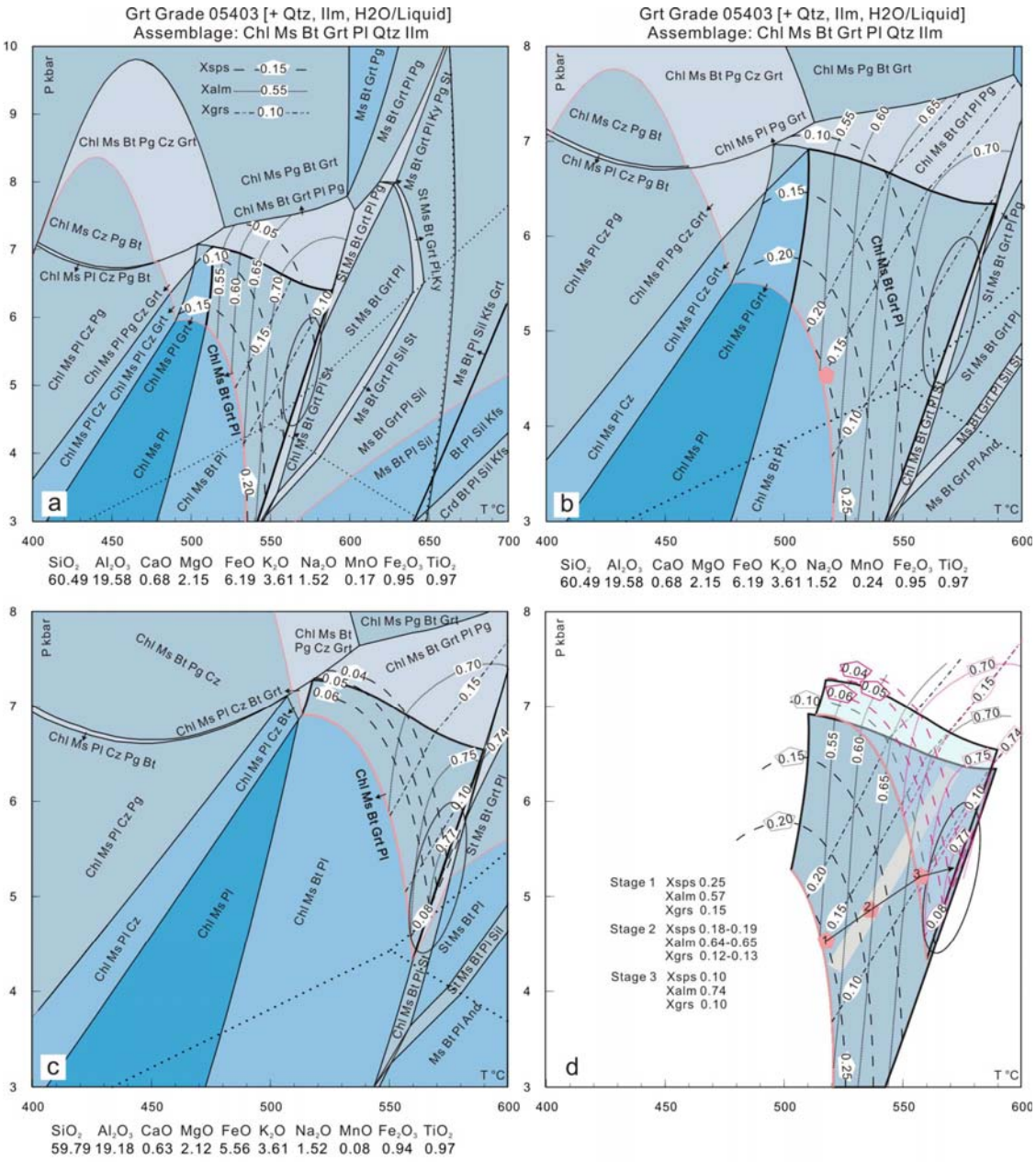

Figure 4-1. *P–T* pseudosections with garnet composition isopleths for sample 05403 in the MnNCKFMASHTO system. The equilibrium mineral assemblage is Chl + Ms + Bt + Grt + Pl + Qtz + Ilm (variance 5). The depth of shading reflects increased variance. Bulk compositions used in (**a**) is the original XRF analysis, in (**b**) is the high-MnO composition and in (**c**) is the garnet-fractioned composition. Bulk compositions in molar proportions are listed in Table 4-2. The stability field and garnet composition isopleths of (**b**) (isopleths shown in black lines) and (**c**) (isopleths shown in red lines) are compiled together in (**d**). The average *P–T* 1σ uncertainty ellipse is plotted in all four graphics. Mineral abbreviations follow Kretz (1983).

core to the rim. This result is different from the conclusion of Whitney et al. (1996a), who argued for a retrograde *P–T* path with decreasing pressure and temperature from the outer core to the rim.

4.2.2 Staurolite Zone

The *P–T* pseudosection constructed for sample 05501 is shown in Figure 4-2. The stability field of the equilibrium mineral assemblage, Chld + Bt + Ms + Pl + Grt + St + Qtz + Ilm, is so narrow in terms of temperature that it appears as a thick line in the pseudosection. The *P–T* range covered is ~ 4.3–6.8 kbar and 545–565°C. The calculated average *P–T* uncertainty ellipse encloses the upper part of the stability field.

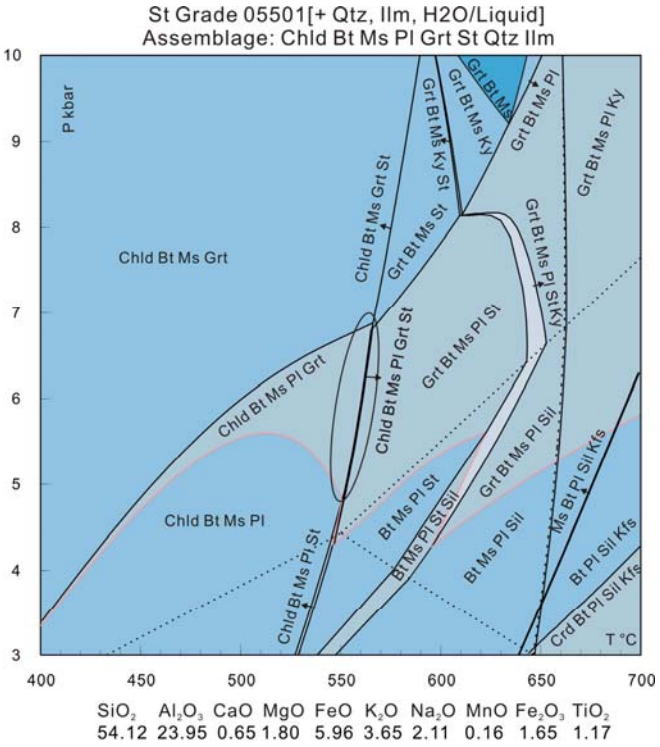

Figure 4-2. *P–T* pseudosection for sample 05501 in the MnNCKFMASHTO system. The mineral assemblage is Chld + Bt + Ms + Pl + Grt + St + Qtz + Ilm (variance 4). The garnet-in line is in pink. The average *P–T* uncertainty ellipse (1σ) is plotted. Mineral abbreviations follow Kretz (1983).

4.2.3 Kyanite Zone

Two samples with different mineral assemblages from the kyanite zone were selected for phase equilibria modeling with the purpose of constraining the *P–T* range by overlapping the stability fields of the two samples. Sample 077092 contains the assemblage Ms + Bt + Pl + Grt + St + Ky + Qtz + Ilm. Trace amounts of fibrolitic sillimanite are also observed. Sample 077401 contains the assemblage Ms + Grt + Bt + Pl + Qtz + Ilm.

The topology of the two pseudosections is very different (Figure 4-3). The stability field of the mineral assemblage of sample 077092 is ~ 5.5–6.9 kbar and 600–610°C. The pressure may be lower than 5.5 kbar given the presence of fibrolitic sillimanite. The stability field of the mineral assemblage of sample 077401 is ~ 4.8–10 kbar and 585–755°C, which is much larger than that of sample 077092. The intersection of the two stability fields is generally consistent with the average *P–T* result (1σ uncertainty), which is 6.4 ± 1.1 kbar and 600 ± 29°C (Figure 4-3c).

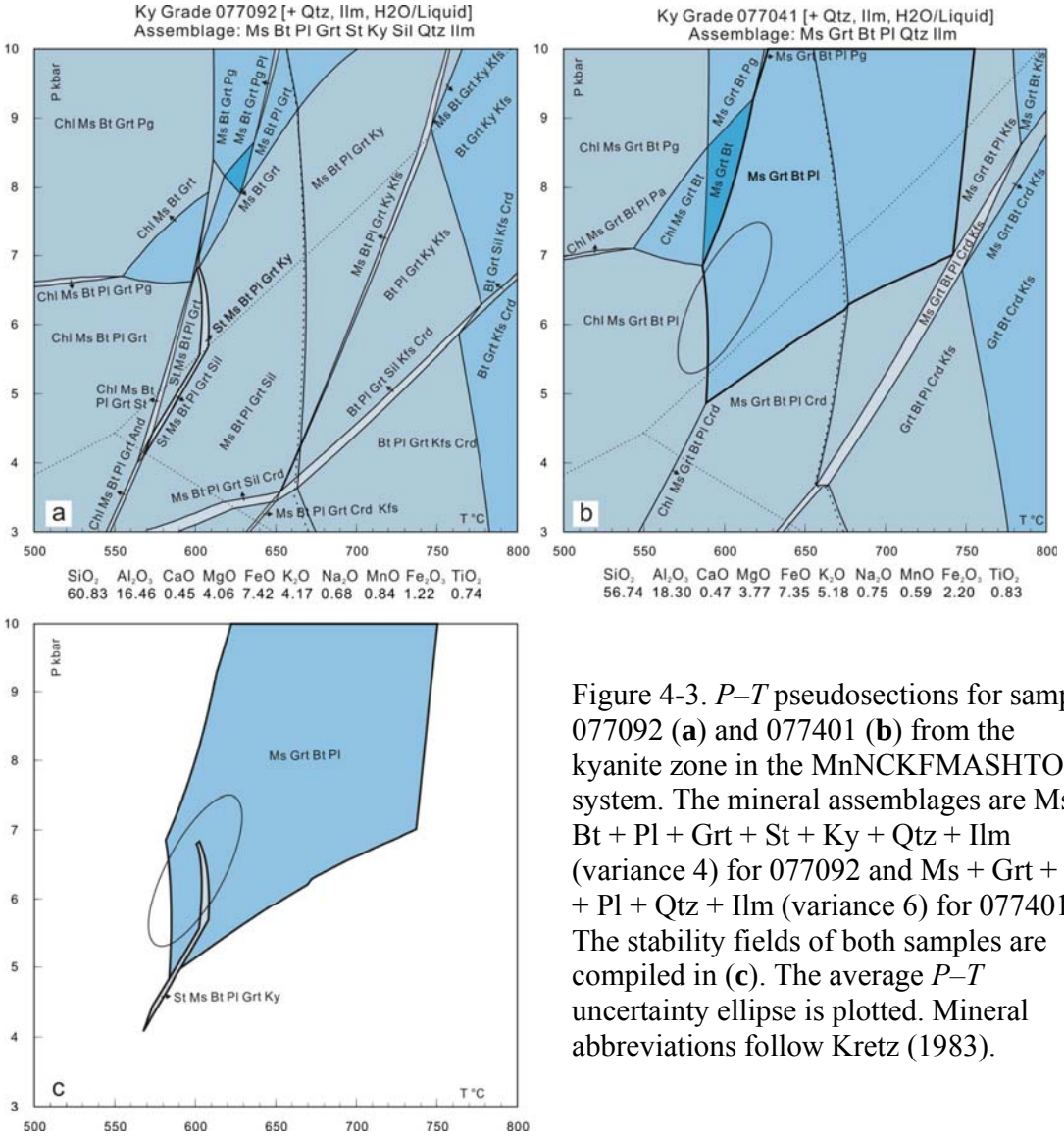

Figure 4-3. *P–T* pseudosections for sample 077092 (**a**) and 077401 (**b**) from the kyanite zone in the MnNCKFMASHTO system. The mineral assemblages are Ms + Bt + Pl + Grt + St + Ky + Qtz + Ilm (variance 4) for 077092 and Ms + Grt + Bt + Pl + Qtz + Ilm (variance 6) for 077401. The stability fields of both samples are compiled in (**c**). The average *P–T* uncertainty ellipse is plotted. Mineral abbreviations follow Kretz (1983).

4.2.4 Sillimanite–K-feldspar Zone

Two samples with the same mineral assemblage but different bulk compositions from the sillimanite–K-feldspar zone were selected for phase equilibria modeling. Both samples contain the assemblage Pl + Grt + Bt + Sil + Kfs + Qtz + Ilm. The stability fields of the equilibrium mineral assemblage in the two pseudosections are very different (Figure 4-4). The stability field of the equilibrium

mineral assemblage in sample 07905 is ~ 6.9–8.8 kbar and 730–750°C, whereas in sample 07908 it is ~ 5.8–10 kbar and 730–830°C. The average *P–T* uncertainty ellipse overlaps the intersection of the two stability fields (Figure 4-4c).

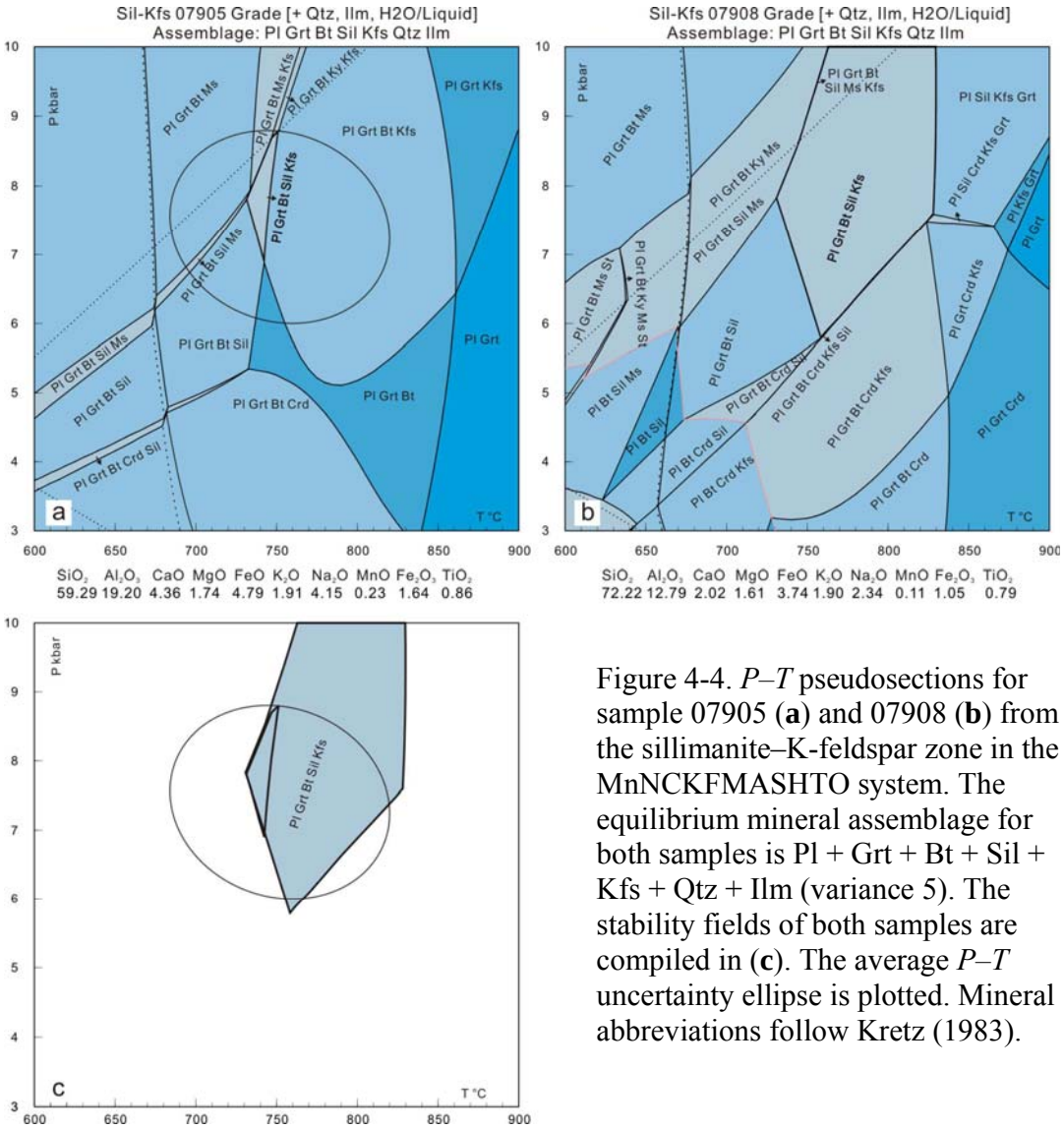

Figure 4-4. *P–T* pseudosections for sample 07905 (**a**) and 07908 (**b**) from the sillimanite–K-feldspar zone in the MnNCKFMASHTO system. The equilibrium mineral assemblage for both samples is Pl + Grt + Bt + Sil + Kfs + Qtz + Ilm (variance 5). The stability fields of both samples are compiled in (**c**). The average *P–T* uncertainty ellipse is plotted. Mineral abbreviations follow Kretz (1983).

4.3 Discussion

The stability fields and the average *P–T* results of all four zones are compiled in Figure 4-5. In general, the mineral assemblages in each successive zone from low to high grade record higher pressures and temperatures than the preceding zone. The

exception is the staurolite zone, in which the temperature is lower than the peak temperature of the garnet zone. This anomaly in the context of the Barrovian sequence may be a result of overstepping of prograde metamorphic reactions, a kinetic effect related to slow break down of refractory porphyroblasts, or a combination of both processes. Based on nucleation theory, considerable overstepping of an equilibrium boundary is required before rates of nucleation become significant even on a geological time scale (Rubie, 1998). The narrow stability field of the assemblage St + Ctd + Grt + Pl + Ms + Bt + Qtz + Ilm in sample 05501 could be overstepped easily before the chloritoid-consuming reaction began. In addition, the dissolution of compact porphyroblastic phases such as chloritoid is slow compared to the transformation of matrix sheet silicates (Waters & Lovegrove, 2002). Depending on the amount of overstepping and the kinetics of the chloritoid-consuming reaction, it may be that a significant portion of the original chloritoid became metastable in the St + Grt + Pl + Ms + Bt + Qtz + Ilm field. Thus, the temperature recorded by the current mineral assemblage may be lower than the peak temperature experienced by the rock along its *P–T* path.

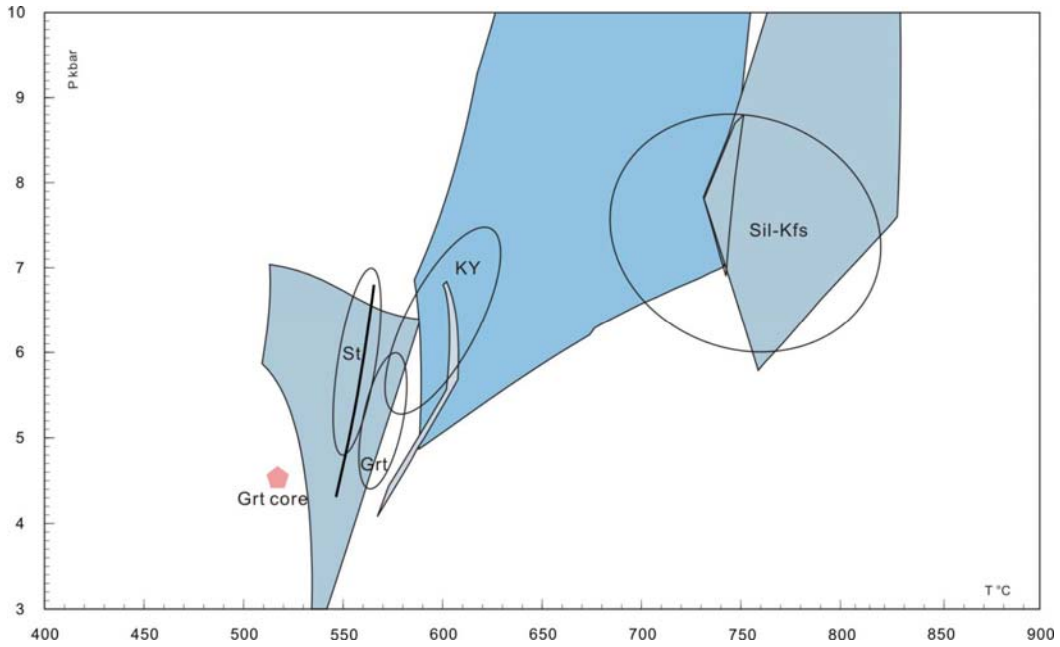

Figure 4-5. The *P–T* stability fields and the average *P–T* uncertainty ellipses of samples from the garnet, staurolite, kyanite and sillimanite–K-feldspar zones.

Chapter 5: Monazite Geochronology

This chapter will first introduce the analytical methods used to obtain monazite dates, followed by the statistical methods used to analyze monazite dates, the quality control of age data, and lastly the application of this protocol to samples from the garnet, staurolite, kyanite and sillimanite–K-feldspar zones.

5.1 Analytical Methods

The analytical techniques for chemical dating of monazite were originally proposed in the early 1990s (Suzuki et al., 1991) and improved during the past two decades (e.g., Pyle et al., 2005b; Jercinovic & Williams, 2005; Williams et al., 2006; Suzuki and Kato, 2008). The techniques are still in development with different analytical protocols used by different researchers (e.g., Pyle et al., 2005b; Williams et al., 2006; Suzuki and Kato, 2008). The protocol used at the University of Maryland is based on Pyle et al. (2005b) and was set up initially by Barry Reno and Dr. Philip Piccoli.

5.1.1 Monazite X-ray Mapping

Wavelength dispersive X-ray element composition maps and backscattered electron images of monazite were collected to identify compositional zoning in monazite. The JEOL JXA-8900 SuperProbe in the Nanoscale Imaging Spectroscopy and Properties Laboratory (NISP) at the University of Maryland was used to obtain the X-ray element composition maps and quantitative monazite compositions in the following section. An accelerating voltage of 15 kV and a cup current of 200 nA were used to collect X-ray maps of Th, U, Pb and Y, and backscattered electron images

simultaneously. Peak search and single channel analyzer (SCA) scans were conducted on natural monazite standards. A step size of 0.2–0.5 μm and a counting time of 200 ms were used. The step size was adjusted based on the size of the monazite, which is primarily a compromise between the collection time and the quality of an individual map.

5.1.2 Monazite Chemical Dating

Quantitative analysis of monazite was undertaken only after examining monazite X-ray element composition maps to distinguish different compositional domains.

The first step of each analytical session was to collect high-resolution wavelength dispersive (WD) scans on both reference and unknown monazites. The WD spectra regions containing Y on the TAP crystal and Pb, Th and U peaks on the PET crystals were scanned. These spectra were used to verify the background positions and identify peak and background interferences. It is generally not necessary to change the background positions appreciably between analytical sessions.

The second step was to set up the element and electron optic system (EOS) conditions. An accelerating voltage of 15 kV and a cup current of 200 nA were used for analysis. Th, U, Pb, Y, Ce, P, Si and Ca were analyzed simultaneously using four spectrometers. The X-ray line, crystal, peak position, background position, counting time, SCA settings and standards for each element are listed in Table 5-1. A peak search for each element (Table 5-1) was conducted on the relevant standard using the corresponding crystal. This was followed immediately by the SCA scan on the

appropriate channel. The SCA settings were adjusted to balance the counting rate and the width of the scan window. The pulse discriminators were set to the differential mode (DIFF) in order to filter out escape peaks that would interfere with element analysis and to filter out higher order reflections from other elements.

Table 5-1. Analytical conditions for EPMA dating of monazite.

Standard	Element	X-ray	Peak	Crystal	Back(+)	Back(-)	Peak (s)	Back (s)	Gain	High V	Base L	Window
$PbCO_3$	Pb	Ma	169.211	PETJ	4.7	2.8	240	120	64	1700	0.7	2.1
YPO_4	Y	La	69.916	TAP	1	1	30	15	32	1700	0.5	5.5
YPO_4	P	Ka	66.708	TAP	4	3	10	5	32	1700	0.5	5.5
UO_2	U	Mb	118.872	PETH	2.5	3	80	40	16	1700	0.5	1.5
$ThSiO_4$	Th	Ma	132.426	PETJ	2.5	3.5	80	40	8	1740	0.5	2.5
$ThSiO_4$	Si	Ka	77.310	TAP	5	1.5	100	50	32	1700	0.5	4.5
Grt-12442	Ca	Ka	107.446	PETJ	2.5	2.5	60	30	8	1650	0.5	1.5
$CePO_4$	Ce	La	82.047	PETJ	1.5	1.5	10	5	32	1700	0.5	2.7

The third step was to standardize each element. Standardization of Th and Si is carried out on $ThSiO_4$, Pb on $PbCO_3$, U on UO_2, Y and P on YPO_4 and Ca on garnet standard (12442/USGS GTAL). A 30 μm beam diameter (5 μm for other standards) is used for YPO_4, $CePO_4$ and $PbCO_3$ to reduce the possibility of sample destruction.

The last step was to quantitatively analyze monazite. Element (peak and background positions, count times etc.) and EOS conditions (accelerating voltage, current etc.) are the same as those of the standardization except that a 3–5 μm beam was used for all analysis. The average composition of other major elements in the reference monazite was used in the ZAF correction.

5.1.3 Monazite Date and Uncertainty Calculations

As was introduced in Chapter 1, monazite dates calculated from the oxide concentration in wt.% are based on the following equation:

$$\frac{PbO}{W_{PbO}} = \frac{ThO_2}{W_{ThO_2}} \cdot (e^{\lambda_{232}t} - 1) + \frac{UO_2}{W_{UO_2}} \cdot \frac{1}{138.88} \cdot (e^{\lambda_{235}t} - 1) + \frac{UO_2}{W_{UO_2}} \cdot \frac{137.88}{138.88} \cdot (e^{\lambda_{238}t} - 1)$$, where W_i refers to the molecular weight of i (i = PbO, UO_2, ThO_2). Y and Th interference on Pb and Th interference on U are corrected according to the method of Pyle et al. (2005b). The uncertainty on an individual date is obtained by propagating the uncertainty on each element through the following equation:

$$\sigma_t = \sqrt{\frac{\sigma_{Pb}^2 - \left(\frac{Ma_{Pb208}}{Ma_{Th232}} \cdot e^{\lambda_{Th232}t} - \frac{Ma_{Pb208}}{Ma_{Th232}}\right)^2 \cdot (\sigma_{Th}^2) - \left[\left(\frac{Ma_{Pb206}}{Ma_{U238}} \cdot \frac{137.88}{138.88} \cdot e^{\lambda_{U238}t} - \frac{Ma_{Pb206}}{Ma_U} \cdot \frac{137.88}{138.88}\right) + \left(\frac{Ma_{Pb207}}{Ma_U} \cdot \left(1 - \frac{137.88}{138.88}\right) \cdot e^{\lambda_{U235}t} - \frac{Ma_{Pb207}}{Ma_U} \cdot \left(1 - \frac{137.88}{138.88}\right)\right)\right]^2 \cdot (\sigma_U^2)}{\left(\frac{Ma_{Pb208}}{Ma_{Th232}} \cdot e^{\lambda_{Th232}t} \cdot Th \cdot \lambda_{Th232} + \frac{Ma_{Pb206}}{Ma_U} \cdot \frac{137.88}{138.88} \cdot e^{\lambda_{U238}t} \cdot U \cdot \lambda_{U238} + \frac{Ma_{Pb207}}{Ma_U} \cdot \left(1 - \frac{137.88}{138.88}\right) \cdot e^{\lambda_{U235}t} \cdot U \cdot \lambda_{U235}\right)^2}}$$

where Ma is the atomic mass of the isotope or element shown in the subscript, λ is the decay constant of the corresponding isotope shown in the subscript, σ^2 is the variance of element concentrations and Th and U are concentrations of the elements. A program written in C code by Barry Reno was used to calculate the date and uncertainty of monazite.

5.2 Statistical Analysis of Monazite Ages

One disadvantage of the chemical dating method is the relatively large uncertainty related to an individual monazite date. However, the small sampling volume (3–5 μm beam diameter) allows for a relatively large number of analyses, which can be used to reduce the uncertainty on an age. Analyses are assumed to follow a normal distribution if they sample one single age domain, which formed

during one single metamorphic event. A normality test of the monazite data set is necessary because normality is critical in many statistical methods (e.g., analysis of variance). When this assumption is violated, interpretation may not be valid. In addition, a non-normal distribution may indicate mixing of samples from different age domains. Therefore, the first step in the statistical analysis is to evaluate the normality of monazite age data using both graphical and numerical methods. Comparison of ages from different populations is commonly required in geochronology studies. The second step in the statistical analysis is to compare the mean of different populations using the one-way analysis of variance (ANOVA) method. The third step is to quantify the mean and variance of a sample.

5.2.1 Normality Test

The methods of testing normality can be classified into graphical methods and numerical methods. Graphical methods display the distributions of random variables or differences between an empirical distribution and a theoretical distribution, whereas numerical methods conduct statistical tests of normality or present summary statistics (Park, 2006). Graphical methods are easy to visualize, whereas numerical methods are more objective. In this thesis, the box-and-whisker plot (Tukey, 1977; Helsel, 1989) is used as a graphical method and the Shapiro-Wilk test (Shapiro & Wilk, 1965) is used as a numerical method to test the normality of monazite age data.

Box-and-Whisker Plot

A box-and-whisker plot (also referred as boxplot) consists of a center line (the median) splitting a box defined by the first quartile and the third quartile of the data set (Tukey, 1977; e.g., Figure 5-1). Whiskers are lines drawn from the end of the box

to the last observation within 1.5 times of the length of the box (Helsel, 1989). Data that lie beyond the whiskers are plotted individually. The mean is plotted as a diamond symbol in this thesis. Boxplots can be used to graphically summarize the distribution of data sets. If normally distributed, the first quartile and third quartile are symmetric about the median and the median and mean are located at the same position. Boxplots can also be used to graphically compare multiple data sets.

Shapiro-Wilk Normality Test

The Shapiro-Wilk normality test is an analysis of variance test for normality developed by Shapiro & Wilk (1965). The original test was designed for a sample size of [3, 50], and was extended to large samples up to 2000 (Royston, 1982a; 1982b). The W test statistic is defined by $W = \frac{(\sum_{i=1}^{n} a_i y_i)^2}{\sum_{i=1}^{n} (y_i - \bar{y})^2}$,

where $a' = (a_1, ..., a_n) = \frac{m'V^{-1}}{(m'V^{-1}V^{-1}m)^{1/2}}$, $m' = (m_1, ..., m_n)$ is the vector of expected values of standard normal order statistics, V is the corresponding $n \times n$ covariance matrix, $y' = (y_1, ..., y_n)$ denotes a vector of ordered random observations, and $\bar{y}$ is the sample mean. The W test can be computed in statistical software like SAS, STATA and SPSS. SPSS 16.0 was used to compute most of the statistical analyses in this thesis. SPSS presents the value of the W statistic, degree of freedom (df) and the p-value (Sig.). A p-value of greater than 0.05 indicates normal distribution at the 95% confidence level.

5.2.2 Data Comparison

Boxplots can give an intuitive comparison of multiple data sets. However, this graphical method does not provide objective criterion to determine if the variables follow the same distribution. Interpretations are, to some extent, a matter of judgment. Therefore, the Levene test (Levene, 1960) and the one-way analysis of variance (one-way ANOVA) method are introduced to compare normally distributed data sets.

A normal distribution, N (μ, σ^2), is uniquely determined by its mean and variance. Two variables follow the same normal distribution if and only if they have the same mean and variance. The Levene test is an inferential statistical tool used to assess the equality of variance (also called homogeneity of variance) in different samples, which is required for some statistical tests like the ANOVA method and the t-test. The Levene test does not require a normal distribution of data sets. The test computed in SPSS presents the F value and the p-value. If the F value is small and the p-value is greater than 0.05, the variances are homogeneous at the 95% confidence level.

The one-way ANOVA method is used to test whether several means are equal across one variable. It assumes normality, equal variance, and independent observations of the data sets. Among the results presented by SPSS, the degrees of freedom in and between groups, the F value and the p-value are of interest. Again, if the p-value is greater than 0.05, the means are equal, otherwise, they are not all equal. If more than two data sets are tested, the post-hoc tests option is selected to examine individual mean differences.

5.2.3 Estimation of the Mean Age

For a normally distributed random variable $X \sim N(\mu, \sigma^2)$, the sample mean $\bar{X}$ and sample variance S^2 are unbiased estimators of μ and σ^2, respectively. The sample mean $\bar{X}$ follows the normal distribution $N(\mu, \sigma^2/n)$, where n is the sample size. Therefore, we can constrain the sample mean to a range of certain confidence levels (e.g., 95%) based on the sample mean and standard error of a normally distributed random sample. However, this classical statistical method has poor performance on samples with outliers. Robust statistics are designed to account for outliers and other small departures from model distribution. The hyperbolic tangent estimators or the tanh-estimators, were developed and proved to be optimally robust (Hampel et al., 1981). Powell et al. (2002) introduced the tanh estimators to improve isochron calculations and Kelsey et al. (2003) applied this method to calculate the mean of monazite chemical ages.

Powell et al. (2002) proposed that the bootstrap method should be used to calculate age uncertainties, which is a resampling procedure with replacement. A percentile-bootstrap confidence interval of the mean is calculated by choosing n samples randomly with replacement from a data set, calculating the mean ($\bar{X}$), and repeating this process m times. In the m ordered values of $\bar{X}$, the $.025^{th}$ and $.975^{th}$ percentiles give the 95% confidence interval of the sample mean $\bar{X}$.

The sample mean and 95% confidence interval will be calculated using the tanh estimator and bootstrap methods proposed by Powell et al. (2002).

5.3 Quality Control of Analysis

The precision and accuracy related to the electron probe microanalysis was monitored by analyzing reference monazites of known age (Trebilcock and GSC-8153). Trebilcock monazite has a $^{235}U/^{207}Pb$ age of 272±2 Ma, and a $^{238}U/^{206}Pb$ age of ca. 279 Ma (Tomascak et al., 1996). There is no available $^{232}Th/^{208}Pb$ age. Chemical ages of ca. 280 Ma have been reported (Pyle et al., 2005b). The GSC-8153 monazite has a $^{232}Th/^{208}Pb$ age of 501±11 Ma, a $^{238}U/^{206}Pb$ age of 505±2 Ma and a $^{235}U/^{207}Pb$ age of 494±9 Ma (Reno et al., in review). Monazite EPMA ages of these standards from different analytical sessions are presented in Table 5-2 and Figure 5-1.

The uncertainty related to locating analytical points on monazite X-ray element composition maps and sampling other minerals is monitored by the chemical composition, especially the SiO_2 concentration. The SiO_2 concentration is ~2.4 wt% for Trebilcock monazite, ~1.4 wt% for GSC-8153, and usually less than 1 wt% for metamorphic monazite from the samples of this study. A higher SiO_2 concentration may indicate sampling of silicate minerals. Analyses with SiO_2 concentration higher than 2.4 wt% are removed from the dataset. Representative monazite analyses and calculated dates and uncertainties are listed in Appendix F.

Table 5-2. Monazite ages of Trebilcock and GSC-8153 from different analytical sessions.

	Trebilcock			GSC-8153		
Date	Mean	2 sd.	# Analysis	Mean	2 sd.	# Analysis
4/4/2007	275.8	1.1	24			
4/12/2007	276.0	1.7	18	508.7	4.5	18
5/24/2007	274.0	2.5	12	508.4	2.1	33
3/14/2008	277.5	1.4	36	506.7	2.4	38
3/3/2009	274.6	1.1	55	509.7	2.3	43

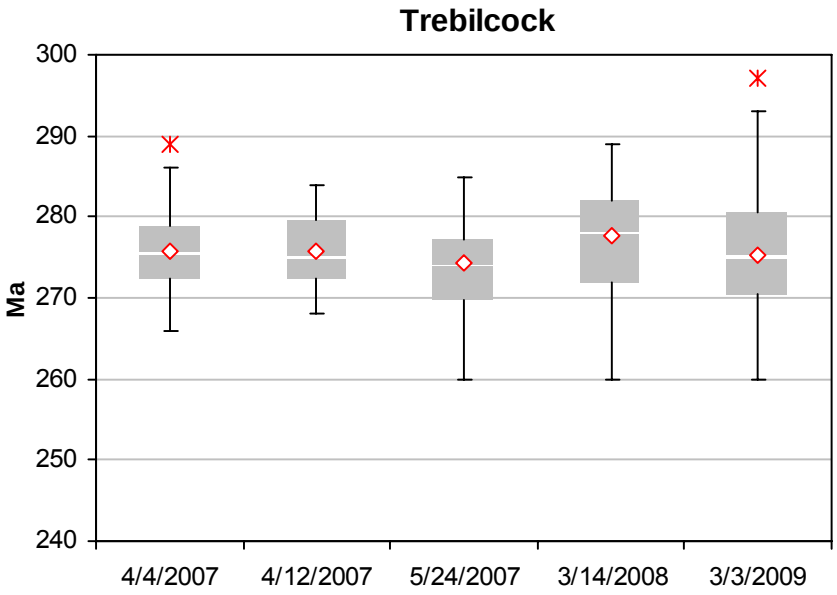

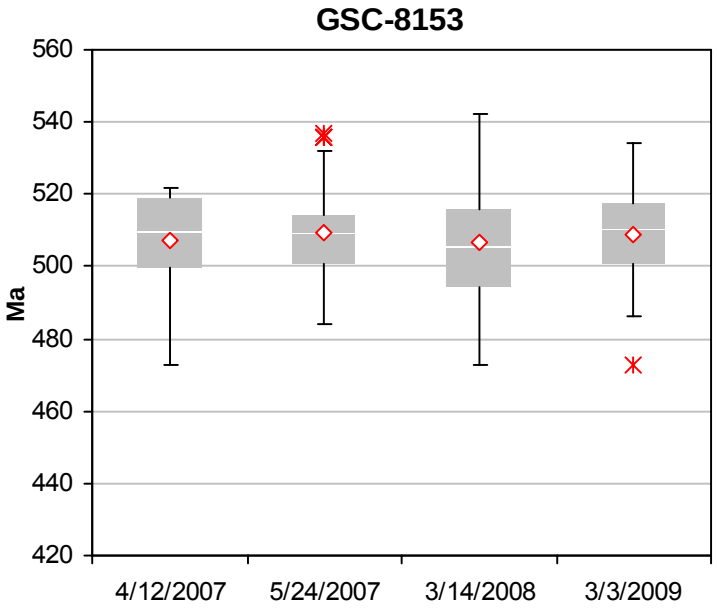

Figure 5-1. Boxplots of Trebilcock (a) and GSC-8153 (b) monazite ages from different analytical sessions. The diamond is the mean and the stars are outliers.

5.4 Applications

5.4.1 Monazite Geochronology

Monazite in sample DC-94-2c and 07310 from the garnet zone does not show compositional zoning in X-ray element composition maps (Figure 5-2). Monazite was not found within garnet in sample 07310 but a limited number of small-sized grains (~ 10 μm) were identified in DC-94-2c. Data were classified into "in garnet" and "in matrix" groups. The p-values of the normality test, homogeneity of variances test and the ANOVA of the two groups from sample DC-94-2c are all greater than 0.05 (Table 5-3, 5-4, 5-5), therefore, they were grouped together to obtain the tanh age and bootstrap uncertainty. The ages from sample DC-94-2c and 07310 are 453±10 Ma and 455±6 Ma, respectively (Table 5-6).

Monazite in sample 05501 from the staurolite zone occurs both within garnet and in the matrix. Monazite within garnet does not show compositional zoning in X-ray element composition maps, whereas those in the matrix show high-Th cores and low-Th rims (Figure 5-2). The p-values of the normality test, homogeneity of variances test and the ANOVA of the two groups from the high-Th cores and low-Th rims are all greater than 0.05 (Table 5-3, 5-4, 5-5), therefore, they were grouped together to obtain the tanh age and bootstrap uncertainty. The ages of monazite within garnet and those in the matrix are 451±9 Ma and 438±8 Ma, respectively (Table 5-6).

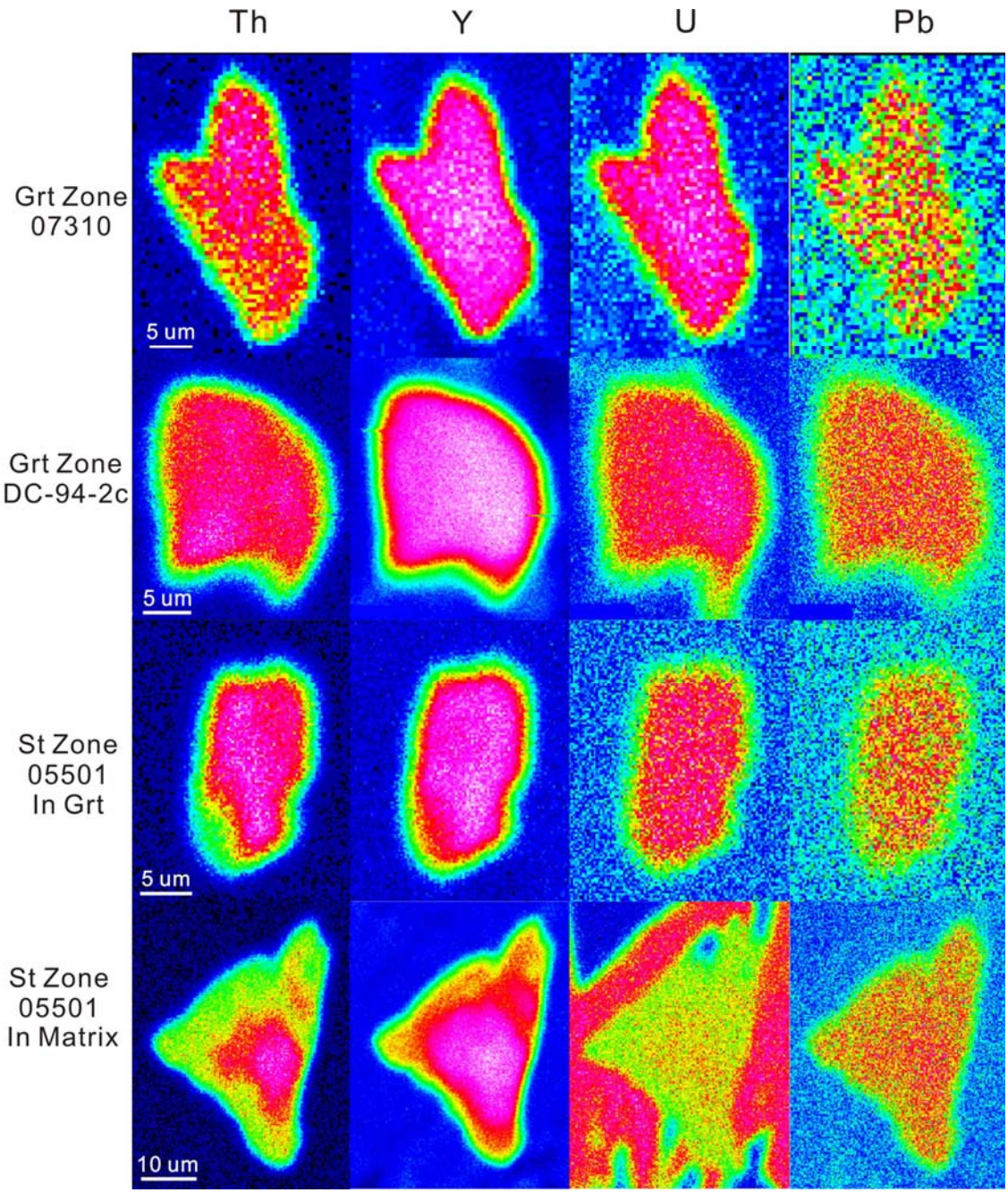

Figure 5-2. Representative monazite X-ray element composition maps of Th, Y, U and Pb from the garnet and staurolite zones.

Monazite in sample DC-94-12 and 077401 from the kyanite zone occurs both within garnet and in the matrix. However, those within garnet are small in size (5–10 μm) and the limited number of analyses show high SiO_2 concentration, which may

indicate sampling of garnet. Therefore, no mean age was obtained from monazite within garnet. Matrix monazite in sample DC-94-12 does not show clear core and rim distinction and the ages are strictly normal with a p-value of 0.999 (Table 5-3). Therefore they are interpreted to belong to one age domain. Monazite in sample 077401 has medium-Y cores, high-Y rims and low-Y overgrowths (Figure 5-3). The low-Y overgrowth is limited to a few grains and generally too small to obtain multiple analyses. Data from the cores are normally distributed, whereas those from the rims are skewed to the younger ages (Table 5-3, 5-4, 5-5, Figure 5-4). The non-normal distribution of data from the rims may indicate sampling of multiple age domains. Comparison of the two groups using statistical tests is not performed because the violation of normal distribution, however, the majority of the data overlaps in the boxplot (Figure 5-4). The tanh age and bootstrap uncertainty for sample DC-94-12 and the core and rim domains of sample 077401 are 478±6 Ma, 431±4 Ma and 425±8 Ma, respectively (Table 5-6).

Monazite in sample 059C1 and 07905 from the sillimanite-K-feldspar zone occurs both within garnet and in the matrix. Sample 07905 is about 4 km east of sample 059C1. The p-values of the normality test, homogeneity of variances test and the ANOVA of monazite ages from the “in garnet” and “in matrix” groups from sample 059C1 are all greater than 0.05 (Table 5-3, 5-4, 5-5), therefore, they were grouped together to obtain the tanh age and bootstrap uncertainty. Monazite in the garnet rim of sample 07905 shows a high-Th core and a low-Th rim (Figure 5-3). Cracks in garnet pass through the monazite grain. Statistical tests indicates that ages from the core and rim domains are indistinguishable from each other (Table 5-3, 5-4,

5-5), therefore, they were grouped together to obtain the tanh age and bootstrap uncertainty. Monazite in the matrix from sample 07905 shows low-Th cores and high-Th rims (Figure 5-3). Ages from these two groups are both normally distributed with common variance, but the ANOVA analysis shows that they are different ages (Table 5-5). The ages from monazite within garnet, in the matrix core and rim domains of sample 07905 are 507±6 Ma, 533±7 Ma and 506±4 Ma, respectively (Table 5-6). The age of monazite in sample 059C1 is 472±5 Ma.

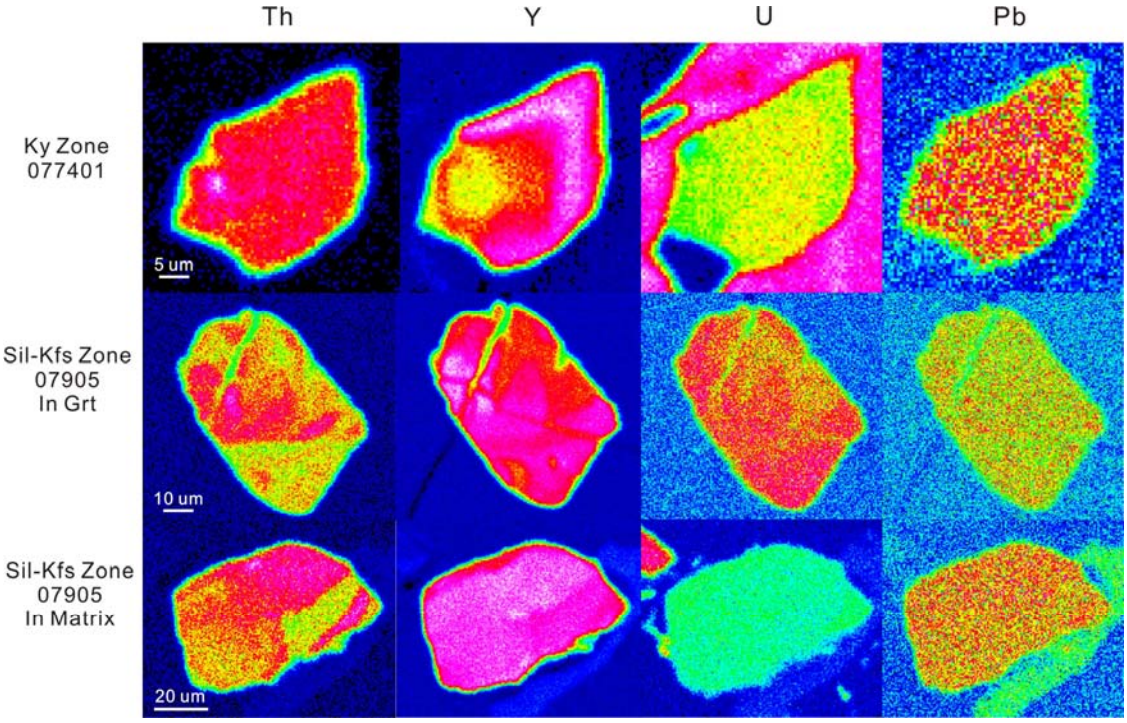

Figure 5-3. Representative monazite X-ray element composition maps of Th, Y, U and Pb from the kyanite and sillimanite-K-feldspar zones.

Boxplots of monazite dates from each sample are shown in Figure 5-4. A summary plot of the means and uncertainties of each sample is shown in Figure 5-5. The ages are classified into five groups: the 533±7 Ma age from the sillimanite-K-feldspar zone, the 507±6 and 506±4 Ma ages from the sillimanite-K-feldspar zone,

the 472±5 Ma age from the sillimanite-K-feldspar zone and the 478±6 Ma age from the kyanite zone, the 455±6, 453±10 and 451±9 Ma ages from the staurolite and garnet zones, and the 438±8, 431±4 and 425±8 Ma ages from the kyanite and staurolite zones.

Table 5-3. Results of the normality tests.

Shapiro-Wilk Tests of Normality					
Zone	Sample	Location	W	df	p-value
Grt	DC-94-2c	In Grt	0.928	8	0.502
Grt	DC-94-2c	In Matrix	0.956	14	0.656
St	05501	Core	0.945	12	0.563
St	05501	Rim	0.955	14	0.638
Ky	DC-94-12	In Matrix	0.991	19	0.999
Ky	077401	Core	0.952	26	0.258
Ky	077401	Rim	0.836	18	0.005
Sil-Kfs	059C1	In Grt	0.972	24	0.727
Sil-Kfs	059C1	In Matrix	0.937	18	0.26
Sil-Kfs	07905	In-Grt Core	0.964	11	0.819
Sil-Kfs	07905	In-Grt Rim	0.954	32	0.187
Sil-Kfs	07905	In-Matrix Core	0.972	10	0.905
Sil-Kfs	07905	In-Matrix Rim	0.965	52	0.135

df: degree of freedom

Table 5-4. Results of the homogeneity of variances tests.

Test of Homogeneity of Variances						
Zone	Sample	Location	F	df1	df2	p-value
Grt	DC-94-2c	Grt+Matrix	0.227	1	20	0.639
St	05501	Core+Rim	0.155	1	24	0.225
Sil-Kfs	059C1	Grt+Matrix	0.405	1	40	0.528
Sil-Kfs	07905	In-Grt Core+Rim	0.010	1	41	0.921
Sil-Kfs	07905	In-Matrix Core+Rim	2.87	1	60	0.096

df1: degree of freedom between groups
df2: degree of freedom within groups

Table 5-5. Results of the ANOVA.

Zone	Sample	Location	F	df1	df2	df3	p-value
Grt	DC-94-2c	Grt + Matrix	1.89	1	20	21	0.184
St	05501	Core + Rim	0.318	1	24	25	0.578
Sil-Kfs	059C1	Grt + Matrix	2.81	1	40	41	0.101
Sil-Kfs	07905	In-Grt Core + Rim	1.48	1	41	42	0.231
Sil-Kfs	07905	In-Matrix Core + Rim	0.647	1	60	61	0.014

df1: degree of freedom between groups
df2: degree of freedom within groups
df3: degree of freedom in total

Table 5-6. The tanh ages and bootstrap uncertainties.

Zone	Sample	Location	Age	2 sd	# Data
Grt	DC-94-2c	Grt + Matrix	453	10	22
Grt	07310	In Matrix	455	6	33
St	05501	In Grt	451	9	15
St	05501	In Matrix	438	8	26
Ky	077401	Core	431	4	26
Ky	077401	Rim	425	8	18
Ky	DC-94-12	In Matrix	478	6	19
Sil-Kfs	059C1	Grt + Matrix	472	5	42
Sil-Kfs	07905	In Grt	507	6	43
Sil-Kfs	07905	In-Matrix Rim	506	4	52
Sil-Kfs	07905	In-Matrix Core	533	7	10

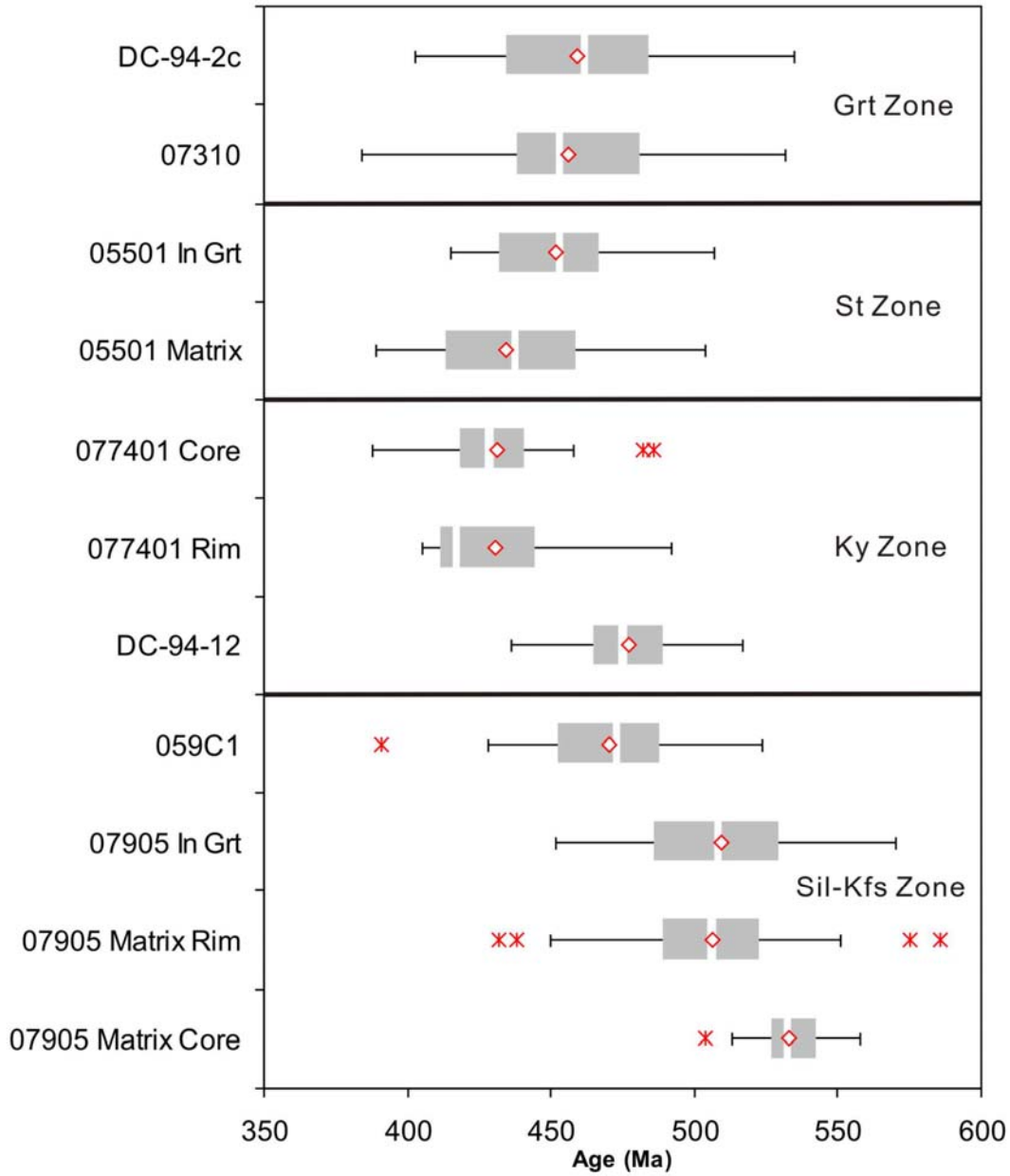

Figure 5-4. Boxplots of monazite ages from the garnet, staurolite, kyanite and sillimanite-K-feldspar zones. The diamond is the mean and the stars are outliers.

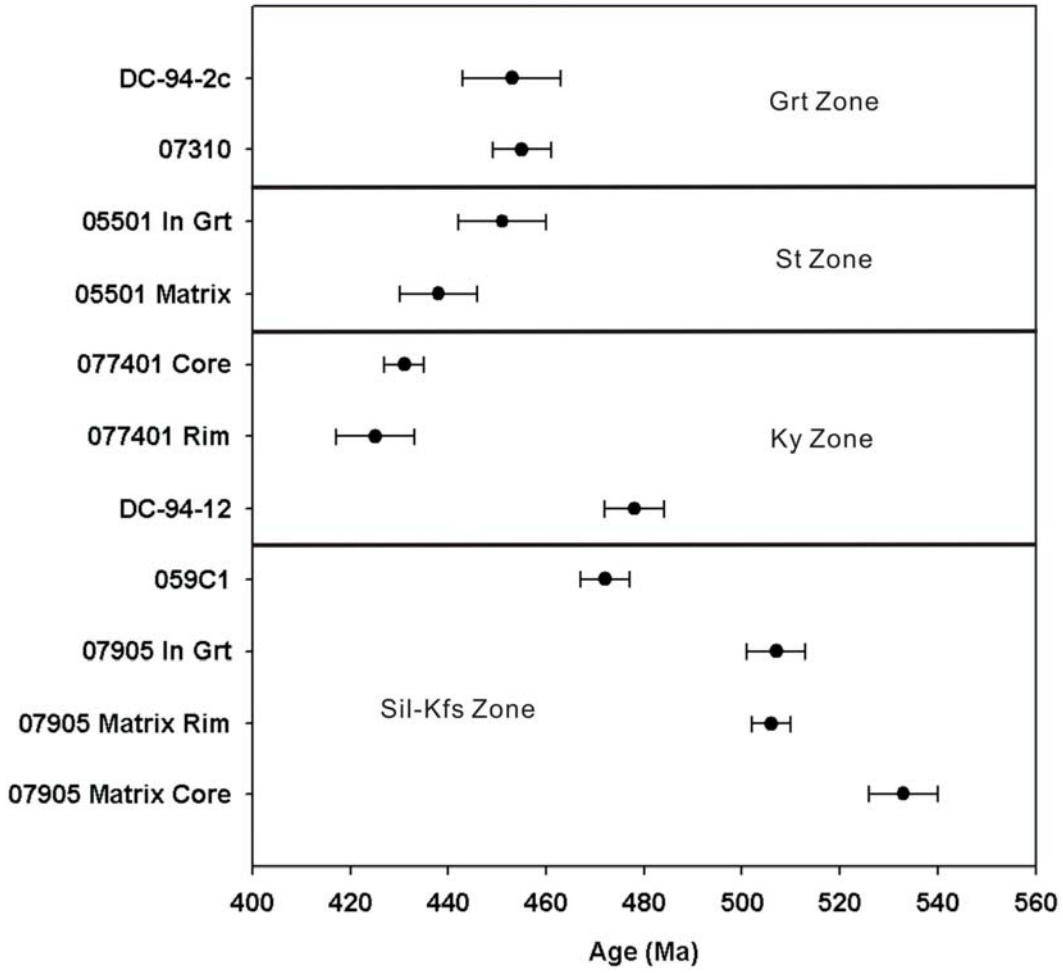

Figure 5-5. Summary of monazite ages from the garnet, staurolite, kyanite and sillimanite-K-feldspar zones. Error bars represent 95% bootstrap confidence intervals.

5.4.2 Interpretation and Discussion

Geochronological data relating to the age of metamorphism in the research area has been reported by Long (1962) and Bence & McLelland (1976). Long (1962) interpreted the ca. 430 Ma Rb-Sr muscovite and whole rock age as the minimum age of a metamorphic event, and proposed that this had been followed by a regional

thermal event at ca. 360–350 Ma (based on K-Ar and Rb-Sr biotite and muscovite ages). Bence & McLelland (1976) obtained $^{40}Ar/^{39}Ar$ biotite and muscovite ages from ca. 435 to 370 Ma and interpreted them as cooling ages from the Taconic Orogeny due to continuous loss of argon during exhumation. The deposition age of the Walloomsac Formation in the study area (Figure 2-1) is determined to be 460–455 Ma based on the occurrence of graptolites in the same formation in New York and Vermont (Hames et al., 1991, and references therein). One geochronological study in Massachusetts (northeast of Dutchess County) reported an $^{40}Ar/^{39}Ar$ hornblende age of ca. 445 Ma from the staurolite zone (Hames et al., 1991), whereas another study in the same area reported an $^{40}Ar/^{39}Ar$ cooling age of 466±5 Ma, and interpreted this to be the best estimate for the Taconic metamorphic peak (Sutter et al., 1985).

The Barrovian sequence in the study area has been ascribed to the Taconic metamorphism (Drake et al., 1989), but may be overprinted by the later Acadian metamorphism in the east (Hames et al., 1991). However, these studies are based on $^{40}Ar/^{39}Ar$ or K-Ar cooling ages other than ages from monazite or zircon that have higher closure temperature and might more closely date the age of metamorphism. Therefore, the monazite ages of this study provide new age constraints on the Taconic thermal peak, and allow a better understanding of the tectonic evolution of the southwestern sector of the Northern Appalachians. The monazite ages will be discussed in detail in the following sections.

The 533±7 Ma Age

The 533±7 Ma monazite core age in sample 07905 from the sillimanite-K-feldspar zone is unusual in the New England Appalachians. Similar ages have been

reported from the Waterbury Dome in Connecticut (535–525 Ma monazite age; Dietsch & Jercinovic, 2005). In the Southern Appalachians in Virginia and North Carolina, Early Cambrian ages of ca. 530 Ma were obtained from monazite and interpreted to be peri-Gondwanan in origin (Hibbard et al., 2003). Although rare in the Northern Appalachians, the occurrence of Early Cambrian ages from Dutchess County (this study) and Waterbury Dome (Dietsch & Jercinovic, 2005) may indicate an Early Cambrian thermal event in the formation of the Northern Appalachians that has not been previously widely identified or fully characterized. Further research on the petrographic relationships between the mafic dikes and the schist, the structural contact, and the ages of the dikes, pegmatite and schist are necessary to better understand this event.

The 507±6 and 506±4 Ma Ages

In the Northern Appalachians, similar ages were reported from the Baie Verte Oceanic Tract in the Notre Dame Subzone in Newfoundland (507–490 Ma; van Staal, 2005), the Moretown and Cram Hill Formations in Vermont (502±4 Ma; Ratcliffe, 2006) and the Waterbury Dome in Connecticut (508–507 Ma; Dietsch & Jercinovic, 2005). Sample 07905 is located in the Rowe-Moretown zone on the geological map of Karabinos et al. (2008). The Rowe-Moretown zone in New England is the equivalent of the Notre Dame Subzone in New Foundland (van Staal et al., 1998). These Middle to Late Cambrian ages were interpreted to correspond to subduction of early oceanic tracts formed in the Iapetus Ocean (Hibbard et al., 2007). In the North-Central Appalachians, magmatic arc complexes yield ages of 515 to 502 Ma, which are defined as the Potomac Orogeny (Faill, 1997). The ca. 500 Ma monazite ages of

this study provide geochronological evidence of the existence of a pre-Taconic event in southwestern New England.

The 478±6 and 472±5 Ma Ages

In Newfoundland, similar ages (480–468 Ma) were obtained from the Annieopsquotch accretionary tract which formed in an arc-backarc environment east of the Dashwoods microcontinent (Zagorevski et al., 2006). In New England, similar ages (485–470 Ma) from the Shelburne Falls Arc in Massachusetts and New Hampshire have been reported (Karabinos et al., 2008). The Shelburne Falls Arc, which lies east of the study area and is separated from the study area by the Rowe-Moretown zone, formed above an east-dipping subduction zone, perhaps on a continental fragment rifted from Laurentia (Karabinos et al., 2008). The 478±6 and 472±5 Ma ages from Dutchess County may record the beginning of the collision between Laurentia and the Shelburne Falls arc, which may define the beginning of the Taconic Orogeny in this area.

The 455±6, 453±10 and 451±9 Ma Ages

In Newfoundland, similar ages were reported from the Dashwoods microcontinent and the associated Notre Dame Arc, corresponding to a second phase of the Notre Dame Arc magmatism (469–458 Ma) and the end of the collision of the Dashwoods and the Annieopsquotch accretionary tracts with the Laurentian margin (455–450 Ma) (van Staal, 2005). In New England, similar ages were reported from the Bronson Hill arc (454–442 Ma; Tucker & Robinson, 1990). The 455–451 Ma ages from the study area are interpreted to record the effect of collision of the

Bronson Hill arc with the Laurentian margin during the late stage of the Taconic Orogeny.

The 438±8, 431±4 and 425±8 Ma Ages

In Newfoundland, similar ages (435–420 Ma) from volcanic, plutonic and metamorphic rocks were identified and the event responsible for them was named the Silurian Orogeny by Dunning et al. (1990), which is also called the Salinic Orogeny by van Staal (2005). This plutonic event has been ascribed to the breakoff of a west-dipping, down-going slab of the Annieopsquotch accretionary tract, the Exploits Subzone, and the Gander Zone (van Staal, 2005). In New England, similar ages were reported from the granite sills in the Berkshire Massif in Massachusetts (ca. 434 Ma; Karabinos et al., 2008), volcanic rocks in the Connecticut Valley (423±4 Ma; Aleinikoff & Karabinos, 1990) and the Cortlandt Complex in New York (ca. 423 Ma; Ratcliffe et al., 1982). This post-peak magmatism in New England may only affect parts of the overlying rocks. Whitney et al. (1996a) reported that the upper staurolite and kyanite zone rocks contain clear evidence for extensive fluid infiltration and mineral-fluid reaction. Fluid infiltrated the metapelitic schists along channels (now represented by veins) and triggered high-temperature metasomatic reactions (Whitney et al., 1996a). The contemporary Cortlandt Complex (~ 30 km south of the study area) may be related to the fluid infiltration. Although the vein volume of the study area has not been quantitatively measured, it is significantly higher in the kyanite zone (sample 077401, 431±4 and 425±8 Ma) than in other zones based on visual estimates in the field. Therefore, the Barrovian metamorphic sequence in Dutchess

County may be partially overprinted by fluid flow related to contemporaneous magmatism during the Salinic Orogeny.

In summary, monazite from the Barrovian Sequence in southeastern New York and western Connecticut records metamorphic and related events from the Early Cambrian, through the Late Cambrian, to the Ordovician and Silurian. These ages fill data gaps in southwestern New England, helping to constrain the beginning of the Taconic Orogeny and adding to the geochronological database of the Taconic and Salinic orogenic events.

Chapter 6: Conclusions

The average *P–T* results for the garnet, staurolite, kyanite and sillimanite-K-feldspar zones are (1σ uncertainty): 5.2±0.8 kbar, 570±12°C; 5.9±1.1 kbar, 557±12°C; 6.4±1.1 kbar, 600±29°C; and 7.4±1.4 kbar, 752±68°C, respectively. Phase equilibria modeling in the MnNCKFMASHTO system yields peak *P–T* results consistent with the average *P–T* conditions. Growth zoning in garnet from the garnet zone records a temperature increase of about 50°C and a pressure increase of about 0.6 kbar from the core to the rim. The *P–T* estimation is different from the conclusion of Whitney et al. (1996a), probably due to the use of different thermodynamic datasets and a multi-equilibrium *P–T* estimation method rather than the conventional thermobarometric methods used by Whitney et al. (1996a).

Five groups of ages are identified from monazite geochronology (2σ uncertainties): a 533±7 Ma age from the sillimanite-K-feldspar zone, 507±6 and 506±4 Ma ages from the sillimanite-K-feldspar zone, a 472±5 Ma age from the sillimanite-K-feldspar zone and a 478±6 Ma age from the kyanite zone, 455±6, 453±10 and 451±9 Ma ages from the staurolite and garnet zones, and 438±8, 431±4 and 425±8 Ma ages from the kyanite and staurolite zones. The ca. 533 Ma age may indicate an Early Cambrian thermal event in the formation of the Northern Appalachians that has not been previously identified and characterized. The ca. 507 Ma event maybe related to the subduction of an early oceanic tract in the Iapetus ocean. The ca. 480–470 Ma event most likely marks the beginning of the Taconic Orogeny in the study area, which may be due to the collision of the Shelburne Falls Arc with Laurentia. The ca. 455–451 Ma event marks the end of the Taconic

Orogeny, due to the formation of the Bronson Hill Arc and the collision with Laurentia. The ca. 438–425 Ma event is consistent with the Salinic Orogeny and may be related to magmatism and fluid infiltration.

Appendices

Appendix A Mineral compositions used for the average P–T calculations

Table 1. Muscovite and biotite analyses.

	Grt Zone			St Zone			Ky Zone		Sil-Kfs Zone
	Ms 1†	Ms 2†	Bt	Ms 1‡	Ms 2‡	Bt	Ms	Bt	Bt
SiO_2	46.64	47.88	35.39	46.01	46.72	35.32	46.28	36.08	34.96
TiO_2	0.20	0.16	1.76	0.17	0.18	1.74	0.49	1.45	2.89
Al_2O_3	37.98	36.14	19.86	38.46	38.99	19.68	37.75	19.48	18.55
FeO	1.16	1.49	22.09	0.90	0.98	20.92	0.92	18.03	22.12
MnO	0.02	0.05	0.02	0.03	0.02	0.07	0.03	0.05	0.07
MgO	0.53	0.99	8.31	0.37	0.37	9.20	0.64	11.85	8.06
CaO	0.01	0.01	0.00	0.01	0.01	0.00	0.00	0.00	0.02
Na_2O	1.17	0.92	0.15	1.81	1.90	0.17	1.11	0.31	0.13
K_2O	9.39	9.63	9.14	8.44	8.53	8.96	9.58	9.14	9.99
F	0.01	0.00	–	0.02	0.02	–	0.03	–	–
Total	97.11	97.28	96.72	96.20	97.71	96.07	96.82	96.40	96.80

† Ms 1: average of muscovite close to garnet, Ms 2: single analysis in vein, high SiO_2
‡ Ms 1: average of muscovite close to garnet, Ms 2: average of ms close to chloritoid

Table 2. Plagioclase and orthoclase analyses.

	Grt Zone	St Zone	Ky Zone	Sil-Kfs Zone	
	Pl	Pl rim	Pl rim	Pl rim	Kfs average
SiO_2	62.30	64.31	61.51	59.30	64.67
Al_2O_3	24.03	23.45	25.10	26.16	18.38
FeO	0.34	0.06	0.01	0.03	0.07
MnO	–	–	–	–	0.01
CaO	4.94	3.69	5.94	7.36	0.01
Na_2O	8.89	9.76	8.42	7.40	0.18
K_2O	0.05	0.04	0.07	0.08	16.54
Total	100.55	101.32	101.04	100.33	99.85

Table 3. Garnet analyses.

	Grt Zone	St Zone	Ky Zone		Sil-Kfs Zone	
	Rim	Rim	Core average	Rim	Core average	Rim
SiO_2	36.34	36.41	36.51	36.47	36.38	36.45
TiO_2	0.18	0.15	0.12	0.00	0.03	0.09
Al_2O_3	20.99	20.96	20.70	20.64	20.63	20.87
Fe_2O_3	0.09	0.66	0.80	0.54	0.75	0.12
FeO	36.17	36.05	28.16	30.98	29.66	31.74
MnO	1.76	2.07	6.44	5.00	6.56	4.63
MgO	1.77	2.11	2.97	2.57	2.50	2.45
CaO	1.95	1.37	2.96	2.33	2.15	2.25
Total	99.23	99.73	98.59	98.48	98.59	98.58

Table 4. Chlorite, staurolite and chloritoid analyses.

	Grt Zone	St Zone	
	Chl average	St rim	Chld average
SiO_2	24.88	28.72	25.26
TiO_2	0.05	0.33	0.01
Al_2O_3	22.79	54.04	40.91
FeO	28.06	13.62	23.94
MnO	0.05	0.08	0.18
MgO	11.68	1.12	2.34
CaO	0.00	0.00	0.00
Total	87.51	97.91	92.65

Appendix B Method of calculating the effective bulk composition of samples containing zoned garnet.

In the method below, it is assumed that (1) garnet is spherical and monotonically zoned, (2) the compositional profile of garnet in two dimensional space can be extended to three dimensions, and (3) all garnet in this sample has the same composition as the garnet analyzed.

The fraction of oxide i (F^i) removed from the bulk composition is $F^i = \frac{M_G^i}{M_S} = \frac{V_G \times \rho_G^i}{V_S \times \rho_S}$, where M_G^i is the mass of oxide i in garnet (G), M_S is the mass of the schist (S), V is the volume, ρ is the density.

$\because\ M_G^i = V_G \times \rho_G^i$

$\therefore\ \rho_G^i = \dfrac{M_G^i}{V_G} = \dfrac{M_G \times C_G^i}{V_G}$, where C_G^i is the concentration of oxide i in garnet.

Therefore, we can calculate the concentration of oxide i in garnet using the following equation:

$$C_G^i = \frac{\iiint_\Omega \mu(r,\varphi,\theta) r^2 \sin\varphi dr d\varphi d\theta}{\iiint_\Omega r^2 \sin\varphi dr d\varphi d\theta}, \text{ where } \mu(r,\varphi,\theta) = C_{Core}^i + r \times \frac{C_{Rim}^i - C_{Core}^i}{R},$$

R is the radius of the garnet.

$$C_G^i = \frac{\int_0^R (r^2 C_{Core}^i + r^3 \frac{C_{Rim}^i - C_{Core}^i}{R}) dr \int_0^\pi \sin\varphi d\varphi \int_0^{2\pi} d\theta}{\int_0^R r^2 dr \int_0^\pi \sin\varphi d\varphi \int_0^{2\pi} d\theta}$$

$$= \frac{\frac{4}{3}\pi R^3 (\frac{3}{4} C_{Rim}^i + \frac{1}{4} C_{Core}^i)}{\frac{4}{3}\pi R^3}$$

$$= \frac{3}{4} C_{Rim}^i + \frac{1}{4} C_{Core}^i$$

This result means that for a monotonically zoned element in garnet, the average concentration of this element is equal to three quarters of the concentration at the rim plus one quarter of the concentration at the core.

$$F^i = \frac{M_G^i}{M_S} = \frac{V_G \times \rho_G^i}{V_S \times \rho_S}$$

$$= Mode_G \times \frac{\rho_G \cdot C_G^i}{\rho_S}$$

$$= Mode_G \cdot \frac{\rho_G}{\rho_S} \cdot (\frac{3}{4} C_{Rim}^i + \frac{1}{4} C_{Core}^i)$$

The fraction of the area of all garnet in a thin section is used as an approximation for the mode. The mode of garnet in sample 05403 is 1.26 %.

The density of garnet is calculated using the density of endmembers and the average fraction of each endmember (Table 1) in the garnet. The calculated density of garnet is 4.20 g/cm^3.

Table 1. Density of garnet.

	Density g/cm^3	Fraction mole%
Alm	4.318	0.75
Prp	3.582	0.06
Grs	3.594	0.08
Sps	4.190	0.11
Grt	4.20	

Density of endmembers from Deer et al., 1992.

The density of the rock is calculated by measuring the mass and volume of the rock. The density calculated is 2.77 g/cm^3.

The interior of garnet in sample 05403 from the garnet zone (from the core to a position ~ 50 μm from the rim: B-B' in Figure 3-2) was removed from the bulk composition. The results of this modeling suggest that the effective MnO concentration in the rock was 0.08 wt.%.

Appendix C Standards used for mineral analyses.

Mineral	SiO_2	TiO_2	Al_2O_3	FeO	MgO	MnO	CaO	Na_2O	K_2O	F	Cl
Muscovite	Muscovite	Hb-Kakanui	Muscovite	Hb-Kakanui	Hb-Kakanui	Rhodonite	Hb-Kakanui	Microcline	Muscovite	Topaz	Scapolite
Biotite	Biotite-Lemhi	Biotite-Lemhi	Biotite-Lemhi	Biotite-Lemhi	Biotite-Lemhi	Rhodonite	Hb-Kakanui	Microcline	Biotite-Lemhi	Topaz	Biotite-Lemhi
Staurolite	Staurolite	Hb-Kakanui	Kyanite	Staurolite	Staurolite	Rhodonite	Hb-Kakanui				
Chlorite	Staurolite	Hb-Kakanui	Garnet-12442	Garnet-12442	Hb-Kakanui	Rhodonite	Plagioclase				
Chloritoid	Staurolite	Hb-Kakanui	Kyanite	Garnet-12442	Hb-Kakanui	Rhodonite	Plagioclase				
K-feldspar	Microcline		Microcline	Hb-Kakanui		Rhodonite	Plagioclase	Microcline	Microcline		
Plagioclase	Plagioclase	Hb-Kakanui	Plagioclase	Staurolite	Saturolite	Rhodonite	Plagioclase	Plagioclase	Microcline		
Garnet	Garnet-12442	Hb-Kakanui	Garnet-12442	Garnet-12442	Garnet-12442	Rhodonite	Garnet-12442				

Appendix D Mineral compositions from different metamorphic zones.

Table 1. Muscovite analyses from the garnet zone, sample 05403.

	1#1	1#2	1#3	2#1	2#2	2#3	2#4	2#5	2#6	3#1	3#2	4#1	4#2	4#3
SiO_2	46.53	46.72	47.58	46.72	46.31	46.33	46.98	46.88	46.65	46.23	46.58	47.88	47.49	46.72
TiO_2	0.18	0.20	0.24	0.22	0.25	0.12	0.21	0.19	0.21	0.23	0.19	0.16	0.22	0.16
Al_2O_3	38.57	37.83	37.11	37.81	37.80	37.77	38.11	38.11	37.81	38.59	38.28	36.14	36.51	37.27
FeO	1.09	1.21	1.07	1.15	1.20	1.15	1.12	1.11	1.28	1.30	1.18	1.49	1.31	1.18
MnO	0.01	0.00	0.01	0.04	0.00	0.00	0.04	0.03	0.02	0.00	0.08	0.05	0.00	0.00
MgO	0.46	0.52	0.65	0.58	0.58	0.46	0.50	0.56	0.55	0.44	0.44	0.99	0.97	0.77
CaO	0.00	0.01	0.00	0.00	0.00	0.02	0.03	0.02	0.04	0.00	0.02	0.01	0.00	0.00
Na_2O	1.09	1.00	1.03	1.18	1.20	1.26	1.23	1.31	1.12	1.24	1.32	0.92	0.90	1.02
K_2O	9.40	9.81	9.65	9.44	9.49	9.35	9.19	9.05	9.39	9.46	9.42	9.63	9.69	9.69
F	0.00	0.00	0.00	0.03	0.02	0.00	0.00	0.01	0.05	0.03	0.00	0.00	0.02	0.06
Total	97.34	97.30	97.33	97.15	96.85	96.46	97.41	97.25	97.09	97.53	97.52	97.28	97.10	96.84
Si	6.01	6.06	6.15	6.06	6.03	6.05	6.06	6.06	6.06	5.98	6.02	6.21	6.17	6.09
Al^{IV}	1.99	1.94	1.85	1.94	1.97	1.95	1.94	1.94	1.94	2.02	1.98	1.79	1.83	1.91
Al^{VI}	3.89	3.84	3.81	3.84	3.83	3.86	3.86	3.86	3.84	3.87	3.86	3.73	3.75	3.81
Ti	0.02	0.02	0.02	0.02	0.02	0.01	0.02	0.02	0.02	0.02	0.02	0.02	0.02	0.02
Fe	0.12	0.13	0.12	0.12	0.13	0.13	0.12	0.12	0.14	0.14	0.13	0.16	0.14	0.13
Mn	0.00	0.00	0.00	0.00	0.00	0.00	0.00	0.00	0.00	0.00	0.01	0.01	0.00	0.00
Mg	0.09	0.10	0.12	0.11	0.11	0.09	0.10	0.11	0.11	0.09	0.08	0.19	0.19	0.15
Ca	0.00	0.00	0.00	0.00	0.00	0.00	0.00	0.00	0.01	0.00	0.00	0.00	0.00	0.00
Na	0.27	0.25	0.26	0.30	0.30	0.32	0.31	0.33	0.28	0.31	0.33	0.23	0.23	0.26
K	1.55	1.62	1.59	1.56	1.58	1.56	1.51	1.49	1.56	1.56	1.55	1.59	1.61	1.61
F	0.00	0.00	0.00	0.01	0.01	0.00	0.00	0.00	0.02	0.01	0.00	0.00	0.01	0.02
Ca+Na+K	1.82	1.88	1.85	1.86	1.88	1.88	1.83	1.82	1.84	1.87	1.89	1.83	1.83	1.87
OCT	4.12	4.09	4.07	4.10	4.10	4.09	4.10	4.11	4.11	4.12	4.10	4.10	4.10	4.10

Cations calculated on a 22-oxygen equivalents basis.

OCT=Al^{VI}+Ti+Fe+Mn+Mg. "1#2" means the second analysis on muscovite 1.

Table 1 continued. Muscovite analyses from the staurolite zone, sample 05501.

	1#1	1#2	1#3	2#1	2#2	2#3	3#1	3#2	4#1	4#2	4#3	4#4	4#5	4#6
SiO_2	46.27	46.28	46.10	46.18	45.74	45.51	47.34	46.54	46.69	46.74	46.36	46.70	46.76	46.60
TiO_2	0.17	0.17	0.18	0.16	0.17	0.16	0.17	0.16	0.18	0.20	0.17	0.21	0.18	0.20
Al_2O_3	38.81	38.83	37.89	38.20	38.75	38.26	39.11	38.96	39.10	38.93	39.07	39.03	38.82	38.91
FeO	0.88	0.92	0.84	1.01	0.92	0.82	0.93	1.12	1.01	0.95	1.01	1.03	0.85	0.90
MnO	0.07	0.00	0.00	0.01	0.00	0.11	0.03	0.00	0.05	0.00	0.06	0.00	0.00	0.02
MgO	0.36	0.41	0.40	0.38	0.26	0.37	0.38	0.28	0.37	0.36	0.40	0.39	0.43	0.36
CaO	0.02	0.01	0.01	0.00	0.00	0.00	0.00	0.03	0.00	0.00	0.03	0.02	0.00	0.00
Na_2O	2.09	1.99	1.66	1.31	1.73	2.07	2.15	2.03	1.90	1.81	1.77	1.90	1.78	1.88
K_2O	8.27	8.49	8.65	8.54	8.52	8.20	8.10	8.33	8.34	8.82	8.72	8.51	8.87	8.57
F	0.00	0.03	0.02	0.05	0.00	0.04	0.00	0.04	0.01	0.02	0.05	0.00	0.04	0.00
Total	96.92	97.12	95.73	95.83	96.09	95.53	98.20	97.48	97.64	97.82	97.61	97.78	97.72	97.44
Si	5.99	5.98	6.04	6.04	5.97	5.98	6.03	5.99	5.99	6.00	5.97	5.99	6.01	6.00
Al^{IV}	2.01	2.02	1.96	1.96	2.03	2.02	1.97	2.01	2.01	2.00	2.03	2.01	1.99	2.00
Al^{VI}	3.90	3.90	3.89	3.92	3.93	3.90	3.90	3.90	3.91	3.89	3.90	3.90	3.89	3.90
Ti	0.02	0.02	0.02	0.02	0.02	0.02	0.02	0.02	0.02	0.02	0.02	0.02	0.02	0.02
Fe	0.09	0.10	0.09	0.11	0.10	0.09	0.10	0.12	0.11	0.10	0.11	0.11	0.09	0.10
Mn	0.01	0.00	0.00	0.00	0.00	0.01	0.00	0.00	0.01	0.00	0.01	0.00	0.00	0.00
Mg	0.07	0.08	0.08	0.08	0.05	0.07	0.07	0.05	0.07	0.07	0.08	0.08	0.08	0.07
Ca	0.00	0.00	0.00	0.00	0.00	0.00	0.00	0.00	0.00	0.00	0.00	0.00	0.00	0.00
Na	0.52	0.50	0.42	0.33	0.44	0.53	0.53	0.51	0.47	0.45	0.44	0.47	0.44	0.47
K	1.36	1.40	1.45	1.42	1.42	1.37	1.32	1.37	1.37	1.45	1.43	1.39	1.45	1.41
F	0.00	0.01	0.01	0.02	0.00	0.02	0.00	0.02	0.01	0.01	0.02	0.00	0.01	0.00
Ca+Na+K	1.89	1.90	1.87	1.76	1.86	1.90	1.85	1.88	1.84	1.90	1.88	1.87	1.90	1.88
OCT	4.09	4.09	4.08	4.13	4.10	4.09	4.09	4.09	4.11	4.08	4.11	4.10	4.08	4.09

Table 1 continued. Muscovite analyses from the kyanite zone, sample 077401.

	1#1	1#2	1#3	1#4	2#1	2#2	2#3	2#4	2#5	3#1	3#2	3#3	3#4	3#5
SiO_2	46.20	46.43	46.49	46.00	46.35	46.72	47.02	45.38	46.06	45.99	46.19	45.48	46.44	46.54
TiO_2	0.48	0.32	0.59	0.58	0.54	0.57	0.53	0.55	0.41	0.60	0.53	0.32	0.52	0.53
Al_2O_3	38.14	37.22	37.72	37.91	37.83	38.19	38.37	37.77	37.72	37.54	38.01	38.51	38.38	37.99
FeO	0.94	1.06	0.85	0.83	0.80	0.85	0.87	0.83	0.81	0.96	0.95	0.90	0.78	0.97
MnO	0.02	0.00	0.11	0.00	0.00	0.07	0.02	0.00	0.00	0.00	0.00	0.00	0.01	0.03
MgO	0.56	0.75	0.63	0.63	0.65	0.61	0.62	0.62	0.55	0.63	0.64	0.50	0.60	0.55
CaO	0.00	0.00	0.00	0.00	0.00	0.01	0.02	0.02	0.00	0.00	0.00	0.00	0.01	0.00
Na_2O	1.06	1.15	1.07	1.14	1.14	1.16	1.18	1.13	1.25	1.12	1.08	1.20	1.20	1.18
K_2O	9.76	9.67	9.49	9.41	9.73	9.83	9.70	9.59	9.45	9.83	9.68	9.56	9.54	9.62
F	0.06	0.02	0.04	0.01	0.00	0.05	0.02	0.05	0.00	0.02	0.00	0.00	0.00	0.03
Total	97.19	96.62	96.98	96.50	97.04	98.05	98.33	95.91	96.25	96.68	97.09	96.47	97.48	97.43
Si	6.00	6.06	6.04	6.00	6.02	6.01	6.03	5.97	6.03	6.01	6.00	5.95	6.00	6.02
Al^{IV}	2.00	1.94	1.96	2.00	1.98	1.99	1.97	2.03	1.97	1.99	2.00	2.05	2.00	1.98
Al^{VI}	3.84	3.79	3.81	3.83	3.81	3.81	3.82	3.83	3.84	3.79	3.82	3.88	3.84	3.82
Ti	0.05	0.03	0.06	0.06	0.05	0.06	0.05	0.05	0.04	0.06	0.05	0.03	0.05	0.05
Fe	0.10	0.12	0.09	0.09	0.09	0.09	0.09	0.09	0.09	0.10	0.10	0.10	0.08	0.11
Mn	0.00	0.00	0.01	0.00	0.00	0.01	0.00	0.00	0.00	0.00	0.00	0.00	0.00	0.00
Mg	0.11	0.15	0.12	0.12	0.13	0.12	0.12	0.12	0.11	0.12	0.12	0.10	0.12	0.11
Ca	0.00	0.00	0.00	0.00	0.00	0.00	0.00	0.00	0.00	0.00	0.00	0.00	0.00	0.00
Na	0.27	0.29	0.27	0.29	0.29	0.29	0.29	0.29	0.32	0.28	0.27	0.30	0.30	0.30
K	1.62	1.61	1.57	1.57	1.61	1.61	1.59	1.61	1.58	1.64	1.60	1.59	1.57	1.59
F	0.02	0.01	0.02	0.00	0.00	0.02	0.01	0.02	0.00	0.01	0.00	0.00	0.00	0.01
Ca+Na+K	1.88	1.90	1.84	1.85	1.90	1.91	1.88	1.90	1.89	1.92	1.88	1.90	1.87	1.88
OCT	4.09	4.09	4.10	4.10	4.08	4.08	4.08	4.10	4.08	4.08	4.10	4.11	4.09	4.09

Table 2. Biotite analyses from the garnet (05403) and staurolite (05501) zones.

	Garnet Zone 05403						Staurolite Zone 05501								
	2#1	2#2	3#1	3#2	3#3	3#4	2#1	2#2	2#3	2#4	2#5	2#6	2#7	2#8	2#9
SiO_2	33.98	34.15	35.36	35.32	35.38	35.50	35.22	35.60	35.22	35.13	35.31	35.29	35.39	35.24	35.47
TiO_2	1.40	1.47	1.66	1.73	1.76	1.90	1.64	1.64	1.79	1.76	1.83	1.85	1.98	1.57	1.56
Al_2O_3	19.56	19.95	20.13	20.06	19.85	19.39	19.68	20.30	20.12	19.37	19.66	19.56	19.38	19.91	19.15
FeO	22.49	22.97	22.42	22.00	21.99	21.94	21.28	19.87	21.00	21.15	20.43	21.38	21.17	20.99	20.98
MnO	0.01	0.11	0.00	0.07	0.02	0.00	0.01	0.00	0.05	0.09	0.13	0.15	0.14	0.04	0.01
MgO	8.99	9.23	8.31	8.43	8.36	8.13	9.28	9.14	9.24	9.06	8.97	9.10	9.30	9.14	9.55
CaO	0.00	0.00	0.00	0.00	0.00	0.00	0.00	0.00	0.00	0.00	0.00	0.00	0.00	0.00	0.00
Na_2O	0.14	0.16	0.11	0.16	0.19	0.13	0.20	0.21	0.18	0.19	0.20	0.16	0.13	0.15	0.14
K_2O	8.09	8.22	8.99	9.16	9.17	9.23	8.83	9.27	9.08	8.79	9.02	9.05	9.04	8.94	8.65
Total	94.67	96.27	96.99	96.94	96.74	96.21	96.13	96.06	96.70	95.55	95.59	96.54	96.52	95.99	95.54
Si	5.26	5.21	5.34	5.33	5.35	5.40	5.34	5.37	5.31	5.36	5.37	5.34	5.35	5.34	5.40
Al^{IV}	2.74	2.79	2.66	2.67	2.65	2.60	2.66	2.63	2.69	2.64	2.63	2.66	2.65	2.66	2.60
Al^{VI}	0.83	0.79	0.92	0.90	0.89	0.88	0.85	0.98	0.88	0.84	0.90	0.83	0.80	0.90	0.83
Ti	0.16	0.17	0.19	0.20	0.20	0.22	0.19	0.19	0.20	0.20	0.21	0.21	0.23	0.18	0.18
Fe	2.91	2.93	2.83	2.78	2.78	2.79	2.70	2.51	2.65	2.70	2.60	2.70	2.68	2.66	2.67
Mn	0.00	0.01	0.00	0.01	0.00	0.00	0.00	0.00	0.01	0.01	0.02	0.02	0.02	0.01	0.00
Mg	2.07	2.10	1.87	1.90	1.89	1.84	2.10	2.05	2.07	2.06	2.03	2.05	2.09	2.06	2.17
Ca	0.00	0.00	0.00	0.00	0.00	0.00	0.00	0.00	0.00	0.00	0.00	0.00	0.00	0.00	0.00
Na	0.04	0.05	0.03	0.05	0.05	0.04	0.06	0.06	0.05	0.06	0.06	0.05	0.04	0.05	0.04
K	1.60	1.60	1.73	1.76	1.77	1.79	1.71	1.78	1.74	1.71	1.75	1.75	1.74	1.73	1.68
Ca+Na+K	1.64	1.65	1.76	1.81	1.82	1.83	1.77	1.84	1.80	1.77	1.81	1.79	1.78	1.77	1.72
OCT	5.98	6.01	5.80	5.78	5.76	5.73	5.83	5.72	5.81	5.81	5.75	5.81	5.81	5.81	5.85

Cations calculated on a 22-oxygen equivalents basis.

OCT=Al^{VI}+Ti+Fe+Mn+Mg. "1#2" means the second analysis on biotite 1.

Table 2 continued. Biotite analyses from the kyanite zone, sample 077401.

	1#1	1#2	1#3	1#4	1#5	1#6	1#7	1#8	2#1	2#2	2#3	2#4	2#5	2#6	2#7	2#8
SiO_2	35.91	35.82	36.24	36.37	36.38	36.64	36.11	35.99	35.84	35.79	36.23	36.05	35.82	36.20	35.95	35.91
TiO_2	1.45	1.40	1.38	1.43	1.40	1.31	1.36	1.42	1.55	1.52	1.54	1.56	1.44	1.51	1.50	1.46
Al_2O_3	18.95	19.36	19.53	19.58	19.53	19.40	19.48	19.58	19.14	19.48	19.54	19.50	19.78	19.72	19.35	19.79
FeO	18.15	18.05	18.23	18.02	17.84	17.79	18.46	17.71	18.30	18.35	17.83	17.97	18.62	18.05	17.53	17.59
MnO	0.00	0.03	0.21	0.07	0.06	0.00	0.00	0.00	0.04	0.15	0.06	0.06	0.04	0.00	0.01	0.10
MgO	11.81	11.90	12.01	12.08	11.95	12.10	12.04	11.89	11.75	11.84	11.82	11.59	11.98	11.58	11.43	11.76
CaO	0.00	0.01	0.03	0.00	0.00	0.00	0.00	0.00	0.00	0.00	0.00	0.00	0.00	0.00	0.00	0.00
Na_2O	0.29	0.34	0.33	0.33	0.33	0.32	0.34	0.33	0.28	0.25	0.31	0.33	0.31	0.31	0.29	0.32
K_2O	9.00	9.03	8.93	9.07	8.79	9.06	9.09	9.13	9.23	9.31	9.29	9.27	9.33	9.36	9.05	9.30
Total	95.57	95.96	96.89	96.95	96.29	96.62	96.90	96.06	96.15	96.69	96.63	96.34	97.33	96.73	95.11	96.22
Si	5.40	5.36	5.37	5.38	5.41	5.43	5.36	5.37	5.37	5.33	5.38	5.38	5.31	5.37	5.41	5.35
Al^{IV}	2.60	2.64	2.63	2.62	2.60	2.57	2.64	2.63	2.63	2.67	2.62	2.62	2.69	2.63	2.59	2.65
Al^{VI}	0.76	0.78	0.78	0.79	0.82	0.81	0.77	0.81	0.75	0.76	0.80	0.80	0.76	0.83	0.85	0.83
Ti	0.16	0.16	0.15	0.16	0.16	0.15	0.15	0.16	0.18	0.17	0.17	0.17	0.16	0.17	0.17	0.16
Fe	2.28	2.26	2.26	2.23	2.22	2.20	2.29	2.21	2.29	2.29	2.21	2.24	2.31	2.24	2.21	2.19
Mn	0.00	0.00	0.03	0.01	0.01	0.00	0.00	0.00	0.01	0.02	0.01	0.01	0.00	0.00	0.00	0.01
Mg	2.65	2.66	2.65	2.66	2.65	2.67	2.66	2.65	2.62	2.63	2.62	2.58	2.65	2.56	2.57	2.61
Ca	0.00	0.00	0.00	0.00	0.00	0.00	0.00	0.00	0.00	0.00	0.00	0.00	0.00	0.00	0.00	0.00
Na	0.09	0.10	0.09	0.09	0.09	0.09	0.10	0.09	0.08	0.07	0.09	0.10	0.09	0.09	0.08	0.09
K	1.73	1.73	1.69	1.71	1.67	1.71	1.72	1.74	1.76	1.77	1.76	1.76	1.76	1.77	1.74	1.77
Ca+Na+K	1.81	1.83	1.79	1.80	1.76	1.80	1.82	1.83	1.84	1.84	1.85	1.86	1.85	1.86	1.82	1.86
OCT	5.85	5.86	5.87	5.85	5.85	5.83	5.87	5.83	5.84	5.86	5.81	5.81	5.88	5.80	5.79	5.81

Table 2 continued. Biotite analyses from the sillimanite-K-feldspar zone, sample 07905.

	1#1	1#2	1#3	1#4	1#5	2#1	2#2	2#4	2#5	3#1	3#2	3#3
SiO_2	34.79	35.05	35.02	35.31	34.84	34.94	35.24	34.73	34.87	35.05	34.99	34.64
TiO_2	2.66	2.52	2.44	2.38	2.65	3.36	3.50	3.57	3.40	2.73	2.82	2.72
Al_2O_3	18.31	18.80	18.88	18.65	18.61	18.48	18.64	18.21	18.36	18.59	18.61	18.52
FeO	21.73	22.17	22.64	22.35	22.03	21.94	22.46	21.88	21.77	22.20	22.30	21.93
MnO	0.15	0.15	0.00	0.08	0.00	0.03	0.10	0.13	0.11	0.07	0.07	0.00
MgO	8.25	8.14	8.21	8.34	8.19	7.97	7.84	7.87	7.86	7.96	8.10	8.04
CaO	0.00	0.00	0.00	0.00	0.00	0.00	0.04	0.00	0.00	0.08	0.06	0.07
Na_2O	0.11	0.04	0.10	0.10	0.14	0.19	0.15	0.10	0.15	0.14	0.13	0.15
K_2O	10.11	10.16	10.14	10.25	10.10	9.90	9.81	9.80	9.89	9.86	10.01	9.87
Total	96.11	97.04	97.43	97.46	96.57	96.81	97.76	96.28	96.41	96.68	97.09	95.94
Si	5.35	5.34	5.32	5.36	5.33	5.32	5.32	5.32	5.34	5.35	5.33	5.33
Al^{IV}	2.65	2.66	2.68	2.64	2.67	2.68	2.68	2.68	2.66	2.65	2.67	2.67
Al^{VI}	0.67	0.71	0.70	0.69	0.69	0.64	0.64	0.61	0.65	0.70	0.67	0.69
Ti	0.31	0.29	0.28	0.27	0.31	0.39	0.40	0.41	0.39	0.31	0.32	0.31
Fe	2.79	2.82	2.88	2.84	2.82	2.80	2.84	2.81	2.79	2.84	2.84	2.82
Mn	0.02	0.02	0.00	0.01	0.00	0.00	0.01	0.02	0.01	0.01	0.01	0.00
Mg	1.89	1.85	1.86	1.89	1.87	1.81	1.76	1.80	1.79	1.81	1.84	1.84
Ca	0.00	0.00	0.00	0.00	0.00	0.00	0.01	0.00	0.00	0.01	0.01	0.01
Na	0.03	0.01	0.03	0.03	0.04	0.06	0.04	0.03	0.05	0.04	0.04	0.04
K	1.98	1.97	1.97	1.98	1.97	1.93	1.89	1.92	1.93	1.92	1.95	1.94
Ca+Na+K	2.02	1.99	1.99	2.01	2.01	1.98	1.94	1.95	1.98	1.97	1.99	2.00
OCT	5.68	5.69	5.71	5.70	5.68	5.64	5.65	5.65	5.63	5.67	5.68	5.67

Table 3. Plagioclase analyses from the garnet (05403) and staurolite (05501) zones.

	Garnet Zone 05403			Staurolite Zone 05501											
	1#1	1#2	2#3	1#2	1#3	1#4	1#5	1#6	1#7	1#8	2#2	2#3	2#4	2#5	2#6
SiO_2	62.15	62.15	62.60	66.31	67.59	67.09	64.52	68.07	65.26	64.31	62.14	63.23	61.38	62.54	63.58
Al_2O_3	24.01	24.29	23.78	22.06	21.17	21.06	22.79	20.88	22.88	23.45	23.25	24.47	24.30	23.90	23.11
FeO	0.39	0.38	0.25	0.03	0.05	0.01	0.07	0.00	0.07	0.06	0.07	0.09	0.10	0.12	0.19
CaO	5.07	5.05	4.69	2.36	1.36	1.46	3.17	1.03	3.21	3.69	4.60	5.03	5.01	4.72	3.98
Na_2O	8.77	8.97	8.95	10.42	11.08	10.89	9.84	11.11	9.83	9.76	8.91	9.16	8.60	9.19	9.29
K_2O	0.02	0.04	0.07	0.02	0.03	0.04	0.05	0.04	0.02	0.04	0.07	0.03	0.17	0.03	0.02
Total	100.42	100.87	100.35	101.20	101.28	100.55	100.45	101.13	101.27	101.32	99.04	102.00	99.56	100.51	100.17
Si	2.75	2.74	2.76	2.88	2.92	2.92	2.83	2.94	2.84	2.80	2.78	2.75	2.73	2.76	2.80
Al	1.25	1.26	1.24	1.13	1.08	1.08	1.18	1.06	1.17	1.20	1.22	1.25	1.28	1.24	1.20
Fe	0.01	0.01	0.01	0.00	0.00	0.00	0.00	0.00	0.00	0.00	0.00	0.00	0.00	0.00	0.01
Ca	0.24	0.24	0.22	0.11	0.06	0.07	0.15	0.05	0.15	0.17	0.22	0.23	0.24	0.22	0.19
Na	0.75	0.77	0.77	0.88	0.93	0.92	0.84	0.93	0.83	0.82	0.77	0.77	0.74	0.79	0.79
K	0.00	0.00	0.00	0.00	0.00	0.00	0.00	0.00	0.00	0.00	0.00	0.00	0.01	0.00	0.00
Or	0.00	0.00	0.00	0.00	0.00	0.00	0.00	0.00	0.00	0.00	0.00	0.00	0.01	0.00	0.00
Ab	0.76	0.76	0.77	0.89	0.93	0.93	0.85	0.95	0.85	0.83	0.78	0.77	0.75	0.78	0.81
An	0.24	0.24	0.22	0.11	0.06	0.07	0.15	0.05	0.15	0.17	0.22	0.23	0.24	0.22	0.19

Cations calculated on a 8-oxygen basis.
"1#2" means the second analysis on plagioclase 1.

Table 3 continued. Plagioclase analyses from the kyanite zone, sample 077401.

	1#1	1#2	1#3	1#4	2#1	2#2	2#3	2#4	2#5	2#6
SiO_2	60.22	61.44	61.49	60.52	61.51	62.82	60.89	61.64	60.77	61.40
Al_2O_3	24.88	24.79	24.82	24.83	25.10	25.45	24.81	24.29	25.18	24.78
FeO	0.05	0.04	0.04	0.01	0.01	0.02	0.00	0.01	0.04	0.02
CaO	6.12	5.94	5.30	6.27	5.94	5.87	5.90	5.53	6.24	5.63
Na_2O	8.19	8.28	8.62	8.30	8.42	8.54	8.32	8.37	8.05	8.38
K_2O	0.03	0.04	0.06	0.04	0.07	0.02	0.07	0.05	0.07	0.06
Total	99.50	100.50	100.32	99.97	101.04	102.72	99.99	99.88	100.34	100.27
Si	2.69	2.71	2.72	2.69	2.70	2.71	2.71	2.74	2.69	2.72
Al	1.31	1.29	1.29	1.30	1.30	1.30	1.30	1.27	1.31	1.29
Fe	0.00	0.00	0.00	0.00	0.00	0.00	0.00	0.00	0.00	0.00
Ca	0.29	0.28	0.25	0.30	0.28	0.27	0.28	0.26	0.30	0.27
Na	0.71	0.71	0.74	0.72	0.72	0.71	0.72	0.72	0.69	0.72
K	0.00	0.00	0.00	0.00	0.00	0.00	0.00	0.00	0.00	0.00
Or	0.00	0.00	0.00	0.00	0.00	0.00	0.00	0.00	0.00	0.00
Ab	0.71	0.71	0.74	0.70	0.72	0.72	0.72	0.73	0.70	0.73
An	0.29	0.28	0.25	0.29	0.28	0.28	0.28	0.27	0.30	0.27

Table 3 continued. Plagioclase analyses from the sillimanite-K-feldspar zone, sample 07905.

	1#1	1#2	1#3	1#4	1#5	1#6	1#7	2#1	2#2	2#3	2#4	2#5	2#6	2#7	2#8	2#9	2#10
SiO_2	59.30	58.79	58.72	59.05	59.21	58.82	60.37	58.03	59.76	60.23	58.44	59.19	59.71	58.18	58.04	58.99	58.36
Al_2O_3	26.16	25.90	26.11	26.57	26.03	26.09	26.04	26.44	26.54	26.01	26.09	26.33	27.49	26.82	26.95	27.26	26.63
FeO	0.03	0.01	0.05	0.05	0.05	0.11	0.21	0.01	0.06	0.07	0.01	0.03	0.01	0.04	0.02	0.02	0.00
CaO	7.36	7.57	7.72	7.91	7.51	7.31	6.83	7.92	7.64	7.13	7.52	7.75	8.14	8.21	8.25	8.61	8.17
Na_2O	7.40	7.26	7.20	7.18	7.39	7.17	7.72	7.17	7.60	7.61	7.22	7.23	6.92	6.98	6.96	7.01	6.86
K_2O	0.08	0.09	0.09	0.09	0.09	0.14	0.09	0.10	0.12	0.09	0.08	0.07	0.11	0.10	0.11	0.10	0.08
Total	100.33	99.62	99.90	100.85	100.28	99.63	101.27	99.67	101.72	101.13	99.36	100.61	102.38	100.33	100.31	101.97	100.10
Si	2.64	2.63	2.63	2.62	2.64	2.63	2.66	2.60	2.62	2.65	2.62	2.63	2.60	2.59	2.59	2.59	2.60
Al	1.37	1.37	1.38	1.39	1.37	1.38	1.35	1.40	1.37	1.35	1.38	1.38	1.41	1.41	1.42	1.41	1.40
Fe	0.00	0.00	0.00	0.00	0.00	0.00	0.01	0.00	0.00	0.00	0.00	0.00	0.00	0.00	0.00	0.00	0.00
Ca	0.35	0.36	0.37	0.38	0.36	0.35	0.32	0.38	0.36	0.34	0.36	0.37	0.38	0.39	0.39	0.40	0.39
Na	0.64	0.63	0.62	0.62	0.64	0.62	0.66	0.62	0.65	0.65	0.63	0.62	0.59	0.60	0.60	0.60	0.59
K	0.00	0.01	0.01	0.01	0.01	0.01	0.01	0.01	0.01	0.00	0.00	0.00	0.01	0.01	0.01	0.01	0.00
Or	0.00	0.01	0.01	0.01	0.01	0.01	0.01	0.01	0.01	0.00	0.00	0.00	0.01	0.01	0.01	0.01	0.00
Ab	0.64	0.63	0.62	0.62	0.64	0.63	0.67	0.62	0.64	0.66	0.63	0.63	0.60	0.60	0.60	0.59	0.60
An	0.35	0.36	0.37	0.38	0.36	0.36	0.33	0.38	0.35	0.34	0.36	0.37	0.39	0.39	0.39	0.40	0.40

Table 4. Garnet analyses from the garnet zone, sample 05403.

	1#1	1#3	1#4	1#5	1#6	1#7	1#8	1#9	1#10	1#11	1#12	1#13	1#14	1#15	1#16	1#17	1#18
SiO_2	36.34	36.52	36.44	36.36	36.28	36.27	36.41	36.16	36.43	36.28	36.43	36.38	36.49	36.51	36.21	36.24	36.24
TiO_2	0.18	0.21	0.09	0.14	0.13	0.14	0.20	0.20	0.19	0.28	0.07	0.05	0.17	0.12	0.23	0.24	0.16
Al_2O_3	20.99	20.87	21.03	20.83	20.93	20.84	20.92	20.86	20.86	20.98	20.76	20.75	20.77	20.78	20.70	20.78	20.91
Fe_2O_3	0.09	0.33	0.76	0.73	1.13	1.31	0.68	1.42	0.81	0.96	1.02	0.47	0.87	0.79	0.75	1.01	1.26
FeO	36.17	35.32	33.98	32.48	31.19	29.56	28.29	27.70	30.32	30.42	26.16	26.21	25.99	26.02	25.75	25.50	25.42
MnO	1.76	2.81	3.57	4.34	5.84	7.13	8.30	8.46	5.76	5.61	10.04	10.19	10.34	10.50	10.54	10.55	10.76
MgO	1.77	1.70	1.55	1.42	1.28	1.12	0.98	1.06	1.30	1.26	0.92	0.87	0.88	0.88	0.87	0.86	0.90
CaO	1.95	2.07	2.58	3.29	3.21	3.67	4.11	4.12	4.11	4.12	4.40	4.27	4.49	4.32	4.32	4.55	4.35
Total	99.23	99.79	99.92	99.52	99.89	99.93	99.82	99.83	99.71	99.81	99.71	99.14	99.91	99.83	99.31	99.63	99.88
Si	2.97	2.98	2.97	2.97	2.96	2.96	2.97	2.95	2.97	2.96	2.98	2.98	2.97	2.98	2.97	2.96	2.96
Al^{IV}	0.03	0.02	0.03	0.03	0.04	0.04	0.03	0.05	0.03	0.04	0.02	0.02	0.03	0.02	0.03	0.04	0.04
Al^{VI}	2.00	1.98	1.99	1.98	1.98	1.97	1.98	1.96	1.97	1.97	1.97	1.99	1.97	1.98	1.97	1.97	1.97
Fe^{3+}	0.01	0.02	0.05	0.05	0.07	0.08	0.04	0.09	0.05	0.06	0.06	0.03	0.05	0.05	0.05	0.06	0.08
Ti	0.01	0.01	0.01	0.01	0.01	0.01	0.01	0.01	0.01	0.02	0.00	0.00	0.01	0.01	0.01	0.01	0.01
Fe^{2+}	2.48	2.41	2.32	2.22	2.13	2.02	1.93	1.89	2.07	2.07	1.79	1.80	1.77	1.77	1.77	1.74	1.73
Mn	0.12	0.19	0.25	0.30	0.40	0.49	0.57	0.59	0.40	0.39	0.69	0.71	0.71	0.73	0.73	0.73	0.74
Mg	0.22	0.21	0.19	0.17	0.16	0.14	0.12	0.13	0.16	0.15	0.11	0.11	0.11	0.11	0.11	0.10	0.11
Ca	0.17	0.18	0.22	0.29	0.28	0.32	0.36	0.36	0.36	0.36	0.39	0.38	0.39	0.38	0.38	0.40	0.38
X_{Alm}	0.83	0.81	0.78	0.74	0.72	0.68	0.65	0.64	0.69	0.70	0.60	0.60	0.59	0.59	0.59	0.59	0.58
X_{Prp}	0.07	0.07	0.06	0.06	0.05	0.05	0.04	0.04	0.05	0.05	0.04	0.04	0.04	0.04	0.04	0.04	0.04
X_{Grs}	0.06	0.06	0.08	0.10	0.09	0.11	0.12	0.12	0.12	0.12	0.13	0.13	0.13	0.13	0.13	0.13	0.13
X_{Sps}	0.04	0.07	0.08	0.10	0.14	0.17	0.19	0.20	0.13	0.13	0.23	0.24	0.24	0.24	0.25	0.25	0.25
Mg#	0.08	0.08	0.08	0.07	0.07	0.06	0.06	0.06	0.07	0.07	0.06	0.06	0.06	0.06	0.06	0.06	0.06

Cations calculated on a 12-oxygen basis. X_{Alm} = Fe(II)/(Fe(II)+Mn+Mg+Ca), X_{Grs} = Ca/(Fe(II)+Mn+Mg+Ca), X_{Sps} = Mn/(Fe(II)+Mn+Mg+Ca), X_{Prp} = Mg/(Fe(II)+Mn+Mg+Ca), Mg# = Mg/(Fe(II)+Mg)

Table 4 continued. Garnet analyses from the garnet zone, sample 05403.

	1#19	1#20	1#21	1#22	1#23	1#24	1#25	1#26	1#27	1#28	1#29	1#30	1#31	1#32	1#33	1#34	1#35	1#36
SiO_2	36.35	36.42	36.36	36.52	36.27	36.60	36.38	36.16	36.41	36.56	36.46	36.43	36.41	36.19	36.40	36.39	36.53	36.52
TiO_2	0.18	0.19	0.25	0.14	0.16	0.24	0.12	0.13	0.09	0.03	0.12	0.14	0.11	0.11	0.11	0.07	0.14	0.13
Al_2O_3	20.77	20.65	20.71	20.64	20.65	20.67	20.72	20.80	20.88	20.78	20.57	20.72	20.78	20.73	20.80	20.88	20.76	20.68
Fe_2O_3	1.22	1.34	1.01	0.89	1.41	0.97	1.58	1.75	1.13	1.20	0.55	0.78	0.65	0.91	0.63	1.05	0.27	0.14
FeO	25.27	24.98	25.51	26.21	26.76	28.44	27.71	27.65	28.37	28.88	29.15	30.99	32.23	32.76	33.66	33.89	35.57	36.46
MnO	10.84	10.64	10.59	10.03	9.08	7.94	8.16	8.37	8.13	7.89	7.34	6.18	5.58	4.64	3.97	3.44	2.47	1.99
MgO	0.84	0.83	0.88	0.94	0.98	1.07	1.04	1.02	1.03	1.05	1.08	1.23	1.24	1.37	1.45	1.56	1.65	1.65
CaO	4.58	5.07	4.60	4.50	4.53	4.36	4.50	4.23	4.06	3.90	4.05	3.30	2.75	2.70	2.62	2.68	2.19	1.85
Total	99.93	99.99	99.80	99.78	99.70	100.20	100.05	99.95	99.99	100.19	99.27	99.70	99.69	99.33	99.57	99.85	99.55	99.40
Si	2.97	2.97	2.97	2.98	2.97	2.97	2.97	2.95	2.97	2.98	2.99	2.98	2.98	2.97	2.98	2.97	2.99	2.99
Al^{IV}	0.03	0.03	0.03	0.02	0.03	0.03	0.03	0.05	0.03	0.02	0.01	0.02	0.02	0.03	0.02	0.03	0.01	0.01
Al^{VI}	1.96	1.95	1.96	1.97	1.96	1.96	1.96	1.96	1.97	1.97	1.98	1.97	1.98	1.98	1.98	1.98	1.99	1.99
Fe^{3+}	0.07	0.08	0.06	0.05	0.09	0.06	0.10	0.11	0.07	0.07	0.03	0.05	0.04	0.06	0.04	0.06	0.02	0.01
Ti	0.01	0.01	0.02	0.01	0.01	0.01	0.01	0.01	0.01	0.00	0.01	0.01	0.01	0.01	0.01	0.00	0.01	0.01
Fe^{2+}	1.72	1.70	1.74	1.79	1.83	1.93	1.89	1.89	1.93	1.97	2.00	2.12	2.21	2.25	2.30	2.31	2.43	2.50
Mn	0.75	0.73	0.73	0.69	0.63	0.55	0.56	0.58	0.56	0.54	0.51	0.43	0.39	0.32	0.28	0.24	0.17	0.14
Mg	0.10	0.10	0.11	0.11	0.12	0.13	0.13	0.12	0.12	0.13	0.13	0.15	0.15	0.17	0.18	0.19	0.20	0.20
Ca	0.40	0.44	0.40	0.39	0.40	0.38	0.39	0.37	0.35	0.34	0.36	0.29	0.24	0.24	0.23	0.23	0.19	0.16
X_{Alm}	0.58	0.57	0.58	0.60	0.61	0.65	0.64	0.64	0.65	0.66	0.67	0.71	0.74	0.76	0.77	0.78	0.81	0.83
X_{Prp}	0.03	0.03	0.04	0.04	0.04	0.04	0.04	0.04	0.04	0.04	0.04	0.05	0.05	0.06	0.06	0.06	0.07	0.07
X_{Grs}	0.13	0.15	0.13	0.13	0.13	0.13	0.13	0.13	0.12	0.11	0.12	0.10	0.08	0.08	0.08	0.08	0.06	0.05
X_{Sps}	0.25	0.25	0.25	0.23	0.21	0.18	0.19	0.20	0.19	0.18	0.17	0.14	0.13	0.11	0.09	0.08	0.06	0.05
Mg#	0.06	0.06	0.06	0.06	0.06	0.06	0.06	0.06	0.06	0.06	0.06	0.07	0.06	0.07	0.07	0.08	0.08	0.07

Table 4 continued. Garnet analyses from the staurolite zone, sample 05501.

	1#1	1#2	1#3	1#4	1#5	1#6	1#7	1#8	1#9	1#10	1#11	1#12	1#13	1#14	1#15
SiO_2	36.74	36.41	36.63	36.46	36.62	36.53	36.32	36.68	36.44	36.42	36.32	36.49	36.46	36.43	36.10
TiO_2	0.13	0.15	0.15	0.11	0.14	0.03	0.17	0.20	0.25	0.14	0.15	0.15	0.02	0.16	0.14
Al_2O_3	20.99	20.96	21.15	21.08	20.95	20.94	20.82	20.78	20.95	20.99	21.00	20.89	20.74	20.79	20.87
Fe_2O_3	0.32	0.66	0.56	0.85	0.65	0.78	0.84	0.18	0.20	0.47	0.71	0.56	0.48	0.85	1.09
FeO	36.63	36.05	36.10	35.47	35.27	34.75	34.30	34.27	34.02	33.69	33.00	32.81	32.84	32.01	31.70
MnO	1.99	2.07	2.20	2.42	2.77	3.34	3.70	4.46	4.62	4.89	5.38	5.74	5.98	6.50	6.86
MgO	2.10	2.11	2.04	1.98	2.00	1.90	1.84	1.73	1.65	1.61	1.60	1.48	1.44	1.39	1.35
CaO	1.30	1.37	1.54	1.74	1.76	1.70	1.76	1.70	1.68	1.69	1.78	1.95	1.67	2.05	1.75
Total	100.17	99.73	100.32	100.03	100.11	99.89	99.68	99.97	99.79	99.84	99.88	100.02	99.58	100.11	99.75
Si	2.98	2.97	2.97	2.97	2.98	2.98	2.97	2.99	2.97	2.97	2.97	2.98	2.99	2.97	2.96
Al^{IV}	0.02	0.03	0.03	0.03	0.02	0.02	0.03	0.01	0.03	0.03	0.03	0.02	0.01	0.03	0.04
Al^{VI}	1.99	1.98	1.99	1.99	1.98	1.99	1.98	1.98	1.99	1.99	1.99	1.98	1.99	1.97	1.98
Fe^{3+}	0.02	0.04	0.03	0.05	0.04	0.05	0.05	0.01	0.01	0.03	0.04	0.03	0.03	0.05	0.07
Ti	0.01	0.01	0.01	0.01	0.01	0.00	0.01	0.01	0.02	0.01	0.01	0.01	0.00	0.01	0.01
Fe^{2+}	2.49	2.46	2.45	2.41	2.40	2.37	2.34	2.33	2.32	2.30	2.25	2.24	2.25	2.18	2.17
Mn	0.14	0.14	0.15	0.17	0.19	0.23	0.26	0.31	0.32	0.34	0.37	0.40	0.42	0.45	0.48
Mg	0.25	0.26	0.25	0.24	0.24	0.23	0.22	0.21	0.20	0.20	0.19	0.18	0.18	0.17	0.16
Ca	0.11	0.12	0.13	0.15	0.15	0.15	0.15	0.15	0.15	0.15	0.16	0.17	0.15	0.18	0.15
X_{Alm}	0.83	0.83	0.82	0.81	0.80	0.80	0.79	0.78	0.78	0.77	0.76	0.75	0.75	0.73	0.73
X_{Prp}	0.08	0.09	0.08	0.08	0.08	0.08	0.08	0.07	0.07	0.07	0.07	0.06	0.06	0.06	0.06
X_{Grs}	0.038	0.040	0.04	0.05	0.05	0.05	0.05	0.05	0.05	0.05	0.05	0.06	0.05	0.06	0.05
X_{Sps}	0.05	0.05	0.05	0.06	0.06	0.08	0.09	0.10	0.11	0.11	0.13	0.13	0.14	0.15	0.16
Mg#	0.09	0.09	0.09	0.09	0.09	0.09	0.09	0.08	0.08	0.08	0.08	0.07	0.07	0.07	0.07

Table 4 continued. Garnet analyses from the staurolite zone, sample 05501.

	1#16	1#17	1#18	1#19	1#20	1#21	1#22	1#23	1#24	1#25	1#26	1#27	1#28	1#29	1#30
SiO_2	36.21	36.28	36.23	36.24	36.09	36.31	36.41	36.30	36.26	36.26	36.35	36.21	36.22	36.24	36.26
TiO_2	0.18	0.21	0.18	0.21	0.23	0.15	0.11	0.08	0.09	0.02	0.02	0.11	0.00	0.02	0.02
Al_2O_3	20.89	20.84	20.78	20.80	20.73	20.81	20.70	20.81	20.82	20.81	20.89	20.88	20.81	20.89	20.77
Fe_2O_3	0.85	0.53	0.82	0.44	0.88	0.25	0.51	0.42	0.28	0.70	0.42	0.65	1.06	0.74	0.58
FeO	31.72	31.87	31.51	31.66	31.43	31.80	31.63	31.60	31.72	31.74	31.93	31.78	31.65	31.76	31.96
MnO	6.92	6.93	6.96	7.16	7.29	7.13	7.21	7.16	7.13	6.83	6.96	6.84	6.79	6.76	6.56
MgO	1.37	1.33	1.32	1.27	1.29	1.29	1.30	1.27	1.28	1.33	1.33	1.37	1.35	1.36	1.40
CaO	1.78	1.81	2.01	1.83	1.76	1.74	1.86	1.85	1.73	1.82	1.67	1.75	1.86	1.80	1.78
Total	99.84	99.73	99.72	99.55	99.60	99.45	99.67	99.44	99.29	99.45	99.53	99.53	99.63	99.49	99.26
Si	2.96	2.97	2.97	2.97	2.96	2.98	2.98	2.98	2.98	2.98	2.98	2.97	2.97	2.97	2.98
Al^{IV}	0.04	0.03	0.03	0.03	0.04	0.02	0.02	0.02	0.02	0.02	0.02	0.03	0.03	0.03	0.02
Al^{VI}	1.98	1.98	1.98	1.98	1.97	1.99	1.98	1.99	2.00	1.99	2.00	1.99	1.98	1.99	1.99
Fe^{3+}	0.05	0.03	0.05	0.03	0.05	0.02	0.03	0.03	0.02	0.04	0.03	0.04	0.07	0.05	0.04
Ti	0.01	0.01	0.01	0.01	0.01	0.01	0.01	0.01	0.01	0.00	0.00	0.01	0.00	0.00	0.00
Fe^{2+}	2.17	2.18	2.16	2.17	2.16	2.18	2.17	2.17	2.18	2.18	2.19	2.18	2.17	2.18	2.20
Mn	0.48	0.48	0.48	0.50	0.51	0.50	0.50	0.50	0.50	0.48	0.48	0.48	0.47	0.47	0.46
Mg	0.17	0.16	0.16	0.16	0.16	0.16	0.16	0.15	0.16	0.16	0.16	0.17	0.16	0.17	0.17
Ca	0.16	0.16	0.18	0.16	0.15	0.15	0.16	0.16	0.15	0.16	0.15	0.15	0.16	0.16	0.16
X_{Alm}	0.73	0.73	0.72	0.73	0.72	0.73	0.72	0.73	0.73	0.73	0.73	0.73	0.73	0.73	0.74
X_{Prp}	0.06	0.05	0.05	0.05	0.05	0.05	0.05	0.05	0.05	0.05	0.05	0.06	0.06	0.06	0.06
X_{Grs}	0.05	0.05	0.06	0.05	0.05	0.05	0.05	0.05	0.05	0.05	0.05	0.05	0.06	0.05	0.05
X_{Sps}	0.16	0.16	0.16	0.17	0.17	0.17	0.17	0.17	0.17	0.16	0.16	0.16	0.16	0.16	0.15
Mg#	0.07	0.07	0.07	0.07	0.07	0.07	0.07	0.07	0.07	0.07	0.07	0.07	0.07	0.07	0.07

Table 4 continued. Garnet analyses from the staurolite zone, sample 05501.

	1#31	1#32	1#33	1#34	1#35	1#36	1#37	1#38	1#39	1#40	1#41	1#42	1#43	1#44	1#45
SiO_2	36.20	36.28	36.44	36.31	36.29	36.26	36.39	36.25	36.22	36.55	36.35	36.50	36.35	36.28	36.32
TiO_2	0.13	0.05	0.10	0.16	0.17	0.17	0.21	0.17	0.15	0.13	0.08	0.12	0.05	0.07	0.11
Al_2O_3	20.85	20.81	20.93	20.90	20.73	20.81	20.83	20.77	20.79	20.84	20.82	20.81	20.95	20.76	20.77
Fe_2O_3	1.08	0.90	0.63	0.56	0.17	0.70	0.32	0.93	1.27	0.52	1.20	0.80	0.99	1.33	1.12
FeO	31.94	31.91	32.45	32.54	32.99	33.32	34.19	34.10	34.28	34.89	34.77	35.33	35.19	35.47	35.66
MnO	6.48	6.39	6.20	6.14	5.44	4.97	4.01	3.91	3.68	3.19	2.90	2.66	2.40	2.16	2.11
MgO	1.43	1.43	1.47	1.44	1.50	1.63	1.73	1.77	1.85	1.88	1.97	1.93	1.99	2.08	2.08
CaO	1.84	1.96	1.80	1.74	1.84	1.74	1.85	1.79	1.67	1.84	1.82	1.79	1.83	1.63	1.58
Total	99.83	99.64	99.95	99.73	99.13	99.53	99.49	99.59	99.77	99.79	99.78	99.86	99.66	99.63	99.64
Si	2.96	2.97	2.97	2.97	2.98	2.97	2.98	2.97	2.96	2.98	2.97	2.98	2.97	2.97	2.97
Al^{IV}	0.04	0.03	0.03	0.03	0.02	0.03	0.02	0.03	0.04	0.02	0.03	0.02	0.03	0.03	0.03
Al^{VI}	1.98	1.98	1.99	1.99	1.99	1.98	1.98	1.97	1.97	1.98	1.97	1.98	1.98	1.97	1.97
Fe^{3+}	0.07	0.06	0.04	0.03	0.01	0.04	0.02	0.06	0.08	0.03	0.07	0.05	0.06	0.08	0.07
Ti	0.01	0.00	0.01	0.01	0.01	0.01	0.01	0.01	0.01	0.01	0.01	0.01	0.00	0.00	0.01
Fe^{2+}	2.19	2.19	2.22	2.23	2.27	2.28	2.34	2.34	2.35	2.38	2.37	2.41	2.40	2.43	2.44
Mn	0.45	0.44	0.43	0.43	0.38	0.35	0.28	0.27	0.25	0.22	0.20	0.18	0.17	0.15	0.15
Mg	0.17	0.17	0.18	0.18	0.18	0.20	0.21	0.22	0.23	0.23	0.24	0.23	0.24	0.25	0.25
Ca	0.16	0.17	0.16	0.15	0.16	0.15	0.16	0.16	0.15	0.16	0.16	0.16	0.16	0.14	0.14
X_{Alm}	0.74	0.73	0.74	0.75	0.76	0.77	0.78	0.78	0.79	0.80	0.80	0.81	0.81	0.82	0.82
X_{Prp}	0.06	0.06	0.06	0.06	0.06	0.07	0.07	0.07	0.08	0.08	0.08	0.08	0.08	0.09	0.09
X_{Grs}	0.05	0.06	0.05	0.05	0.05	0.05	0.05	0.05	0.05	0.05	0.05	0.05	0.05	0.05	0.05
X_{Sps}	0.15	0.15	0.14	0.14	0.13	0.12	0.09	0.09	0.09	0.07	0.07	0.06	0.06	0.05	0.05
Mg#	0.07	0.07	0.07	0.07	0.08	0.08	0.08	0.08	0.09	0.09	0.09	0.09	0.09	0.09	0.09

Table 4 continued. Garnet analyses from the kyanite zone, sample 077401.

	1#1	1#2	1#3	1#4	1#5	1#6	1#7	1#8	1#9	1#10	1#11	1#12	1#13	1#14	1#15
SiO_2	37.12	36.98	37.21	37.06	36.95	37.22	37.10	37.08	36.93	36.73	36.98	36.78	36.56	36.72	36.68
TiO_2	0.01	0.00	0.00	0.00	0.00	0.00	0.00	0.03	0.00	0.01	0.01	0.02	0.00	0.00	0.02
Al_2O_3	21.30	21.27	21.18	21.27	21.39	21.20	21.16	20.98	21.07	21.07	21.06	20.99	20.82	21.01	20.98
Fe_2O_3	0.79	0.77	0.75	0.75	0.76	0.79	0.80	0.81	0.84	0.83	0.89	0.91	0.91	0.92	0.93
FeO	28.18	28.24	28.32	28.40	28.48	28.46	28.49	28.52	28.54	28.57	28.56	28.57	28.60	28.62	28.65
MnO	5.37	6.15	6.08	6.06	6.12	6.13	6.22	6.44	6.49	6.47	6.31	6.20	6.17	6.25	6.46
MgO	2.80	2.75	2.80	2.84	3.01	3.08	3.17	3.11	3.18	3.10	2.84	2.85	2.85	2.97	3.11
CaO	1.46	1.47	1.79	2.27	1.92	2.11	1.85	1.84	2.01	2.20	3.34	3.52	3.43	3.16	2.53
Total	100.80	100.80	100.86	100.59	100.67	100.79	100.77	100.62	100.18	99.79	99.40	98.95	98.35	98.91	99.35
Si	2.99	2.99	3.00	2.99	2.98	3.00	2.99	3.00	2.99	2.99	3.01	3.00	3.01	3.00	2.99
Al^{IV}	0.01	0.01	0.00	0.01	0.02	0.00	0.01	0.00	0.01	0.01	0.00	0.00	0.00	0.00	0.01
Al^{VI}	2.02	2.02	2.02	2.02	2.02	2.01	2.00	2.00	2.01	2.01	2.02	2.03	2.02	2.03	2.01
Fe^{3+}	0.00	0.00	0.00	0.00	0.00	0.00	0.01	0.00	0.00	0.00	0.00	0.00	0.00	0.00	0.00
Ti	0.00	0.00	0.00	0.00	0.00	0.00	0.00	0.00	0.00	0.00	0.00	0.00	0.00	0.00	0.00
Fe^{2+}	2.21	2.18	2.15	2.10	2.11	2.09	2.10	2.11	2.07	2.06	1.96	1.95	1.96	1.97	2.02
Mn	0.30	0.34	0.34	0.34	0.34	0.34	0.35	0.36	0.36	0.36	0.35	0.35	0.35	0.35	0.36
Mg	0.34	0.33	0.34	0.34	0.36	0.37	0.38	0.38	0.38	0.38	0.34	0.35	0.35	0.36	0.38
Ca	0.13	0.13	0.15	0.20	0.17	0.18	0.16	0.16	0.17	0.19	0.29	0.31	0.30	0.28	0.22
X_{Alm}	0.74	0.73	0.72	0.71	0.71	0.70	0.70	0.70	0.69	0.69	0.66	0.66	0.66	0.66	0.68
X_{Prp}	0.11	0.11	0.11	0.11	0.12	0.12	0.13	0.12	0.13	0.13	0.12	0.12	0.12	0.12	0.13
X_{Grs}	0.04	0.04	0.05	0.07	0.06	0.06	0.05	0.05	0.06	0.06	0.10	0.10	0.10	0.09	0.07
X_{Sps}	0.10	0.12	0.11	0.11	0.11	0.11	0.12	0.12	0.12	0.12	0.12	0.12	0.12	0.12	0.12
Mg#	0.13	0.13	0.14	0.14	0.15	0.15	0.15	0.15	0.16	0.15	0.15	0.15	0.15	0.16	0.16

Table 4 continued. Garnet analyses from the kyanite zone, sample 077401.

	1#16	1#17	1#18	1#19	1#20	1#21	1#22	1#23	1#24	1#25	1#26	1#27	1#28	1#29
SiO_2	36.80	36.67	36.58	37.01	36.57	36.85	36.77	35.87	36.97	36.88	36.85	36.48	36.22	36.24
TiO_2	0.09	0.20	0.02	0.00	0.03	0.02	0.04	0.01	0.00	0.00	0.01	0.00	0.00	0.00
Al_2O_3	20.92	20.90	21.04	20.93	20.89	21.05	21.00	20.57	20.91	20.98	21.11	20.92	20.98	20.82
Fe_2O_3	0.93	0.94	0.93	0.92	0.90	0.88	0.87	0.85	0.82	0.82	0.82	0.82	0.84	0.85
FeO	28.68	28.69	28.71	28.75	28.79	28.81	28.84	28.85	28.87	28.85	28.80	28.74	28.65	28.56
MnO	6.56	6.63	6.76	6.74	6.77	6.67	6.61	6.36	6.27	6.24	6.13	6.24	6.04	5.28
MgO	3.06	2.97	3.02	3.08	3.11	3.07	2.98	2.93	3.10	2.97	2.83	2.87	2.82	2.77
CaO	2.38	2.43	2.17	2.02	2.03	2.25	2.08	1.89	1.92	2.09	2.07	1.44	1.09	1.60
Total	99.51	99.25	99.58	100.17	99.87	100.48	100.27	98.02	100.04	100.21	100.29	99.86	99.42	99.24
Si	3.00	3.00	2.99	3.00	2.98	2.99	2.99	2.98	3.00	2.99	2.99	2.98	2.98	2.98
Al^{IV}	0.00	0.00	0.01	0.00	0.02	0.01	0.01	0.02	0.00	0.01	0.01	0.02	0.02	0.02
Al^{VI}	2.01	2.01	2.01	2.01	1.99	2.00	2.00	2.00	2.00	2.00	2.01	2.00	2.01	2.00
Fe^{3+}	0.00	0.00	0.00	0.00	0.03	0.02	0.02	0.03	0.00	0.01	0.00	0.03	0.03	0.04
Ti	0.01	0.01	0.00	0.00	0.00	0.00	0.00	0.00	0.00	0.00	0.00	0.00	0.00	0.00
Fe^{2+}	2.02	2.01	2.05	2.06	2.05	2.05	2.08	2.09	2.10	2.10	2.13	2.15	2.19	2.20
Mn	0.37	0.37	0.38	0.38	0.38	0.37	0.37	0.37	0.35	0.35	0.34	0.35	0.34	0.30
Mg	0.37	0.36	0.37	0.37	0.38	0.37	0.36	0.36	0.38	0.36	0.34	0.35	0.35	0.34
Ca	0.21	0.21	0.19	0.18	0.18	0.19	0.18	0.17	0.17	0.18	0.18	0.13	0.10	0.14
X_{Alm}	0.68	0.68	0.69	0.69	0.69	0.69	0.69	0.70	0.70	0.70	0.71	0.72	0.74	0.74
X_{Prp}	0.12	0.12	0.12	0.12	0.13	0.12	0.12	0.12	0.13	0.12	0.11	0.12	0.12	0.11
X_{Grs}	0.07	0.07	0.06	0.06	0.06	0.07	0.06	0.06	0.06	0.06	0.06	0.04	0.03	0.05
X_{Sps}	0.12	0.13	0.13	0.13	0.13	0.13	0.12	0.12	0.12	0.12	0.11	0.12	0.12	0.10
Mg#	0.16	0.15	0.15	0.15	0.16	0.15	0.15	0.15	0.15	0.15	0.14	0.14	0.14	0.13

Table 4 continued. Garnet analyses from the sillimanite-K-feldspar zone, sample 07905.

	1#1	1#2	1#3	1#4	1#5	1#6	1#7	1#8	1#9	1#10	1#11	1#12	1#13	1#14	1#15	1#16	1#17	1#18
SiO_2	36.70	36.68	36.81	36.53	36.57	36.76	36.91	36.67	36.48	36.28	36.44	36.56	36.45	36.53	36.61	36.46	36.58	36.48
TiO_2	0.01	0.00	0.01	0.00	0.00	0.00	0.01	0.01	0.00	0.00	0.01	0.00	0.02	0.01	0.01	0.01	0.01	0.01
Al_2O_3	21.10	21.15	21.09	21.07	21.13	20.94	21.37	21.19	21.06	20.86	20.83	20.85	20.75	20.85	21.04	21.10	21.05	20.94
Fe_2O_3	0.00	0.00	0.00	0.00	0.00	0.00	0.00	0.00	0.00	0.00	0.00	0.00	0.00	0.00	0.00	0.00	0.00	0.00
FeO	32.21	31.99	31.80	31.24	31.05	30.78	30.50	30.56	30.39	30.65	30.76	30.74	30.64	30.48	30.04	30.01	29.92	29.77
MnO	4.99	5.37	5.56	5.83	6.17	6.16	6.17	6.57	6.61	6.67	6.74	6.79	6.97	6.93	7.10	7.07	7.11	7.16
MgO	2.54	2.61	2.58	2.67	2.61	2.61	2.63	2.57	2.57	2.60	2.60	2.56	2.53	2.55	2.43	2.50	2.49	2.50
CaO	2.15	2.04	1.99	1.98	1.95	1.95	1.95	1.98	1.92	1.98	2.06	2.04	2.05	2.05	2.03	2.05	2.13	2.14
Total	99.70	99.84	99.85	99.33	99.48	99.20	99.54	99.55	99.04	99.04	99.46	99.53	99.40	99.38	99.25	99.19	99.30	99.00
Si	2.99	2.99	3.00	2.99	2.99	3.01	3.01	3.00	3.00	2.99	2.99	3.00	3.00	3.00	3.00	2.99	3.00	3.00
Al^{IV}	0.01	0.01	0.00	0.01	0.01	0.00	0.00	0.00	0.00	0.01	0.01	0.00	0.00	0.00	0.00	0.01	0.00	0.00
Al^{VI}	2.02	2.02	2.02	2.02	2.03	2.02	2.05	2.04	2.04	2.01	2.01	2.01	2.01	2.02	2.04	2.04	2.03	2.03
Fe^{3+}	0.00	0.00	0.00	0.00	0.00	0.00	0.00	0.00	0.00	0.00	0.00	0.00	0.00	0.00	0.00	0.00	0.00	0.00
Ti	0.00	0.00	0.00	0.00	0.00	0.00	0.00	0.00	0.00	0.00	0.00	0.00	0.00	0.00	0.00	0.00	0.00	0.00
Fe^{2+}	2.20	2.18	2.17	2.14	2.12	2.11	2.08	2.09	2.09	2.11	2.11	2.11	2.11	2.09	2.06	2.06	2.05	2.05
Mn	0.28	0.30	0.31	0.33	0.35	0.35	0.35	0.37	0.38	0.38	0.38	0.38	0.40	0.39	0.40	0.40	0.40	0.41
Mg	0.31	0.32	0.31	0.33	0.32	0.32	0.32	0.31	0.31	0.32	0.32	0.31	0.31	0.31	0.30	0.31	0.30	0.31
Ca	0.19	0.18	0.17	0.17	0.17	0.17	0.17	0.17	0.17	0.17	0.18	0.18	0.18	0.18	0.18	0.18	0.19	0.19
X_{Alm}	0.74	0.73	0.73	0.72	0.72	0.72	0.71	0.71	0.71	0.71	0.71	0.71	0.70	0.70	0.70	0.70	0.70	0.69
X_{Prp}	0.10	0.11	0.11	0.11	0.11	0.11	0.11	0.11	0.11	0.11	0.11	0.10	0.10	0.10	0.10	0.10	0.10	0.10
X_{Grs}	0.06	0.06	0.06	0.06	0.06	0.06	0.06	0.06	0.06	0.06	0.06	0.06	0.06	0.06	0.06	0.06	0.06	0.06
X_{Sps}	0.09	0.10	0.11	0.11	0.12	0.12	0.12	0.13	0.13	0.13	0.13	0.13	0.13	0.13	0.14	0.14	0.14	0.14
Mg#	0.12	0.13	0.13	0.13	0.13	0.13	0.13	0.13	0.13	0.13	0.13	0.13	0.13	0.13	0.13	0.13	0.13	0.13

Table 4 continued. Garnet analyses from the sillimanite-K-feldspar zone, sample 07905.

	1#19	1#20	1#21	1#22	1#23	1#24	1#25	1#26	1#27	1#28	1#29	1#30	1#31	1#32	1#33	1#34	1#35	1#36
SiO_2	36.55	36.64	36.56	36.54	36.62	36.56	36.60	36.55	36.57	36.36	36.53	36.62	36.45	36.62	36.65	36.66	36.65	36.64
TiO_2	0.00	0.01	0.01	0.00	0.01	0.00	0.00	0.00	0.01	0.00	0.00	0.00	0.01	0.00	0.01	0.02	0.00	0.02
Al_2O_3	20.95	20.95	21.03	21.03	20.97	20.87	21.01	20.99	21.04	21.09	21.04	21.02	21.01	20.91	21.04	20.85	20.91	20.85
Fe_2O_3	0.00	0.00	0.00	0.00	0.00	0.00	0.00	0.00	0.00	0.00	0.00	0.00	0.00	0.00	0.00	0.00	0.00	0.00
FeO	29.80	29.79	29.94	29.93	30.28	30.26	30.47	30.21	30.63	30.46	30.75	30.65	31.07	31.12	31.54	31.82	31.90	32.51
MnO	7.11	7.11	7.15	7.13	7.08	6.93	6.93	6.84	6.82	6.66	6.56	6.32	6.19	6.10	5.86	5.60	5.33	4.87
MgO	2.51	2.48	2.49	2.52	2.52	2.59	2.56	2.50	2.62	2.59	2.64	2.63	2.64	2.58	2.62	2.53	2.50	2.53
CaO	2.09	2.06	2.06	2.05	2.04	2.05	1.98	1.98	1.99	1.97	1.94	2.02	2.02	2.01	1.97	1.99	2.06	2.12
Total	99.02	99.03	99.24	99.20	99.52	99.25	99.55	99.06	99.67	99.14	99.46	99.27	99.39	99.34	99.68	99.46	99.35	99.54
Si	3.01	3.01	3.00	3.00	3.00	3.00	3.00	3.00	2.99	2.99	2.99	3.00	2.99	3.00	2.99	3.00	3.00	3.00
Al^{IV}	0.00	0.00	0.00	0.00	0.00	0.00	0.00	0.00	0.01	0.01	0.01	0.00	0.01	0.00	0.01	0.00	0.00	0.00
Al^{VI}	2.03	2.03	2.03	2.03	2.02	2.02	2.02	2.04	2.02	2.03	2.02	2.03	2.02	2.02	2.02	2.01	2.02	2.00
Fe^{3+}	0.00	0.00	0.00	0.00	0.00	0.00	0.00	0.00	0.00	0.00	0.00	0.00	0.00	0.00	0.00	0.00	0.00	0.00
Ti	0.00	0.00	0.00	0.00	0.00	0.00	0.00	0.00	0.00	0.00	0.00	0.00	0.00	0.00	0.00	0.00	0.00	0.00
Fe^{2+}	2.05	2.05	2.05	2.05	2.07	2.08	2.09	2.08	2.10	2.09	2.11	2.10	2.13	2.13	2.15	2.18	2.18	2.22
Mn	0.40	0.40	0.41	0.40	0.40	0.39	0.39	0.39	0.39	0.38	0.37	0.36	0.35	0.35	0.33	0.32	0.30	0.28
Mg	0.31	0.30	0.31	0.31	0.31	0.32	0.31	0.31	0.32	0.32	0.32	0.32	0.32	0.32	0.32	0.31	0.31	0.31
Ca	0.18	0.18	0.18	0.18	0.18	0.18	0.17	0.17	0.17	0.17	0.17	0.18	0.18	0.18	0.17	0.17	0.18	0.19
X_{Alm}	0.70	0.70	0.70	0.70	0.70	0.70	0.70	0.71	0.70	0.71	0.71	0.71	0.71	0.72	0.72	0.73	0.74	0.74
X_{Prp}	0.10	0.10	0.10	0.10	0.10	0.11	0.11	0.10	0.11	0.11	0.11	0.11	0.11	0.11	0.11	0.10	0.10	0.10
X_{Grs}	0.06	0.06	0.06	0.06	0.06	0.06	0.06	0.06	0.06	0.06	0.06	0.06	0.06	0.06	0.06	0.06	0.06	0.06
X_{Sps}	0.14	0.14	0.14	0.14	0.14	0.13	0.13	0.13	0.13	0.13	0.13	0.12	0.12	0.12	0.11	0.11	0.10	0.09
Mg#	0.13	0.13	0.13	0.13	0.13	0.13	0.13	0.13	0.13	0.13	0.13	0.13	0.13	0.13	0.13	0.12	0.12	0.12

Table 5. Chlorite analyses from the garnet zone, sample 05403.

	1#1	1#2	1#3	1#4	1#5	1#6	2#1	3#1	4#1
SiO_2	24.64	24.71	24.05	24.45	24.16	24.32	24.50	25.00	25.14
TiO_2	0.06	0.08	0.03	0.08	0.03	0.08	0.05	0.05	0.05
Al_2O_3	22.81	23.11	23.16	22.81	22.92	23.01	23.17	23.02	22.17
FeO	27.58	27.81	28.04	27.38	27.26	27.47	28.42	27.90	27.87
MnO	0.05	0.06	0.05	0.08	0.04	0.06	0.06	0.04	0.05
MgO	11.50	11.39	11.38	11.69	11.51	11.50	11.27	11.70	12.07
Total	86.66	87.16	86.71	86.49	85.93	86.45	87.46	87.70	87.36
Si	5.31	5.29	5.31	5.28	5.25	5.25	5.25	5.32	5.38
Al^{IV}	2.69	2.71	2.69	2.72	2.75	2.75	2.75	2.68	2.62
Al^{VI}	3.10	3.13	0.00	3.08	3.12	3.11	3.10	3.09	2.97
Ti	0.01	0.01	0.01	0.01	0.01	0.01	0.01	0.01	0.01
Fe(ii)	4.97	4.98	3.10	4.94	4.95	4.96	5.09	4.96	4.99
Mn	0.01	0.01	4.97	0.01	0.01	0.01	0.01	0.01	0.01
Mg	3.69	3.64	0.01	3.76	3.73	3.70	3.60	3.71	3.85

Cations calculated on a 28-oxygen equivalents basis

"1#2" means the second analysis on chlorite 1

Chlorite 1 is in Qtz-rich band, 2, 3, and 4 are close to garnet and too small to get multiple analyses.

Table 6. Chloritoid and staurolite analyses from the staurolite zone.

	Chloritoid														
	g1#1	g1#2	g1#4	g1#5	g1#6	g1#7	g1#8	g1#9	g1#10	g1#11	1#1	1#2	1#3	1#4	1#5
SiO_2	25.13	25.12	25.22	25.17	25.39	25.19	24.94	25.06	25.46	25.34	25.42	25.51	25.33	25.12	25.35
TiO_2	0.05	0.02	0.01	0.01	0.00	0.00	0.01	0.00	0.02	0.00	0.00	0.02	0.02	0.00	0.00
Al_2O_3	40.99	40.90	40.94	40.91	40.84	40.93	40.83	40.52	41.03	40.52	41.03	40.95	40.84	40.97	41.16
FeO	23.82	24.06	24.30	24.04	23.96	23.58	23.91	24.03	24.37	23.84	23.83	23.86	23.43	23.90	24.08
MnO	0.17	0.16	0.15	0.17	0.16	0.17	0.18	0.20	0.16	0.18	0.18	0.16	0.18	0.18	0.20
MgO	2.15	2.25	2.19	2.27	2.39	2.36	2.39	2.29	2.19	2.22	2.13	2.36	2.51	2.49	2.55
Total	92.32	92.51	92.82	92.58	92.74	92.24	92.26	92.11	93.24	92.10	92.59	92.86	92.31	92.67	93.33
Si	2.06	2.06	2.06	2.06	2.08	2.07	2.05	2.07	2.07	2.09	2.08	2.08	2.08	2.06	2.06
Ti	0.00	0.00	0.00	0.00	0.00	0.00	0.00	0.00	0.00	0.00	0.00	0.00	0.00	0.00	0.00
Al	3.97	3.96	3.95	3.95	3.94	3.96	3.96	3.94	3.94	3.93	3.96	3.94	3.95	3.95	3.95
Fe	1.64	1.65	1.66	1.65	1.64	1.62	1.65	1.66	1.66	1.64	1.63	1.63	1.61	1.64	1.64
Mn	0.01	0.01	0.01	0.01	0.01	0.01	0.01	0.01	0.01	0.01	0.01	0.01	0.01	0.01	0.01
Mg	0.26	0.28	0.27	0.28	0.29	0.29	0.29	0.28	0.27	0.27	0.26	0.29	0.31	0.30	0.31

Cations calculated on a 12-oxygen equivalents basis

"1#2" means the second analysis on chloritoid 1

Chloritoid g1 and 2 are close to garnet, chloritoid 1 is close to staurolite.

Table 6 continued. Chloritoid and staurolite analyses from the staurolite zone.

	Chloritoid							Staurolite						
	1#6	1#7	1#8	2#1	2#3	2#4	2#6	2#1	2#2	2#3	2#4	2#5	2#6	2#7
SiO_2	25.40	25.23	25.20	25.35	25.35	25.04	25.32	28.47	28.25	28.52	28.83	28.64	28.23	28.72
TiO_2	0.00	0.00	0.03	0.01	0.00	0.00	0.04	0.28	0.36	0.20	0.18	0.17	0.41	0.33
Al_2O_3	40.98	40.99	40.77	40.98	40.98	40.94	41.01	53.96	54.47	53.84	53.65	54.09	53.65	54.04
FeO	23.71	23.95	23.90	23.90	24.07	24.23	24.00	13.77	13.89	13.88	14.09	13.82	13.98	13.62
MnO	0.18	0.17	0.17	0.18	0.21	0.26	0.24	0.08	0.08	0.06	0.08	0.06	0.08	0.08
MgO	2.40	2.39	2.47	2.37	2.40	2.41	2.34	1.16	1.21	1.20	1.22	1.23	1.18	1.12
Total	92.67	92.73	92.56	92.80	93.02	92.88	92.94	97.72	98.27	97.72	98.05	98.02	97.52	97.91
Si	2.08	2.06	2.07	2.07	2.07	2.05	2.07	2.06	2.03	2.06	2.08	2.06	2.05	2.07
Ti	0.00	0.00	0.00	0.00	0.00	0.00	0.00	0.02	0.02	0.01	0.01	0.01	0.02	0.02
Al	3.95	3.95	3.94	3.95	3.94	3.95	3.95	4.60	4.62	4.59	4.56	4.59	4.59	4.59
Fe	1.62	1.64	1.64	1.63	1.64	1.66	1.64	0.83	0.84	0.84	0.85	0.83	0.85	0.82
Mn	0.01	0.01	0.01	0.01	0.01	0.02	0.02	0.00	0.01	0.00	0.00	0.00	0.00	0.00
Mg	0.29	0.29	0.30	0.29	0.29	0.29	0.28	0.13	0.13	0.13	0.13	0.13	0.13	0.12

Table 7. K-feldspar analyses from the sillimanite-K-feldspar zone, sample 07905.

	1#1	1#2	1#3	2#1	3#1	3#2	3#3	3#4	4#1	4#2	5#1	6#1	7#1	8#1	9#1
SiO_2	63.84	64.84	64.67	63.75	65.10	64.97	66.15	64.72	63.68	63.75	65.77	64.35	63.85	65.03	65.88
Al_2O_3	18.38	18.37	18.31	19.49	18.82	18.21	18.62	18.42	18.60	18.05	18.49	18.71	18.73	18.00	19.20
FeO	0.02	0.02	0.05	0.06	0.01	0.01	0.01	0.13	0.22	0.19	0.08	0.01	0.03	0.01	0.07
MnO	0.00	0.00	0.01	0.00	0.03	0.00	0.00	0.00	0.02	0.00	0.06	0.00	0.00	0.00	0.00
CaO	0.00	0.00	0.00	0.76	0.02	0.00	0.02	0.03	0.00	0.01	0.02	0.20	0.11	0.01	0.06
Na_2O	0.25	0.17	0.20	0.59	0.15	0.17	0.15	0.18	0.17	0.23	0.18	0.42	0.50	0.09	0.30
K_2O	16.63	16.60	16.50	15.46	16.45	16.51	16.84	16.42	16.59	16.25	16.63	16.02	15.57	16.61	16.55
Total	99.11	100.00	99.73	100.12	100.57	99.89	101.80	99.90	99.28	98.49	101.23	99.70	98.78	99.75	102.05
Si	2.99	3.00	3.00	2.94	2.99	3.01	3.00	3.00	2.98	3.00	3.00	2.98	2.98	3.01	2.98
Al	1.01	1.00	1.00	1.06	1.02	0.99	1.00	1.00	1.02	1.00	1.00	1.02	1.03	0.98	1.02
Fe	0.00	0.00	0.00	0.00	0.00	0.00	0.00	0.00	0.01	0.01	0.00	0.00	0.00	0.00	0.00
Mn	0.00	0.00	0.00	0.00	0.00	0.00	0.00	0.00	0.00	0.00	0.00	0.00	0.00	0.00	0.00
Ca	0.00	0.00	0.00	0.04	0.00	0.00	0.00	0.00	0.00	0.00	0.00	0.01	0.01	0.00	0.00
Na	0.02	0.01	0.02	0.05	0.01	0.02	0.01	0.02	0.02	0.02	0.02	0.04	0.05	0.01	0.03
K	0.99	0.98	0.98	0.91	0.96	0.97	0.98	0.97	0.99	0.97	0.97	0.95	0.93	0.98	0.96
Or	0.98	0.99	0.98	0.91	0.99	0.98	0.99	0.98	0.98	0.98	0.98	0.95	0.95	0.99	0.97
Ab	0.02	0.01	0.02	0.05	0.01	0.02	0.01	0.02	0.02	0.02	0.02	0.04	0.05	0.01	0.03
An	0.00	0.00	0.00	0.04	0.00	0.00	0.00	0.00	0.00	0.00	0.00	0.01	0.01	0.00	0.00

Cations calculated on an 8-oxygen basis.

"1#2" means the second analysis on K-feldspar 1.

Appendix E Whole rock compositions (wt.%).

Table 1. Whole rock compositions (wt.%) from the sub-chlorite, chlorite and biotite zones.

Zone	Sub-Chl								Chl				Bt				
Sample	07101	07102	07104	07105	07106	07107	07109	0713B	07205	07208	07211	07212	07302	07217	07304	07307	07405
SiO_2	60.09	53.82	61.89	67.81	83.04	71.06	67.82	70.05	76.57	72.49	67.56	67.10	68.65	62.31	62.93	56.12	45.31
TiO_2	0.64	0.73	0.94	0.73	0.31	0.59	0.62	0.62	0.36	0.49	0.63	0.55	0.62	0.97	1.01	1.11	1.56
Al_2O_3	12.97	11.27	16.01	11.78	5.59	10.94	12.97	14.71	9.49	12.96	14.89	13.94	15.59	18.81	18.51	21.50	32.58
$Fe_2O_3^T$	5.48	4.80	6.79	5.07	2.23	4.42	6.77	4.18	4.74	4.66	6.52	6.69	6.02	9.04	7.77	11.04	9.70
MnO	0.06	0.07	0.06	0.07	0.13	0.11	0.19	0.03	0.25	0.06	0.04	0.19	0.08	0.13	0.30	0.25	0.16
MgO	2.98	2.42	2.31	1.84	0.70	1.77	3.70	4.43	4.15	4.09	5.36	6.41	3.60	2.77	2.74	3.34	2.49
CaO	13.62	22.42	7.10	9.15	5.23	6.49	4.01	0.23	1.24	0.32	0.22	0.17	0.11	0.16	0.26	0.22	0.29
Na_2O	2.05	2.80	2.01	1.83	1.33	2.03	1.60	4.11	1.67	3.89	0.34	0.68	1.94	1.96	2.06	1.73	1.20
K_2O	2.11	1.54	2.88	1.85	1.40	2.25	2.47	1.81	1.35	1.23	4.49	4.02	3.08	3.32	4.54	4.43	6.69
P_2O_5	0.16	0.18	0.18	0.17	0.14	0.16	0.17	0.13	0.17	0.11	0.11	0.10	0.10	0.13	0.15	0.17	0.12
Total	100.16	100.05	100.17	100.30	100.10	99.82	100.32	100.30	99.99	100.30	100.16	99.85	99.79	99.60	100.27	99.91	100.10
LOI	12.48	15.79	8.21	8.61	4.73	6.67	7.12	3.01	3.78	2.86	4.31	4.00	3.65	4.13	4.81	4.80	5.85
FeO	4.09	2.42	4.10	3.83	1.80	2.99	4.63	3.21	3.16	3.54	3.95	1.79	4.15	7.19	5.26	8.61	7.52
Fe_2O_3	0.92	2.11	2.23	0.81	0.23	0.89	1.62	0.61	1.23	0.73	2.13	4.70	1.41	1.05	1.92	1.47	1.34

Table 2. Whole rock compositions (wt.%) from the garnet and staurolite zones.

Zone	Grt									St		
Sample	07309	07310	07408	07408A	07409	05401A	05401B	05403A	05403B	07606	05501A	05501B
SiO_2	67.87	76.02	55.28	57.91	56.50	58.25	57.62	62.44	62.32	79.05	56.37	56.37
TiO_2	0.52	0.32	1.24	1.17	1.03	1.11	1.11	1.00	1.01	0.52	1.21	1.23
Al_2O_3	11.58	7.60	23.27	24.02	20.05	24.03	24.36	20.33	20.05	10.04	24.96	24.94
$Fe_2O_3^T$	6.94	10.32	10.62	8.53	8.47	8.85	8.75	8.09	8.05	4.76	8.61	8.62
MnO	1.71	0.12	0.27	0.20	0.13	0.14	0.14	0.17	0.18	0.03	0.17	0.16
MgO	3.88	3.78	2.74	1.91	3.24	1.99	1.97	2.23	2.21	1.45	1.87	1.89
CaO	3.20	0.24	1.08	0.62	5.16	0.32	0.33	0.70	0.70	0.91	0.68	0.68
Na_2O	0.50	0.16	2.14	1.66	3.04	1.14	1.15	1.57	1.56	0.30	2.19	2.20
K_2O	3.20	1.41	3.13	3.92	1.81	4.19	4.17	3.71	3.74	3.22	3.82	3.78
P_2O_5	0.29	0.14	0.17	0.16	0.21	0.16	0.14	0.11	0.11	0.15	0.16	0.16
Total	99.69	100.11	99.94	100.10	99.64	100.18	99.74	100.35	99.93	100.43	100.04	100.03
LOI	3.15	2.68	4.15	4.08	2.30	4.33	4.49	3.41	2.65	4.56	3.86	4.12
FeO	5.01	7.91	7.77	5.72	6.47	2.96	2.45	1.81	1.17	3.58	2.90	2.00
Fe_2O_3	1.37	1.53	1.98	2.17	1.28	5.28	5.67	5.65	6.19	0.78	5.14	5.96

Table 3. Whole rock compositions (wt.%) from the kyanite and sillimanite-K-feldspar zones.

Zone	Ky								Sil-Kfs				
Sample	077011	077031	077041A	077041B	077061	077092A	077092B	077101	07804	07905A	07905B	07908A	07908B
SiO_2	67.06	46.12	58.76	58.32	61.37	61.98	62.44	58.59	61.49	59.59	60.35	73.30	72.97
TiO_2	0.57	0.81	0.86	0.86	0.68	0.76	0.76	0.63	0.75	0.87	0.87	0.80	0.80
Al_2O_3	13.89	17.91	18.82	18.93	16.59	16.99	16.68	13.56	16.98	19.40	19.45	12.89	13.01
$Fe_2O_3^T$	6.73	25.69	10.66	10.73	7.99	9.70	9.67	17.71	7.14	6.99	7.10	5.27	5.27
MnO	0.37	1.36	0.60	0.61	0.65	0.85	0.87	2.51	0.15	0.23	0.23	0.11	0.11
MgO	5.86	4.26	3.88	3.90	6.46	4.16	4.14	3.36	3.59	1.76	1.76	1.63	1.63
CaO	0.38	0.70	0.49	0.49	0.77	0.45	0.47	1.09	3.52	4.41	4.42	2.05	2.05
Na_2O	0.79	0.44	0.77	0.78	1.00	0.70	0.69	0.43	3.01	4.18	4.21	2.37	2.37
K_2O	3.92	2.88	5.36	5.32	4.05	4.28	4.25	1.96	3.43	1.93	1.94	1.92	1.93
P_2O_5	0.11	0.14	0.11	0.12	0.12	0.13	0.12	0.30	0.16	0.05	0.05	0.11	0.11
Total	99.68	100.31	100.31	100.06	99.68	100.00	100.09	100.14	100.22	99.41	100.38	100.45	100.25
LOI	1.67	2.45	2.94	3.20	1.58	2.08	2.37	2.44	2.00	1.10	1.17	1.24	1.25
FeO	5.52	16.91	2.93	2.56	7.11	2.78	1.42	15.52	5.65	1.07	1.78	0.20	1.11
Fe_2O_3	0.60	6.90	6.96	7.35	0.09	6.23	7.42	0.46	0.86	5.33	4.79	4.56	3.74

Appendix F Monazite analyses (wt.%) and calculated dates and uncertainties.

Sample	Location	UO_2	ThO_2	PbO	Y_2O_3	Ce_2O_3	CaO	SiO_2	P_2O_5	Date	Error
DC-94-2c											
3#1	In Grt	0.470	3.007	0.080	0.702	34.16	0.489	1.508	27.49	442	24
3#2	In Grt	0.552	2.164	0.133	0.770	21.06	0.527	0.228	27.61	428	22
3#3	In Grt	0.553	2.708	0.162	0.961	30.06	0.497	1.778	27.42	426	23
3#4	In Grt	0.533	2.781	0.312	0.902	21.57	0.494	2.638	27.21	484	23
3#6	In Grt	0.547	1.806	0.049	0.681	24.85	0.575	0.203	27.66	403	20
3#7	In Grt	0.395	2.380	0.064	0.729	25.87	0.475	1.132	27.79	483	25
3#8	In Grt	0.445	1.870	0.066	0.484	34.98	0.653	0.392	27.74	439	20
3#9	In Grt	0.432	1.943	0.070	0.773	34.62	0.500	1.513	27.44	468	24
4#1	In Matrix	0.344	1.727	0.067	0.673	34.06	0.539	0.267	27.37	434	24
4#2	In Matrix	0.333	1.988	0.069	0.564	34.35	0.537	1.135	27.40	459	25
4#7	In Matrix	0.479	2.370	0.084	0.995	33.46	0.623	0.479	26.93	418	21
4#8	In Matrix	0.407	2.318	0.090	0.943	33.21	0.551	0.262	27.36	486	24
4#9	In Matrix	0.363	2.302	0.066	0.705	34.77	0.544	0.245	27.42	464	24
4#10	In Matrix	0.350	1.781	0.075	0.692	33.76	0.571	0.255	27.42	500	23
4#11	In Matrix	0.361	1.881	0.051	0.727	27.10	0.659	0.597	27.57	466	21
4#12	In Matrix	0.415	2.331	0.072	0.980	34.78	0.558	0.235	27.22	497	23
4#13	In Matrix	0.451	1.932	0.068	1.004	34.69	0.580	0.212	27.23	494	22
4#14	In Matrix	0.472	2.693	0.078	1.001	35.25	0.569	0.329	26.38	535	22
6#3	In Matrix	0.197	1.838	0.056	1.077	26.17	0.607	0.329	27.88	436	23
6#5	In Matrix	0.254	2.402	0.073	1.137	33.05	0.612	1.339	28.21	437	21
6#6	In Matrix	0.245	2.163	0.075	1.249	33.95	0.617	0.615	28.06	425	22
6#7	In Matrix	0.243	2.350	0.072	1.236	34.50	0.624	0.372	27.88	478	22
07310											
2#1	In Matrix	0.317	1.187	0.040	0.209	33.64	0.57	0.278	27.65	424	46
2#2	In Matrix	0.322	1.387	0.042	0.222	33.20	0.57	0.264	27.65	405	41
2#3	In Matrix	0.326	1.141	0.046	0.195	32.42	0.57	0.126	27.65	481	45
2#4	In Matrix	0.326	1.262	0.050	0.158	33.34	0.57	0.190	27.65	505	44
5#1	In Matrix	0.329	3.997	0.102	1.224	29.55	0.57	0.291	27.65	458	22
5#2	In Matrix	0.331	3.715	0.089	1.203	29.78	0.57	0.310	27.65	419	23
5#3	In Matrix	0.329	3.568	0.093	1.201	30.49	0.57	0.253	27.65	457	23
5#4	In Matrix	0.355	3.365	0.099	1.278	30.42	0.57	0.235	27.65	497	24
5#5	In Matrix	0.310	3.116	0.080	1.205	29.88	0.57	0.258	27.65	438	26
5#6	In Matrix	0.363	2.689	0.077	1.229	30.13	0.57	0.182	27.65	448	27
5#7	In Matrix	0.328	2.963	0.088	1.205	32.06	0.57	0.239	27.65	491	26
6#1	In Matrix	0.425	2.386	0.077	0.577	32.06	0.57	0.216	27.65	472	28
6#2	In Matrix	0.437	3.174	0.089	0.373	31.76	0.57	0.212	27.65	453	24
6#3	In Matrix	0.436	2.099	0.069	0.607	32.06	0.57	0.181	27.65	451	30
6#4	In Matrix	0.454	2.362	0.076	0.623	31.80	0.57	0.182	27.65	458	28
6#5	In Matrix	0.419	2.426	0.077	0.596	32.06	0.57	0.182	27.65	465	28
9#2	In Matrix	0.324	3.482	0.099	1.096	30.23	0.57	0.289	27.65	497	23

Sample	Location	UO_2	ThO_2	PbO	Y_2O_3	Ce_2O_3	CaO	SiO_2	P_2O_5	Date	Error
07310											
9#3	In Matrix	0.333	3.074	0.093	0.993	31.12	0.57	0.456	27.65	514	25
9#4	In Matrix	0.398	2.743	0.090	1.239	29.79	0.57	0.271	27.65	505	26
12#1	In Matrix	0.390	2.574	0.072	0.246	31.98	0.57	0.252	27.65	440	28
12#2	In Matrix	0.411	2.368	0.075	0.271	31.67	0.57	0.255	27.65	472	28
12#3	In Matrix	0.411	2.162	0.067	0.224	31.51	0.57	0.190	27.65	447	30
10#2	In Matrix	0.336	2.564	0.073	0.923	31.84	0.57	0.290	27.65	456	29
10#3	In Matrix	0.274	2.047	0.050	0.794	31.70	0.57	0.204	27.65	386	36
10#4	In Matrix	0.350	2.098	0.062	0.906	31.35	0.57	0.200	27.65	432	32
10#5	In Matrix	0.303	1.906	0.051	0.798	32.46	0.57	0.274	27.65	401	36
11#2	In Matrix	0.437	2.693	0.097	1.324	30.36	0.57	0.751	27.65	532	26
11#4	In Matrix	0.333	2.045	0.062	1.182	31.04	0.57	0.387	27.65	442	33
7#1	In Matrix	0.586	2.756	0.092	0.801	30.44	0.57	0.281	27.65	453	23
7#2	In Matrix	0.303	1.966	0.063	0.788	31.19	0.57	0.301	27.65	487	36
7#3	In Matrix	0.304	2.180	0.062	0.799	30.82	0.57	0.238	27.65	442	33
7#4	In Matrix	0.278	1.949	0.055	0.644	31.26	0.57	0.174	27.65	436	37
7#5	In Matrix	0.318	2.163	0.055	0.860	31.85	0.57	0.199	27.65	384	33
05501											
2#1	In Grt	0.357	3.648	0.089	0.399	31.52	0.813	0.232	27.44	429	21
2#2	In Grt	0.443	4.703	0.119	1.004	28.85	1.002	0.273	27.58	447	17
4#2	In Grt	0.381	4.786	0.111	0.952	28.22	1.013	0.337	27.19	426	17
4#3	In Grt	0.416	5.507	0.139	1.081	27.54	1.104	0.375	26.99	466	15
2G#1	In Grt	0.386	3.590	0.087	0.556	29.14	0.809	0.282	27.77	415	22
2G#2	In Grt	0.390	4.002	0.106	0.948	27.51	0.886	0.684	28.29	461	20
2G#3	In Grt	0.420	4.491	0.119	1.058	27.04	0.960	0.442	28.49	468	18
2G#4	In Grt	0.419	3.960	0.108	0.975	27.80	0.878	0.327	28.34	467	20
2G#5	In Grt	0.426	4.277	0.112	1.021	26.64	0.939	0.404	27.35	453	19
4G#1	In Grt	0.324	2.768	0.084	0.597	28.55	0.684	0.958	27.95	507	27
4G#2	In Grt	0.390	4.833	0.121	1.104	26.31	0.999	0.429	28.07	457	18
4G#3	In Grt	0.392	4.886	0.116	1.020	26.21	1.007	0.642	28.07	432	17
4G#4	In Grt	0.380	4.972	0.116	0.908	25.98	1.032	1.069	27.65	432	17
4G#5	In Grt	0.402	4.860	0.128	0.973	26.51	1.017	0.450	28.19	481	17
4G#6	In Grt	0.382	4.836	0.115	1.016	26.54	1.011	0.388	28.43	437	18
5#2	In Grt	0.286	2.935	0.058	0.192	26.26	0.824	27.990	21.92	353	25
4#1	In Grt	0.308	4.027	0.093	0.918	25.06	1.084	6.529	23.52	422	20
6#4	In Grt	0.435	3.059	0.080	0.533	30.18	0.690	3.221	26.98	411	23
5#8	Matrix Rim	0.304	2.219	0.061	0.216	32.75	0.496	0.149	27.43	448	31
5#7	Matrix Rim	0.297	2.377	0.072	0.284	32.68	0.526	0.169	27.32	504	30
5#6	Matrix Rim	0.301	2.415	0.065	0.274	31.54	0.638	0.388	25.50	459	29
3#9	Matrix Rim	0.347	2.588	0.075	0.319	31.80	0.579	0.385	27.55	468	27
5#9	Matrix Rim	0.321	2.716	0.066	0.160	31.40	0.597	0.266	27.16	413	27
5#4	Matrix Rim	0.324	2.732	0.064	0.252	32.15	0.652	0.285	27.17	395	27
3#1	Matrix Rim	0.350	2.772	0.071	0.193	31.62	0.622	1.907	27.21	423	26
3#8	Matrix Rim	0.320	2.791	0.068	0.265	31.86	0.606	0.309	27.56	413	27
5#10	Matrix Rim	0.330	2.805	0.079	0.175	31.44	0.621	1.210	25.74	480	26
3#3	Matrix Rim	0.354	2.842	0.074	0.419	31.77	0.624	0.222	27.61	433	25
1#4	Matrix Rim	0.323	3.042	0.059	0.191	30.75	0.755	1.627	26.73	333	25
6#1	Matrix Rim	0.372	3.044	0.080	0.980	30.69	0.663	1.449	27.50	426	24

Sample	Location	UO_2	ThO_2	PbO	Y_2O_3	Ce_2O_3	CaO	SiO_2	P_2O_5	Date	Error
05501											
1#3	Matrix Rim	0.326	3.233	0.090	0.401	31.61	0.698	0.240	27.87	491	24
3#2	Matrix Rim	0.386	3.242	0.088	0.555	31.23	0.692	0.238	27.58	451	23
3#6	Matrix Core	0.415	3.639	0.095	0.954	29.70	0.795	0.239	27.76	436	21
5#1	Matrix Core	0.301	3.795	0.085	0.383	31.41	0.826	0.837	27.37	415	22
6#3	Matrix Core	0.423	3.834	0.105	1.255	29.22	0.883	0.280	27.28	459	20
5#3	Matrix Core	0.338	3.846	0.082	0.233	31.38	1.020	0.862	26.53	389	21
3#7	Matrix Core	0.442	3.867	0.094	1.299	28.81	0.825	0.239	27.51	401	20
6#5	Matrix Core	0.308	4.183	0.092	1.365	26.70	0.901	0.760	28.86	403	20
6#2	Matrix Core	0.459	4.681	0.119	1.364	28.85	0.960	1.263	27.33	439	17
1#1	Matrix Core	0.470	4.884	0.128	1.315	26.97	1.081	0.664	27.05	457	16
3#4	Matrix Core	0.420	4.923	0.129	1.282	27.86	0.967	0.303	27.13	471	17
1#2	Matrix Core	0.444	5.012	0.124	1.293	27.75	1.052	0.507	27.67	439	16
3#5	Matrix Core	0.476	5.334	0.134	1.419	27.23	1.067	0.335	27.46	446	15
5#4	Matrix Core	0.394	5.672	0.121	0.452	30.60	1.134	0.437	26.78	407	15
077401											
1#1	Matrix Rim	0.322	3.923	0.089	1.096	30.40	0.840	0.232	29.36	407	22
1#2	Matrix Rim	0.337	3.891	0.090	1.029	31.15	0.840	0.229	29.36	412	22
1#3	Matrix Rim	0.385	4.160	0.101	1.087	31.22	0.840	0.206	29.36	427	20
1#4	Matrix Rim	0.346	4.057	0.111	1.113	31.00	0.840	0.221	29.36	492	21
2#1	Matrix Rim	0.347	4.078	0.095	0.971	30.52	0.840	0.368	29.36	418	21
2#2	Matrix Rim	0.323	4.012	0.090	1.027	30.70	0.840	0.305	29.36	405	22
2#3	Matrix Rim	0.287	3.832	0.087	0.917	31.22	0.840	0.261	29.36	416	23
2#4	Matrix Rim	0.277	3.762	0.084	0.861	31.41	0.840	0.259	29.36	411	23
2#5	Matrix Rim	0.374	3.880	0.100	1.007	31.32	0.840	0.428	29.36	439	22
4#1	Matrix Rim	0.350	3.883	0.097	0.909	30.88	0.840	0.339	29.36	446	22
4#2	Matrix Rim	0.378	4.038	0.093	0.951	31.11	0.840	0.427	29.36	406	21
7#2	Matrix Rim	0.330	3.941	0.100	0.780	31.44	0.840	0.269	29.36	462	22
7#5	Matrix Rim	0.348	3.688	0.090	0.718	31.44	0.840	0.319	29.36	430	22
13#1	Matrix Rim	0.328	3.829	0.088	0.891	31.69	0.840	0.321	29.36	414	22
13#2	Matrix Rim	0.342	3.983	0.105	0.853	31.82	0.840	0.265	29.36	476	21
13#3	Matrix Rim	0.347	3.965	0.092	0.833	31.56	0.840	0.206	29.36	413	22
13#7	Matrix Rim	0.331	3.715	0.098	0.776	31.65	0.840	0.198	29.36	472	23
13#8	Matrix Rim	0.335	3.821	0.087	0.682	31.70	0.840	0.172	29.36	408	22
1#6	Matrix Core	0.331	4.526	0.097	0.150	31.55	0.840	0.243	29.36	407	19
1#7	Matrix Core	0.335	4.418	0.101	0.237	31.26	0.840	0.195	29.36	431	20
1#9	Matrix Core	0.219	3.860	0.083	0.289	31.51	0.840	0.283	29.36	424	24
2#6	Matrix Core	0.361	4.027	0.102	0.621	32.28	0.840	0.209	29.36	458	21
2#7	Matrix Core	0.283	3.914	0.085	0.386	31.62	0.840	0.213	29.36	410	23
4#3	Matrix Core	0.346	4.267	0.104	0.440	30.49	0.840	0.282	29.36	450	20
4#4	Matrix Core	0.336	4.206	0.098	0.267	31.46	0.840	0.279	29.36	432	21
7#3	Matrix Core	0.340	4.053	0.091	0.260	31.44	0.840	0.201	29.36	415	21

Sample	Location	UO_2	ThO_2	PbO	Y_2O_3	Ce_2O_3	CaO	SiO_2	P_2O_5	Date	Error
077401											
11#1	Matrix Core	0.245	3.657	0.082	0.367	31.00	0.840	0.220	29.36	426	24
11#2	Matrix Core	0.284	4.053	0.086	0.219	31.62	0.840	0.198	29.36	403	22
11#3	Matrix Core	0.246	2.859	0.070	0.331	32.50	0.840	0.196	29.36	446	29
11#4	Matrix Core	0.232	3.441	0.086	0.365	31.42	0.840	0.186	29.36	482	26
11#5	Matrix Core	0.364	4.429	0.102	0.243	31.76	0.840	0.297	29.36	426	20
11#6	Matrix Core	0.258	3.956	0.088	0.137	32.06	0.840	0.181	29.36	429	23
11#7	Matrix Core	0.262	3.926	0.086	0.100	31.10	0.840	0.252	29.36	424	23
11#8	Matrix Core	0.251	3.978	0.079	0.229	31.70	0.840	0.237	29.36	388	23
11#9	Matrix Core	0.358	3.955	0.095	0.187	31.12	0.840	0.211	29.36	434	21
11#10	Matrix Core	0.251	2.835	0.076	0.301	32.68	0.840	0.144	29.36	486	29
11#11	Matrix Core	0.248	3.938	0.087	0.168	31.92	0.840	0.168	29.36	428	23
11#12	Matrix Core	0.337	4.187	0.099	0.148	32.09	0.840	0.260	29.36	439	21
11#13	Matrix Core	0.379	4.221	0.105	0.462	31.44	0.840	0.268	29.36	448	20
13#4	Matrix Core	0.246	4.250	0.091	0.288	32.19	0.840	0.232	29.36	422	22
13#6	Matrix Core	0.180	3.289	0.073	0.177	32.46	0.840	0.166	29.36	441	28
13#9	Matrix Core	0.169	2.992	0.063	0.211	31.44	0.840	0.166	29.36	417	30
13#11	Matrix Core	0.198	3.618	0.080	0.178	31.44	0.840	0.200	29.36	439	25
13#12	Matrix Core	0.203	3.730	0.077	0.183	31.44	0.840	0.207	29.36	414	25
DC-94-12											
4#1	In Matrix	0.349	3.026	0.087	1.564	33.59	0.625	0.136	28.17	468	25
4#3	In Matrix	0.437	4.930	0.125	1.617	31.31	0.923	0.196	27.94	446	17
4#4	In Matrix	0.529	5.368	0.137	2.169	31.87	1.111	0.186	28.28	436	15
4#5	In Matrix	0.296	2.437	0.075	1.660	33.31	0.506	0.116	28.27	485	31
4#6	In Matrix	0.407	4.475	0.126	1.767	32.32	0.961	0.197	28.04	492	19
4#7	In Matrix	0.357	2.801	0.092	1.833	33.08	0.622	0.116	28.35	517	26
4#8	In Matrix	0.525	5.061	0.146	2.147	31.12	1.134	0.177	28.14	485	16
4#9	In Matrix	0.462	4.470	0.132	2.045	30.66	0.951	0.213	28.11	498	18
5#1	In Matrix	0.610	4.519	0.132	1.993	31.33	0.953	1.484	27.99	457	16
5#2	In Matrix	0.403	3.967	0.108	1.681	31.80	0.800	1.155	27.76	461	20
5#3	In Matrix	0.724	4.455	0.142	2.092	31.09	0.993	0.168	28.02	471	16
5#4	In Matrix	0.456	3.039	0.096	1.725	32.85	0.647	0.143	28.07	473	23
5#5	In Matrix	0.487	3.695	0.118	1.836	31.88	0.830	0.238	28.17	501	20
5#6	In Matrix	0.681	7.203	0.186	1.844	30.13	1.376	0.377	27.86	453	12
5#7	In Matrix	0.552	6.021	0.160	1.636	31.12	1.146	0.314	27.95	469	14
5#8	In Matrix	0.755	4.665	0.150	2.142	30.82	1.055	0.235	27.87	475	15
5#9	In Matrix	0.639	4.333	0.138	2.018	31.25	0.948	0.212	27.93	486	17
5#10	In Matrix	0.393	4.162	0.122	1.625	32.01	0.832	0.262	27.92	510	20
5#11	In Matrix	0.545	4.340	0.131	1.908	31.47	0.937	0.270	28.11	482	18

Sample	Location	UO_2	ThO_2	PbO	Y_2O_3	Ce_2O_3	CaO	SiO_2	P_2O_5	Date	Error
059C1											
1#1	In Grt	0.354	4.291	0.123	2.061	29.50	1.157	0.097	27.94	488	19
1#2	In Grt	0.492	4.642	0.125	1.928	28.96	1.081	0.199	27.65	453	17
1#3	In Grt	0.524	4.779	0.134	1.988	28.66	1.118	0.211	27.72	464	16
1#4	In Grt	0.328	2.680	0.088	1.589	30.53	0.677	0.150	27.79	524	27
1#5	In Grt	0.385	3.048	0.096	1.467	30.76	0.832	0.134	27.91	501	24
1#6	In Grt	0.440	3.673	0.111	1.860	29.78	0.959	0.182	27.70	489	20
1#7	In Grt	0.480	3.352	0.105	1.712	30.20	0.885	0.139	27.72	479	21
1#8	In Grt	0.791	4.042	0.124	1.435	29.56	1.099	0.165	27.13	428	16
1#9	In Grt	0.557	3.430	0.117	1.776	30.46	0.974	0.098	27.79	503	20
1#10	In Grt	0.524	3.565	0.112	1.791	30.14	0.969	0.095	27.65	483	20
1#11	In Grt	0.517	3.597	0.113	1.737	30.02	0.949	0.112	27.65	482	20
1#12	In Grt	0.405	3.282	0.102	1.611	30.43	0.806	0.137	27.63	499	22
1#12	In Grt	0.536	3.625	0.112	1.771	30.38	0.963	0.115	27.87	469	19
1#13	In Grt	0.410	3.923	0.115	1.833	29.13	0.939	0.175	27.40	493	20
1#14	In Grt	0.332	2.811	0.081	1.568	30.68	0.700	0.140	27.50	461	26
1#15	In Grt	0.624	4.113	0.129	1.886	29.71	1.136	0.110	27.41	475	17
1#16	In Grt	0.389	3.316	0.092	1.588	30.32	0.813	0.143	27.31	451	22
1#17	In Grt	0.466	4.225	0.110	1.849	29.21	0.994	0.186	27.45	429	18
1#18	In Grt	0.518	3.443	0.108	1.897	30.25	0.965	0.086	27.68	473	20
1#19	In Grt	0.520	3.555	0.112	1.871	29.92	0.971	0.113	27.58	476	20
1#20	In Grt	0.514	3.338	0.107	1.795	30.27	0.917	0.094	27.53	479	20
1#21	In Grt	0.618	3.598	0.113	1.959	29.93	1.024	0.098	27.39	451	18
1#22	In Grt	0.391	3.360	0.101	1.614	30.19	0.804	0.160	27.26	493	22
1#23	In Grt	0.393	3.354	0.098	1.605	30.57	0.821	0.162	27.43	474	22
2#1	In Matrix	0.555	3.839	0.114	1.823	29.98	0.947	0.185	27.24	452	18
2#2	In Matrix	0.462	3.281	0.100	1.622	30.70	0.865	0.160	27.25	391	22
2#3	In Matrix	0.450	3.673	0.110	1.619	30.28	0.863	0.213	27.25	482	20
2#4	In Matrix	0.497	3.253	0.098	1.792	30.23	0.852	0.156	27.41	449	21
2#5	In Matrix	0.584	3.897	0.122	1.899	29.89	0.953	0.167	27.31	473	18
2#6	In Matrix	0.572	3.932	0.122	1.911	29.66	0.956	0.153	27.22	471	18
2#7	In Matrix	0.571	4.093	0.134	1.936	29.62	0.988	0.189	27.32	509	17
2#8	In Matrix	0.562	3.729	0.123	1.807	30.25	1.013	0.121	27.43	498	19
2#9	In Matrix	0.467	3.820	0.105	1.621	30.32	0.921	0.163	27.35	442	19
2#10	In Matrix	0.484	4.402	0.117	1.647	30.17	1.013	0.213	27.30	444	18
2#11	In Matrix	0.517	3.322	0.104	1.780	30.33	0.936	0.129	27.44	467	21
2#12	In Matrix	0.463	2.968	0.092	1.845	30.25	0.769	0.136	27.34	456	23
2#13	In Matrix	0.383	2.739	0.089	1.696	30.70	0.712	0.142	27.44	496	25
2#14	In Matrix	0.435	2.693	0.083	1.805	30.57	0.702	0.137	27.44	447	25
2#15	In Matrix	0.454	2.750	0.093	1.795	30.48	0.710	0.124	27.36	488	24
2#16	In Matrix	0.438	2.878	0.087	1.815	30.83	0.748	0.146	27.57	445	24
2#17	In Matrix	0.549	4.148	0.122	1.902	29.72	0.997	0.185	27.40	463	18
2#18	In Matrix	0.509	3.697	0.108	1.678	30.41	0.968	0.132	27.52	457	19

Sample	Location	UO_2	ThO_2	PbO	Y_2O_3	Ce_2O_3	CaO	SiO_2	P_2O_5	Date	Error
07905											
1#1	In Grt	0.231	2.721	0.083	1.925	28.36	1.018	0.248	28.42	527	29
1#2	In Grt	0.233	2.545	0.084	1.959	28.28	0.994	0.235	28.29	564	30
1#3	In Grt	0.233	2.932	0.090	1.873	28.21	1.099	0.297	27.89	541	27
1#4	In Grt	0.241	2.852	0.084	1.871	28.21	1.100	0.271	27.83	510	27
1#5	In Grt	0.215	2.527	0.082	1.895	28.59	0.991	0.222	28.24	560	31
1#6	In Grt	0.208	2.806	0.075	1.876	28.54	1.088	0.251	28.41	470	29
1#7	In Grt	0.238	2.933	0.084	1.935	28.12	1.097	0.245	28.32	499	27
1#8	In Grt	0.285	3.229	0.091	2.151	27.61	1.120	0.240	28.40	482	25
1#9	In Grt	0.232	2.912	0.083	1.889	28.22	1.074	0.418	28.23	500	27
1#10	In Grt	0.248	3.094	0.095	1.934	27.92	1.056	0.252	28.11	540	26
1#11	In Grt	0.243	2.909	0.089	1.986	28.34	1.020	0.224	28.33	531	27
1#12	In Grt	0.305	3.057	0.089	2.222	27.18	0.938	0.677	27.52	480	25
1#13	In Grt	0.354	2.696	0.091	2.234	27.15	0.652	0.339	27.67	516	26
1#14	In Grt	0.286	2.688	0.094	2.289	27.39	0.770	0.655	27.55	570	27
1#15	In Grt	0.464	3.804	0.116	3.098	25.36	1.385	0.248	28.03	475	19
1#16	In Grt	0.440	3.662	0.115	3.006	25.57	1.367	0.289	27.97	493	20
1#17	In Grt	0.458	3.808	0.127	2.997	25.27	1.421	0.625	27.50	525	19
1#18	In Grt	0.407	3.962	0.128	2.862	25.70	1.327	0.411	27.88	533	19
1#19	In Grt	0.381	3.598	0.108	2.658	27.00	1.163	0.253	28.48	491	21
1#20	In Grt	0.389	3.561	0.115	2.602	27.35	1.111	0.263	28.63	524	21
1#21	In Grt	0.386	3.264	0.105	2.594	27.89	1.111	0.218	29.00	510	23
1#22	In Grt	0.376	2.930	0.096	2.513	27.93	1.019	0.201	28.79	505	25
1#23	In Grt	0.320	2.554	0.086	2.385	28.69	0.896	0.194	28.88	519	28
1#24	In Grt	0.461	2.798	0.106	2.485	27.05	0.625	0.498	28.41	540	23
1#25	In Grt	0.468	2.820	0.103	2.395	27.05	0.640	0.674	28.75	519	23
1#26	In Grt	0.503	2.848	0.096	2.309	27.55	0.662	0.338	28.67	472	23
1#27	In Grt	0.483	2.865	0.103	2.423	27.56	0.632	0.305	28.52	508	23
1#28	In Grt	0.450	2.603	0.097	2.392	27.42	0.580	0.289	28.35	520	25
1#29	In Grt	0.446	3.069	0.096	1.829	27.85	0.670	0.268	28.64	471	23
1#30	In Grt	0.469	3.010	0.099	1.934	27.53	0.657	0.277	28.57	485	23
1#31	In Grt	0.334	2.482	0.080	2.377	28.55	0.877	0.201	28.87	482	28
1#32	In Grt	0.343	2.469	0.093	2.419	28.31	0.904	0.221	28.76	563	28
1#33	In Grt	0.323	2.479	0.088	2.405	28.50	0.844	0.226	28.76	541	28
1#34	In Grt	0.356	2.784	0.090	2.436	27.80	0.722	0.295	28.48	494	26
1#35	In Grt	0.395	3.262	0.099	2.573	27.45	0.948	0.367	28.82	476	23
1#36	In Grt	0.431	2.915	0.097	2.600	27.46	0.960	0.236	28.78	487	24
1#37	In Grt	0.351	3.817	0.109	2.332	27.55	1.059	0.321	28.76	487	21
1#38	In Grt	0.296	3.565	0.093	2.144	28.28	1.045	0.290	28.89	452	23
1#39	In Grt	0.351	3.455	0.113	2.573	27.43	1.074	0.261	28.99	544	22
1#40	In Grt	0.376	3.819	0.109	2.507	27.30	1.075	0.296	28.79	476	21
1#41	In Grt	0.314	3.293	0.099	2.313	27.92	0.942	0.275	28.86	503	24
1#42	In Grt	0.298	3.530	0.103	2.330	27.31	1.424	0.662	28.55	505	23
1#43	In Grt	0.239	3.107	0.092	2.006	28.12	1.276	0.267	28.80	524	27

Sample	Location	UO_2	ThO_2	PbO	Y_2O_3	Ce_2O_3	CaO	SiO_2	P_2O_5	Date	Error
07905											
2#1	Matrix Core	0.233	2.348	0.078	2.240	27.83	1.219	0.178	28.42	543	32
2#2	Matrix Core	0.239	2.336	0.077	2.170	28.20	1.198	0.197	28.53	535	32
2#3	Matrix Core	0.241	2.348	0.080	2.133	28.27	1.161	0.197	28.46	554	32
2#4	Matrix Core	0.245	2.355	0.081	2.183	28.53	1.214	0.195	28.73	558	32
2#5	Matrix Core	0.248	2.391	0.080	2.224	27.80	1.231	0.194	28.57	540	31
2#6	Matrix Core	0.252	2.407	0.077	2.248	28.42	1.229	0.176	28.68	513	31
2#7	Matrix Core	0.266	2.388	0.076	2.224	28.38	1.223	0.184	28.57	504	31
2#8	Matrix Core	0.254	2.440	0.079	2.229	28.30	1.231	0.178	28.68	526	31
2#9	Matrix Core	0.249	2.403	0.079	2.225	28.42	1.229	0.178	28.64	530	31
2#10	Matrix Core	0.250	2.388	0.079	2.245	28.24	1.234	0.181	28.67	530	32
2#11	Matrix Rim	0.377	3.876	0.112	1.951	27.26	0.683	0.492	27.92	490	20
2#12	Matrix Rim	0.385	3.924	0.113	2.051	27.55	0.682	0.501	28.53	486	20
2#13	Matrix Rim	0.292	2.885	0.091	2.235	28.58	0.893	0.277	28.72	522	27
2#14	Matrix Rim	0.287	2.691	0.091	2.334	28.37	0.749	0.252	28.66	586	28
2#15	Matrix Rim	0.272	2.739	0.089	2.381	28.23	0.767	0.241	28.56	535	28
2#16	Matrix Rim	0.308	2.820	0.100	2.388	28.36	0.805	0.238	28.69	575	26
2#17	Matrix Rim	0.385	2.843	0.093	2.467	27.90	0.821	0.245	28.59	495	25
2#18	Matrix Rim	0.380	3.012	0.096	2.461	28.12	0.828	0.234	28.63	492	24
2#19	Matrix Rim	0.362	3.101	0.097	2.381	28.10	0.851	0.230	28.51	498	24
2#20	Matrix Rim	0.329	2.970	0.100	2.386	28.36	0.820	0.228	28.71	543	25
2#21	Matrix Rim	0.320	2.747	0.104	2.340	27.74	0.781	0.222	28.33	602	26
2#22	Matrix Rim	0.303	2.647	0.092	2.320	28.09	0.744	0.232	28.51	551	28
2#23	Matrix Rim	0.283	2.627	0.088	2.328	28.24	0.727	0.255	28.53	542	29
2#24	Matrix Rim	0.297	2.692	0.089	2.352	27.86	0.757	0.230	28.34	530	28
2#25	Matrix Rim	0.313	2.816	0.092	2.377	27.94	0.774	0.231	28.38	523	27
2#26	Matrix Rim	0.335	3.139	0.095	2.391	27.82	0.841	0.233	28.45	496	24
2#27	Matrix Rim	0.344	3.174	0.100	2.414	28.03	0.850	0.231	28.54	510	24
2#28	Matrix Rim	0.319	3.045	0.086	2.457	27.75	0.741	0.284	28.36	455	25
2#29	Matrix Rim	0.325	3.345	0.103	2.398	27.67	0.757	0.387	28.16	516	23
2#30	Matrix Rim	0.343	4.411	0.106	1.897	27.18	0.776	0.647	27.70	432	19
2#31	Matrix Rim	0.305	3.499	0.101	2.528	27.40	0.711	0.408	28.31	492	23

Sample	Location	UO2	ThO2	PbO	Y2O3	Ce2O3	CaO	SiO2	P2O5	Date	Error
07905											
2#32	Matrix Rim	0.298	3.433	0.104	2.539	26.89	0.702	0.389	28.19	520	24
2#33	Matrix Rim	0.296	3.285	0.100	2.496	27.62	0.712	0.354	28.44	513	24
2#34	Matrix Rim	0.334	3.164	0.100	2.398	28.03	0.852	0.246	28.45	519	24
2#35	Matrix Rim	0.327	3.065	0.098	2.386	28.15	0.833	0.235	28.62	520	25
2#36	Matrix Rim	0.311	3.013	0.095	2.444	27.74	0.838	0.236	28.39	512	26
2#37	Matrix Rim	0.328	2.960	0.097	2.452	27.86	0.826	0.227	28.54	526	25
2#38	Matrix Rim	0.302	2.780	0.089	2.380	27.93	0.779	0.236	28.54	514	27
2#39	Matrix Rim	0.295	3.173	0.094	2.320	27.74	0.882	0.281	28.55	500	25
2#40	Matrix Rim	0.306	3.121	0.093	2.303	27.83	0.856	0.272	28.56	492	25
2#41	Matrix Rim	0.279	3.087	0.093	2.283	27.91	0.881	0.269	28.49	511	26
2#42	Matrix Rim	0.318	3.457	0.098	2.475	27.32	0.959	0.303	28.42	475	23
2#43	Matrix Rim	0.322	3.384	0.097	2.520	27.32	0.797	0.362	28.36	475	23
2#44	Matrix Rim	0.295	3.412	0.098	2.503	27.40	0.694	0.384	28.24	491	24
2#45	Matrix Rim	0.301	3.451	0.103	2.516	27.33	0.691	0.403	28.07	507	23
2#46	Matrix Rim	0.296	3.498	0.099	2.533	27.43	0.702	0.405	28.35	486	23
2#47	Matrix Rim	0.289	3.582	0.106	2.538	27.69	0.704	0.432	28.32	510	23
2#48	Matrix Rim	0.324	4.259	0.117	2.092	27.29	0.763	0.584	27.95	494	20
2#49	Matrix Rim	0.300	3.678	0.101	2.360	27.46	0.662	0.535	27.92	478	22
2#50	Matrix Rim	0.290	3.883	0.115	2.445	27.42	0.664	0.550	27.84	526	22
2#51	Matrix Rim	0.294	3.805	0.100	2.469	27.37	0.679	0.509	27.97	462	22
2#52	Matrix Rim	0.286	3.674	0.095	2.547	27.35	0.699	0.459	28.14	450	23
2#53	Matrix Rim	0.288	3.477	0.099	2.529	27.46	0.697	0.406	28.27	493	24
2#54	Matrix Rim	0.294	3.551	0.110	2.454	27.07	0.728	0.426	28.02	539	23
2#55	Matrix Rim	0.294	3.688	0.105	2.421	27.29	0.683	0.474	27.93	493	23
2#56	Matrix Rim	0.277	3.857	0.112	2.466	27.23	0.674	0.527	27.89	520	22
2#57	Matrix Rim	0.294	3.910	0.097	2.435	27.38	0.652	0.551	27.91	438	22
2#58	Matrix Rim	0.329	3.802	0.107	2.342	27.37	0.642	0.577	27.77	486	21
2#59	Matrix Rim	0.289	3.866	0.106	2.435	27.37	0.658	0.604	27.76	484	22
2#60	Matrix Rim	0.290	3.825	0.113	2.488	27.33	0.684	0.548	27.94	525	22
2#61	Matrix Rim	0.291	3.577	0.104	2.472	27.58	0.726	0.446	28.15	505	23
2#62	Matrix Rim	0.286	3.726	0.103	2.424	27.09	0.711	0.520	28.00	484	23

Appendix G UTM coordinates of samples.

Sample	UTM E	UTM N	Zone
2005 field season			
05101	0587380	4617527	Sub-Chl
05102	0587380	4617527	Sub-Chl
051B	0595079	4615162	Sub-Chl
05202	0599539	4611024	Chl
05203	0599539	4611024	Chl
05301	0608218	4612499	Bt
05401	0611077	4612463	Grt
05402	Close to 05401		Grt
05403	Close to 05401		Grt
05501	0611215	4611596	St
05601	0614729	4611783	St
05701	0617571	4610609	Ky
05801			Sil
05802			Sil
05901	0621623	4604668	Sil-Kfs
059B1			Sil-Kfs
059C1			Sil-Kfs
2007 field season			
07101	0586404	4619692	Sub-Chl
07102	0586404	4619692	Sub-Chl
07103	0586404	4619692	Sub-Chl
07104	0585794	4618858	Sub-Chl
07105	0585794	4618858	Sub-Chl
07106	0583162	4616048	Sub-Chl
07107	0579882	4616195	Sub-Chl
07108	0568558	4615691	Sub-Chl
07109	0568558	4615691	Sub-Chl
07110	0568558	4615691	Sub-Chl
07201	0591319	4616431	Chl
07202	0591319	4616431	Chl
07203	0591319	4616431	Chl
07204	0591319	4616431	Chl
07208	0600308	4623144	Chl
07209	0600308	4623144	Chl
07210	0601124	4623952	Chl
07211	0595734	4612902	Chl
07212	0595734	4612902	Chl
07213	0595734	4612902	Chl
07214	0595734	4612902	Chl
07215	0595734	4612902	Chl
07217	0606125	4613994	Bt
07218	0598533	4613929	Bt

Sample	UTM E	UTM N	Zone
07302	0609575	4626430	Bt
07303	0612599	4628178	Bt
07307	0608094	4612462	Bt
07308	0608094	4612462	Bt
07403	0615073	4632360	Bt
07405	0617299	4633576	Bt
07309	0610860	4612477	Grt
07310	0610860	4612477	Grt
07407	0619249	4633003	Grt
07408	0611296	4612366	Grt
07409	0611296	4612366	Grt
07410	0611296	4612366	Grt
07501	0619025	4632069	St
07502	0619025	4632069	St
07601	0619361	4629044	St
07602	0615722	4611453	St
07603	0615722	4611453	St
07604	0615722	4611453	St
07605	0614593	4611740	St
07606	0614593	4611740	St
077011	0617571	4610609	Ky
077021	0617571	4610609	Ky
077031	0617571	4610609	Ky
077032	0617571	4610609	Ky
077401	0617571	4610609	Ky
077051	0617571	4610609	Ky
077061	0617571	4610609	Ky
077071	0617571	4610609	Ky
077081	0617571	4610609	Ky
077091	0617571	4610609	Ky
077092	0617571	4610609	Ky
077101	0617571	4610609	Ky
077111	0617571	4610609	Ky
077121	0617571	4610609	Ky
07802	0624656	4611495	Sil
07803	0624656	4611495	Sil
07804	0625860	4611459	Sil
07805	0625860	4611459	Sil
07901	0619357	4593553	Sil-Kfs
07902	0619357	4593553	Sil-Kfs
07903	0619357	4593553	Sil-Kfs
07904	0623891	4597891	Sil-Kfs
07905	0625094	4600783	Sil-Kfs
07906	0625094	4600783	Sil-Kfs
07907	0625094	4600783	Sil-Kfs
07908	0624623	4603391	Sil-Kfs

References

Aleinikoff, J.N. and Karabinos, P., 1990. Zircon U-Pb data for the Moretown and Barnard Members of the MissisquoiFormation and a dike cutting the Standing Pond Volcanics, southeastern Vermont, in Slack, J.F., ed., Summary results ofthe Glenns Falls CUSMAP Project, New York, Vermont, New Hampshire, *U.S. Geological Survey Bulletin*, **1887**, chapter D, 10 p.

Balk,R.,1936. Structural and petrological studies in Dutche County, New York, PartI. Geologic structure of sedimentary rocks. *Geological Society of America Bulletin*, **47**, 685–774.

Barth, T.F.W., 1936. Structural and petrologic studies in Dutchess County, New York, part II: Petrology and metamorphism of the Paleozoic rocks. *Bulletin of the Geological Society of America*, **47,** 775-850.

Bence, A.E. and McLelland, J.M., 1976. Progressive metamorphism in Dutchess County, New York. *New York State Geological Association Field Guidebook*, 48th Annual Meeting, Vassar College, Poughkeepsie, New York, B-7-1-B-7-27.

Berman, R.G., 1990. Mixing properties of Ca-Mg-Fe-Mn garnets. *American Mineralogist*, **75**, 328-344.

Bowles, J.F.W., 1990. Age dating of individual grains of uraninite in rocks from electron microprobe analyses. *Chemical Geology*, **83**, 47-53.

Boyd, F.R. and Mertzman, S.A., 1987. Composition and structure of the Kaapvaal lithosphere, Southern Africa. *Special Publication - Geochemical Society*, **1**, 13-24.

Cameron-Schimann, M., 1978. Electron microprobe study of uranium minerals and its application to some Canadian deposits. PhD thesis, the University of Alberta.

Coggon, R. and Holland, T.J.B., 2002. Mixing properties of phengitic micas and revised garnet-phengite thermobarometers. *Journal of Metamorphic Geology*, **20**, 683-696.

Deer W.A., Howie R.A. and Zussman J., 1992. An introduction to the rock-forming minerals. 2nd ed. Longman Group Limited, Longman House, Burnt Mill, Harlow.

Dietsch,C. and Jercinovic, M, 2005, Tectonic implications of electron microprobe monazite ages of 525–535, 500–510, and ~ 475 Ma from the Waterbury dome, southwestern New England. *Geological Society of America Abstracts with Program*, **37**, 65.

Drake, A.A. Jr., Sinha, A.K., Laird, J. and Guy, R.E., 1989. The Taconic orogen. In *The appalachina-Ouachita orogen in the United States*. Vol. **F-2**, 101-177.

Faill, R.T., 1997. A geologic history of the north-central Appalachians; Part 1, Orogenesis from the Mesoproterozoic through the Taconic Orogeny. *American Journal of Science*, **297**, 551-619.

Ferry, J.M. and Spear, F.S., 1978. Experimental calibration of the partitioning of Fe and Mg between biotite and garnet. *Contributions to Mineralogy and Petrology*, **66**, 113-117.

Fisher, D.W., Isachsen, Y.W. and Rickard, L.V., 1970. Geologic map of New York: lower Hudson sheet. New York State Geological Survey.

Ghent, E.D. and Stout, M.Z., 1981. Geobarometry and geothermometry of plagioclase-biotite-garnet-muscovite assemblages. *Contributions to Mineralogy and Petrology*, **76**, 92-97.

Hames, W.E., Tracy, R.J., Ratcliffe, N.M. et al., 1991. Petrologic, structural, and geochronological characteristics of the Acadian metamorphic overprint on the Taconide zone in part of southwestern New-England. *American Journal of Science*, **291**(9), 887-913.

Hampel, F.R., Rousseeuw, P.J. and Ronchetti, E., 1981. The change-of-variance curve and optimal redescending M-estimators. *Journal of the American Statistical Association*, **76**, 643-648.

Helsel, D.R., 1989. Boxplots, a graphical method for data analysis. Branch of systems analysis technical memorandum 89.01

Hibbard, J., Tracy, R. and Henika, W, 2003, Smith River allochthon: a southern Appalachian peri-Gondwanan terrane emplaced directly on Laurentia? *Geology*, **31**, 215–218.

Hibbard, J., van Staal, C.R. and Rankin, D.W., 2007. A comparative analysis of pre-Silurian crustal building blocks of the northern and the southern appalachian orogen. *American Journal of Science*, **307**, 23-45.

Hirsch D.M., Prior D.J. and Carlson W.D., 2003. An overgrowth model to explain multiple, dispersed high-Mn regions in the cores of garnet porphyroblasts. *American Mineralogist*, **88**, 131-141.

Hodges, K.V. and Crowley, P.D., 1985. Error estimation and empirical geothermobarometry for pelitic systems. *American Mineralogist*, **70**, 702-709.

Hodges, K.V. and Spear, F.S., 1982. Geothermometry, geobarometry, and the Al_2SiO_5 triple point at Mt. Moosilauke, New Hampshire. *American Mineralogist*, **67**, 1118-1134.

Hoisch, T.D., 1990. Empirical calibration of six geobarometers for the mineral assemblage quartz + muscovite + biotite + plagioclase + garnet. *Contributions to Mineralogy and Petrology*, **104**, 225-234.

Holland, T.J.B. and Powell, R., 1998. An internally consistent thermodynamic dataset for phases of petrological interest. *Journal of Metamorphic Geology*, **16**, 309-343.

Jercinovic, M.J. and Williams, M.L., 2005. Analytical perils (and progress) in electron microprobe trace element analysis applied to geochronology; background acquisition, interferences, and beam irradiation effects. *American Mineralogist*, **90**(4), 526-546.

Johnson, T.E., Brown, M. and Solar, G.S., 2003. Low-pressure subsolidus and suprasolidus phase equilibria in the MnNCKFMASH system: Constraints on conditions of regional metamorphism in western Maine, northern Appalachians. *American Mineralogist*, **88**, 624-638.

Johnson, T. and Brown, M., 2004. Quantitative Constraints on Metamorphism in the Variscides of Southern Brittany - a Complementary Pseudosection Approach. *Journal of Petrology*, **45**, 1237-1259.

Karabinos, P., Stoll, H.M. and Hepburn, J.C, 2003. The Shelburne Falls arc- Lost arc of the Taconic orogeny, in Brady, J., and Cheney, J. (eds.), New England Intercollegiate Geologic Conference, Amherst, Massachusetts, p. B3-1 – B3-17.

Karabinos, P., Morris, D., Hamilton, M. and Rayner, N., 2008. Age, origin, and tectonic significance of Mesoproterozoic and Silurian felsic sills in the Berkshire massif, Massachusetts. *American Journal of Science*, **308**, 787-812.

Kelly, N.M., Clarke, G.L. and Harley, S.L., 2006. Monazite behaviour and age significance in poly-metamorphic high-grade terrains: A case study from the western Musgrave Block, central Australia. *Lithos*, **88**(1-4), 100-134.

Kelsey, D.E., Powell, R., Wilson, C.J.L. et al., 2003. (Th+U)-Pb monazite ages from Al-Mg-rich metapelites, Rauer Group, east Antarctica. *Contributions to Mineralogy and Petrology*, **146**(3), 326-340.

Kelts, A.B., Ren, M.H., and Anthony, E.Y., 2008. Monazite occurrence, chemistry, and chronology in the granitoid rocks of the Lachlan Fold Belt, Australia: An electron microprobe study. *American Mineralogist*, **93**, 373-383.

Koziol, A.M. and Newton, R.C., 1989. Redetermination of the anorthite breakdown reaction and improvement of the plagioclase-garnet-Al_2SiO_5-quartz barometer. *American Mineralogist*, **73**, 216-223.

Kretz, R., 1983. Symbols for rock-forming minerals. *Am. Mineral.*, **68**, 277 - 279.

Levene, H., 1960. In contributions to probability and statistics: essays in honor of Harold Hotelling, I. Olkin et al. eds., Stanford University Press, 278-292.

Long, L.E., 1962. Isotopic age study, Dutchess County, New York. *Geological Society of America Bulletin*, **73,** 997-1006.

Mahar, E.M., Baker, J.M., Powell, R. Holland, T.J.B. and Howell, N., 1997. The effect of Mn on mineral stability in metapelites. *Journal of Metamorphic Geology*, **15**, 223-238.

Martin, A.J., Gehrels, G.E., and DeCelles, P.G., 2007. The tectonic significance of (U,Th)/Pb ages of monazite inclusions in garnet from the Himalaya of central Nepal. *Chemical Geology*, **244**, 1-24.

McLelland, J.M. and Fisher, D.W., 1976. Trip C-7, Stratigraphy and structural geology in the Harlem Valley, S.E. Dutchess County, New York. Guidebook, **48,** C-7-1-C-7-37.

McLennan, S.M., Bock, B., Compston, W. et al., 2001. Detrital zircon geochronology of Taconian and Acadian foreland sedimentary rocks in New England. *Journal of Sedimentary Research*, **71**(2), 305-317.

Park, H.M., 2006. Univariate analysis and normality test using SAS, STATA, and SPSS. The Trustees of Indiana University.

Parslow, G.R., Brandstatter, F., Kurat, G. and Thomas, D.J., 1985. Chemical ages and mobility of U and Th in anatectites of the Cree Lake zone, Saskatchewan. *Canadian Mineralogist*, **23**, 543-552.

Powell, R. and Holland, T. J. B., 1988. An internally consistent dataset with uncertainties and correlations; 3, Applications to geobarometry, worked

examples and a computer program. *Journal of Metamorphic Geology*, **6,** 173-204.

Powell, R. and Holland, T. J. B., 1994. Optimal geothermometry and geobarometry. *American Mineralogist*, **79**, 120-133.

Powell, R., Holland, T.J.B. and Worley, B., 1998. Calculating phase diagrams with THERMOCALC: methods and examples. *Journal of Metamorphic Geology*, **16**, 577-588.

Powell, R. and Holland, T. J. B., 2008. On thermobarometry. *Journal of Metamorphic Geology*, **26**, 155-179.

Powell, R., Hergt, J. and Woodhead, J., 2002. Improving isochron calculations with robust statistics and the bootstrap. *Chemical Geology*, **185**, 191-204.

Pyle, J.M., 2006. Temperature-time paths from phosphate accessory phase paragenesis in the Honey Brook Upland and associated cover sequence, SE Pennsylvania, USA. Lithos, 88, 201-232.

Pyle, J. M., Spear, F.S., Cheney, J.T. et al., 2005a. Monazite ages in the Chesham Pond Nappe, SW New Hampshire, USA: Implications for assembly of central New England thrust sheets. *American Mineralogist*, **90**, 592-606.

Pyle, J. M., Spear, F.S., Wark, D.A. et al., 2005b. Contributions to precision and accuracy of monazite microprobe ages. *American Mineralogist*, **90**, 547-577.

Ratcliffe, N.M., Armstrong, R.L., Mose, D.G. et al., 1982. Emplacement history and tectonic significance of the Cortlandt Complex, related plutons, and dike swarms in the Taconide Zone of southeastern New York based on K-Ar and Rb-Sr investigations. *American Journal of Science*, **282**, 358-390.

Ratcliffe, N.M., 2006. Tremadocian to Pridolian accretionary arc, collisional, and post-collisional aspects of the Taconide Zone, Northeastern US. *Geological Society of America Abstracts with Program*, **38**, 9.

Reno, B.L., Piccoli, P.M., Brown, M. and Trouw, R.A.J., in review. Robust Statistical Methods for Assessment and Analysis of Monazite Microprobe Geochronologic Data Applied to the Neoproterozoic Brasília Belt, Brazil. *Chemical Geology*

Royston, J.P., 1982a. An extension of Shapiro and Wilk's W test for normality to large samples. *Appl. Statist.*, **31**(2), 115-124.

Royston, J.P., 1982b. The W test for Normality. *Algorithm AS 181*

Rubie, D.C., 1998. Disequilibrium during metamorphism: the role of nucleation kinetics. In: Treloar, P.J. and O'Brien, P.J. (eds) What Drives Metamorphism and Metamorphic Reactions? Geological Society, London, Special Publications, 138, 199- 214.

Shapiro, S.S. and Wilk, M.B., 1965. An analysis of variance test for normality (complete samples), *Biometrika*, **52**(3-4), 591-611.

Spear F.S. and Daniel C.G., 2001. Diffusion control of garnet growth, Harpswell Neck, Main, USA. *J. Metamorphic Geol*., **19**, 179-195.

Stanley, R.S. and Ratcleffe, N.M., 1985. Tectonic synthesis of the Taconic orogeny in western New England. *Geological Society of America Bulletin*, **96,** 1227-1250.

Sutter, J.F., Ratcliffe, N.M. and Mukasa, S.B., 1985. 40Ar/39Ar and K-Ar data bearing on the metamorphic and tectonic history of western New England. *Geological Society of America Bulletin*, **96**, 123-136.

Suzuki, K., 1991. Middle Precambrian provenance of Jurassic sandstone in the Mino Terrane, central Japan; Th-U-total Pb evidence from an electron microprobe monazite study. *Sedimentary Geology*, **75**, 141-147.

Suzuki, K. and Kato, T., 2008. CHIME dating of monazite, xenotime, zircon and polycrase: protocol, pitfalls and chemical criterion of possibly discordant age data. *Gondwana Research*, In Press.

Tomascak, P.B., Krogstad, E.J. and Walker, R.J., 1996. U-Pb monazite geochronology of granitic rocks from Maine; implications for late Paleozoic tectonics in the Northern Appalachians. *Journal of Geology*, **104**(2), 185-195.

Tucker, R.D. and Robinson, P., 1990. Age and setting of the Bronson Hill magmatic arc: a re-evaluation based on U-Pb zircon ages in southern New England. *Geological Society of America Bulletin*, **102**, 1404-1419.

Tukey, J.W., 1977. Exploratory data analysis. Addision-Wesley, Reading, Mass., 688

van Staal, C.R., 2005. Northern Appalachians. In Encyclopedia of geology. Elsevier Academic Press, Oxford, UK., 81-92.

van Staal, C.R., Dewey, J.F., Mac Niocaill, C. and McKerrow, W.S., 1998. The Cambrian-Silurian tectonic evolution of the Northern Appalachians and British Caledonides; history of a complex, west and southwest Pacific-type segment of Iapetus. In *Lyell: the past is the key to the present*. *Geological Society Special Publications*, **143**, 199-242.

Vidale, R.J., 1974. Vein assemblages and metamorphism in Dutchess County, New York. *Geological Society of America Bulletin*, **85,** 303-306.

Waters, D.J. and Lovegrove, D.P., 2002. Assessing the extent of disequilibrium and overstepping of prograde metamorphic reactions in metapelites from the Bushveld Complex aureole, South Africa. *Journal of Metamorphic Geology*, **20**, 135-149.

White, R.W., Powell, R., Holland, T.J.B. and Worley, B.A., 2000. The effect of TiO2 and Fe2O3 on metapelitic assemblages at greenschist and amphibolite facies conditions: mineral equilibria calculations in the system K2O-FeO-MgO-Al2O3-SiO2-H2O-TiO2-Fe2O3. *Journal of Metamorphic Geology*, **18**, 497-511.

White, R.W., Powell, R. and Clarke, G.L., 2002. The interpretation of reaction textures in Fe-rich metapelitic granulites of the Musgrave Block, central Australia: constraints from mineral equilibria calculations in the system K2O-FeO-MgO-Al2O3-SiO2-H2O-TiO2-Fe2O3. *Journal of Metamorphic Geology*, **20**, 41-55.

White, R.W., Pomroy, N.E. and Powell, R., 2005. An in-situ metatexite-diatexite transition in upper amphibolite facies rocks from Broken Hill, Australia. *Journal of Metamorphic Geology*, **23**, 579-602.

White, R.W., Powell, R. and Holland, T.J.B., 2007. Progress relating to calculation of partial melting equilibria for metapelites. *Journal of Metamorphic Geology*, **25**, 511-527.

Whitney, D. L., Mechum, T. A., Kuehner, S. M. and Dilek, Y. R., 1996a. Progressive metamorphism of pelitic rocks from protolith to granulite facies, Dutchess County, New York, USA; constraints on the timing of fluid infiltration during regional metamorphism. *Journal of Metamorphic Geology*, **14**, 163-181.

Whitney, D.L., Mechum, T.A., Dilek, Y.R. and Kuehner, S.M., 1996b. Modification of garnet by fluid infiltration during regional metamorphism in garnet by through sillimanite-zone rocks, Dutchess County, New York. *American Mineralogist*, **81,** 696-705.

Williams, M.L., Jercinovic, M.J., Hetherington, C.J., 2007. Microprobe monazite geochronology: understanding geologic processes by integrating composition and chronology. *Annu. Rev. Earth Planets. Sci.,* **35,** 137-75.

Williams, M. L., Jervinovic, M.J., Goncalves, P. and Mahan K., 2006. Format and philosophy for collecting, compiling, and reporting microprobe monazite ages. *chemical Geology*, **225**, 1-15.

Zagorevski, A., Rogers, N., van Staal, C.R. et al., 2006. Lower to Middle Ordovician evolution of peri-Laurentian arc and backarc complexes in Iapetus: Constraints from the Annieopsquotch accretionary tract, central Newfoundland. *Geological Society of America Bulletin*, 118, 324-342.

Zagorevski, A., McNicoll, V.J. and van Staal, C.R., 2007. Distinct Taconic, Salinic, and Acadian deformation along the Iapetus suture zone, Newfoundland Appalachians. *Canadian Journal of Earth Sciences*, **44**, 1567-1585.

Zeh A. and Holness M.B., 2003. The effect of reaction overstep on garnet microtextures in metapelitic rocks of the Ilesha Schist belt, SW Nigeria. *Journal of Petrology*, **44**, 967-994

Zen E-an, 1972. The Taconide zone and the Taconic orogeny in the western part of the northern Appalachian orogen. *Geological Society of America Special Paper*, **135**